



QUANTIFYING THE INFLUENCE OF WIND
ADVECTION ON THE URBAN HEAT
ISLAND

By

Richard Bassett

A thesis submitted to The University of Birmingham for the
degree of
DOCTOR OF PHILOSOPHY

School of Geography, Earth and Environmental Sciences

The University of Birmingham

July 2017

UNIVERSITY OF
BIRMINGHAM

University of Birmingham Research Archive

e-theses repository

This unpublished thesis/dissertation is copyright of the author and/or third parties. The intellectual property rights of the author or third parties in respect of this work are as defined by The Copyright Designs and Patents Act 1988 or as modified by any successor legislation.

Any use made of information contained in this thesis/dissertation must be in accordance with that legislation and must be properly acknowledged. Further distribution or reproduction in any format is prohibited without the permission of the copyright holder.

Abstract

The urban heat island (UHI) phenomenon currently effects over half the world's population, and this is set to rise significantly in the near future. Although this anthropogenic-induced warming is well studied, the dynamic nature of the UHI (i.e. with wind) receives little attention. The concept, urban heat advection (UHA), can warm air temperatures in surrounding areas traditionally thought of as rural. This may lead to a misinterpretation of local climate and bias in long-term climate records. Using observational analysis and numerical modelling this thesis investigates these limitations by spatially quantifying UHA. A methodology to separate UHA from the background air temperature was applied to a high-density urban observation network in the city of Birmingham, UK demonstrating mean downwind UHA of 0.4°C and up to 1.2°C at individual stations (wind speeds 2 – 3 m s⁻¹). This UHA methodology was adapted to show that even small urban areas (~1 km²) can produce a mean UHA of 0.6°C under the same wind speeds. Differences in observed UHA between these two urban scales were attributed to complex land-use patterns around the observations, i.e. UHA from multiple sources. To overcome this, the Weather Research & Forecasting numerical model was used to refine the UHA methodology (accounting for regional heat advection) and conduct semi-idealised simulations (hypothetical cities). Here, a square city with 16 km size produced UHA of 2.4°C at the city edge, with 0.5°C warming extending 9 km downwind. A relationship was found between city size and UHA intensity, enabling statistical scaling. Through refinement of model parameters to local conditions, this demonstrated an approach to estimate UHA without the need for computationally expensive simulations.

Acknowledgements

There are several people I would like to thank for helping to make my PhD thesis possible. I would like to thank my Supervisors: Dr. Xiaoming Cai, Prof. Lee Chapman, Dr. Clare Heaviside and Prof. John Thornes. Their guidance and knowledge have been invaluable, and I am very grateful for this over the last few years. I would especially like to thank Xiaoming for the countless hours of discussion, and support he has provided me, not only throughout my PhD but since I began my Undergraduate studies at Birmingham.

I would like to take this opportunity to thank all the reviewers who have contributed to the papers in this thesis, and to the Natural Environment Research Council for providing financial support. This acknowledgement would not be complete without thanking Twingo (the cat). She has never failed to show her, sometimes distracting, encouragement. I would also like to thank my family (and new family in law) and friends.

Finally, I would like to thank my wife Victoria for her relentless support (and of course all the cake and tea I needed to write a PhD!). Thank you so much for putting up with all my quirks over the past few years, it means the world to me and it would only be right to dedicate this PhD to you!

List of Publications arising from this thesis

Bassett, R., Cai, X., Chapman, L., Heaviside, C., Thornes, J.E., Muller, C.L., Young, D.T., Warren, E.L. (2016) ‘Observations of urban heat island advection from a high-density monitoring network’, *Quarterly Journal of the Royal Meteorological Society*, 142, pp. 2434–2441. doi:10.1002/qj.2836.

Bassett, R., Cai, X., Chapman, L., Heaviside, C., Thornes, J.E. (2017) ‘The effects of heat advection on UK weather and climate observations in the vicinity of small urbanised areas’, *Boundary-Layer Meteorology*. doi:10.1007/s10546-017-0263-0.

Bassett, R., Cai, X., Chapman, L., Heaviside, C., Thornes, J.E. (2017) ‘Methodology to separate urban from regional heat advection by use of the Weather Research and Forecasting mesoscale model’, *Quarterly Journal of the Royal Meteorological Society*, 143: 2016–2024. doi:10.1002/qj.3062.

Bassett, R., Cai, X., Chapman, L., Heaviside, C., Thornes, J.E. (Submitted) ‘Semi-idealised urban heat advection simulations using the WRF mesoscale model’.

Table of Contents

<u>Chapter 1. Background</u>	1
1.1. Introduction	2
1.2. Overview of thesis data	10
1.3. Thesis aim and objectives	12
<u>Chapter 2. Observations of urban heat island advection from a high-density monitoring network</u>	16
2.1. Abstract	17
2.2. Introduction	18
2.3. Methods and Background	23
2.3.1. Study Area and Data	23
2.3.2. Urban Heat Island	26
2.3.3. Urban Heat Advection	28
2.3.4. Urban Heat Advection distance	31
2.4. Results and Discussion	33
2.4.1. Urban Heat Island	33
2.4.2. Urban Heat Advection	35
2.4.3. Urban Heat Advection distance	39
2.5. Conclusions	41
<u>Chapter 3. The effects of heat advection on UK weather and climate observations in the vicinity of small urbanised areas</u>	44
3.1. Abstract	45

3.2. Introduction	46
3.2.1. Background	46
3.2.2. Urban Heat Advection	48
3.3. Methods and Background	50
3.3.1. Building fraction data	50
3.3.2. Selection of stations	53
3.3.3. UK baseline temperature	54
3.3.4. Urban heat advection	57
3.4. Results and discussion	60
3.4.1. Case studies	60
3.4.2. Urban heat advection	63
3.4.3. Urban heat-advection footprint	69
3.5. Conclusions	71
 <u>Chapter 4. Methodology to separate urban from regional heat advection by use of the Weather Research and Forecasting mesoscale model</u>	 73
4.1. Abstract	74
4.2. Introduction	75
4.3. Methodology	79
4.3.1. WRF modelling framework	79
4.3.2. Land use and urban canopy parameters	82
4.3.3. WRF simulations	84
4.3.4. Surface observation networks	85
4.3.5. Urban heat advection	88

4.4. Results and discussion	90
4.4.1. Model evaluation	90
4.4.2. Urban Heat Island	91
4.4.3. Urban Heat Advection	94
4.5. Conclusions	99
<u>Chapter 5. Semi-idealised urban heat advection simulations using the WRF mesoscale model</u>	102
5.1. Abstract	103
5.2. Introduction	104
5.3. Methodology	107
5.3.1. WRF configuration	107
5.3.2. Urban heat island and advection	111
5.4. Results and Discussion	117
5.4.1. Semi-idealised urban heat islands	117
5.4.2. Semi-idealised urban heat advection	120
5.4.3. Scaled UHA statistical model	125
5.5. Conclusions	128
<u>Chapter 6. Conclusions</u>	132
6.1. Introduction	133
6.2. Chapter 2. Observations of urban heat island advection from a high-density monitoring network	134
6.3. Chapter 3. The effects of heat advection on UK weather and climate observations in the vicinity of small urbanised areas	136
6.4. Chapter 4. Methodology to separate urban from regional heat advection by use of the Weather Research and Forecasting	137

mesoscale model	
6.5. Chapter 5. Semi-idealised urban heat advection simulations using the WRF mesoscale model	138
6.6. UHA synthesis and concluding remarks	140
<u>References</u>	146
<u>Appendix</u>	171

List of Figures

Chapter 1

Figure 1.1. Hypothetical influence of an urban area “u” on its surrounding environment “e” for: (a) where all wind directions are considered, and (b) for a single wind direction. “r” indicates rural. Adapted from Lowry (1977). 8

Figure 1.2. Overview of thesis structure. 15

Chapter 2

Figure 2.1. Study area and location of BUCL stations, and urban fraction (Ufrac): ranging from 0 (rural) to 1 (urban). Birmingham’s administrative region is outlined with a solid border. The dashed border indicates the outer boundary of observations. 26

Figure 2.2. Hypothetical advection calculation (adapted from Heaviside et al., 2015). Illustration [A] signifies a typical time-mean UHI, assuming that the advection-induced warming is symmetric with respect to two wind directions under the same wind speed and stability group. Therefore, both rural columns will be warmed and the magnitude of the positive bar over the right rural area in [A] is effectively a half of the magnitude of the UHI due to advection in [B]. Illustration [B] considers a single wind direction, left to right, and this hypothetically means no heat is transferred upwind from the urban to left rural column (n.b. the rural background temperature, created by 30

local land use, does not decrease). Illustration [C] is derived by subtracting [A] from [B], i.e. removing the locally heated UHI component (the middle positive bar) and separating the advection-induced component. The negative value in [C] is linked to UHA from the opposing wind direction. The difference between positive and negative bars in [C] is interpreted as the UHA signal.

Figure 2.3. Hypothetical explanation of how [A] UHA $\overline{(T_{UHA(i)}^{(\theta)})}$ and [B] Ufrac difference from the mean $\overline{(\Delta Ufrac_{(i,d)}^{(\theta)})}$ are calculated under a NE wind for a given station (i) located in the centre of the crosshairs. The temperature difference $\overline{(\Delta T_{i-u}^{(\theta)})}$ has a smaller magnitude from the NE (more urbanised sector), i.e. the actual temperature is closer to the urban reference, than SW (less urbanised sector).

Figure 2.4. Spatial interpolation (kriging) of the nocturnal positive UHI intensity $\overline{(\Delta T^+)}$ under low cloud cover in three wind speed groups: WG1 ($< 2 \text{ m s}^{-1}$), WG2 ($2 - 3 \text{ m s}^{-1}$) and WG3 ($> 3 \text{ m s}^{-1}$). The analysis is limited to the outer boundary of observations.

Figure 2.5. Spatial interpolation (kriging) of UHA $\overline{(T_{UHA(i)}^{(\theta)})}$ in three wind speed groups: WG1 ($< 2 \text{ m s}^{-1}$), WG2 ($2 - 3 \text{ m s}^{-1}$) and WG3 ($> 3 \text{ m s}^{-1}$). Within each wind speed group, each box represents a wind direction sector (θ : NW, NE, SE, SW).

Figure 2.6. UHA Box-and-whisker plot $\overline{(T_{UHA(i)}^{(\theta)})}$ using SW and NE wind sectors, in three wind speed groups: WG1 ($< 2 \text{ m s}^{-1}$), WG2 ($2 -$

3 m s⁻¹) and WG3 (> 3 m s⁻¹). The x marker signifies the mean.

Figure 2.7. Pearson's correlation coefficient (r) between [A] UHI 41

$(\overline{\Delta T_{i-u}})$ and Ufrac annuli ($\overline{Ufrac_{(i,d)}^{(ann)}}$), [B] UHA ($\overline{T_{UHA(i)}^{(\theta)}}$) and Ufrac arcs ($\overline{\Delta Ufrac_{(i,d)}^{(\theta)}}$) at 3-km intervals from the stations. * correlation is significant at the 0.01 level.

Chapter 3

Figure 3.1. [a] Urban boundary layer structure and urban plume (after 49

Oke, 1976). [b] Adapted urban plume to show UHA processes: [1] horizontally through the UCL, and [2] horizontal and vertical heat mixing from the urban plume shown through hypothetical eddies.

Figure 3.2. [a] OS VectorMap building data in a 0.5-km radius 52

around the Met Office station at Coningsby, Coltishall and Shawbury (centre stars). [b] Building fraction at 30-degree arcs extending 0.5 km from each station. [c] Mean UHAI for the wind sector θ and station i ($\overline{T_{UHA(i)}^{(\theta)}}$, defined in detail below) in three wind speed groups (WG1, solid blue line: < 2 m s⁻¹, WG2, dashed green line: 2 – 3 m s⁻¹, WG3, dotted red line: > 3 m s⁻¹).

Figure 3.3. Stations used for the baseline temperature series (blue 56 triangles) and advection analysis (red dots).

Figure 3.4. ECMWF ERA-Interim comparison with the baseline 56 temperature series: [a] August 2003, and [b] December 2014.

Figure 3.5. The relationship between 0.5-km upwind building 62

fraction and mean UHAI ($\overline{T_{UHA(i)}^{(\theta)}}$) in three wind speed groups at

Coningsby, Coltishall and Shawbury weather stations (WG1: $< 2 \text{ m s}^{-1}$, WG2: $2 - 3 \text{ m s}^{-1}$, WG3: $> 3 \text{ m s}^{-1}$).

Figure 3.6. The relationship between upwind building fraction and the mean UHAI signal ($\overline{T_{UHA(i)}^{(\theta)}}$) across all stations in three wind speed groups (WG1: $< 2 \text{ m s}^{-1}$, WG2: $2 - 3 \text{ m s}^{-1}$, WG3: $> 3 \text{ m s}^{-1}$). The red square indicates the mean UHA at urban fraction intervals: 0, 0 - 0.1, 0.1 - 0.2, 0.2 - 0.3, 0.3 - 0.4. The vertical lines either side of the mean represent \pm one standard deviation. The dashed blue line at the 0.1 building fractions indicates the urban, rural separation used for statistical analysis in Table 1.

Figure 3.7. Box-and-whisker plot for $\overline{T_{UHA(i)}^{(\theta)}}$ where building fractions > 0.1 for WG1, WG2 and WG3. The x marker signifies the mean and whiskers 1.5 IQR.

Chapter 4

Figure 4.1. (a) Nested configuration of WRF domains at 27, 9, 3 and 1-km resolutions. (b) Domain 4 land use adapted from Corine land cover. The red stars are the location of the observation BUCL and Met Office stations in the region. (c) Domain 4 urban fraction created using a NDVI image taken in July 2013.

Figure 4.2. (a) Time-mean UHI field (domain 4). The black lines represent the urban land-use boundaries. (b) Directional time-mean UHI pattern. Each image is the difference between the time-mean urban and time-mean rural-case simulation for a given wind direction

(θ : NE, SE, SW, NW).

Figure 4.3. (a) Time-mean UHA ($\overline{T_{UHA}^{(\theta)}}$) effects (domain 4) derived 96
using the methodology from Heaviside et al. (2015). This
methodology also contains RHA information. The black lines
represent the urban land-use boundaries and arrows wind direction.
UHA values between -0.1 and 0.1 are not displayed because these
could be natural temperature fluctuations. (b) Regional heat advection
(RHA) effects calculated using the UHA methodology from
Heaviside et al. (2015) on the rural-case time-mean simulations only.
The dashed black lines represent where the urban areas have been
removed.

Figure 4.4. Time-mean UHA ($\overline{T_{UHA}^{(\theta)}}$) effects (domain 4) derived using 98
the new methodology where RHA has been excluded. The black lines
represent the urban land-use boundaries and arrows mean wind
direction. UHA values between -0.1 and 0.1 are not displayed because
these could be natural temperature fluctuations.

Chapter 5

Figure 5.1. (a) WRF domain 1 (the outermost) to 4 (the innermost) 108
configuration. (b) The black square represents the semi-idealised
urban land-use (high-density residential) configuration in domain 4
for the 16-km case. The remainder of the domain was filled with the
USGS land-use category 2, Dryland Cropland and Pasture.

Figure 5.2. Hypothetical UHA calculation that excludes RHA effects. 113
Diagrams named with [A] are for elevated temperatures due to

RHA+UHA (i.e. output of the idealised urban simulations), [B] for elevated temperatures due to RHA only (i.e. output of the rural simulations), and [C] for the difference between [A] and [B] (i.e. elevated temperatures due to UHA only). In the top row, all wind directions (i.e. wind from left to right and right to left) were considered, and the resulting pattern [C1] represents the time-mean UHII field ($\overline{\Delta T}$). In the middle row, only one wind direction (i.e. wind from left to right) is considered, and the resulting [C2] represents the directional time-mean UHII field ($\overline{\Delta T^{(\theta)}}$). In the bottom row, [C2] and [C1] are copied from above, and [C2]-[C1] yields [UHA], which is the UHA field ($\overline{T_{UHA}^{(\theta)}}$) that is free from the local-UHI and RHA effect.

Figure 5.3. (a) Domain 4 time-mean 2 m UHII field ($\overline{\Delta T}$) for each urban size ($L_U = 2, 4, 8, 16$ km) where all wind directions are used. The black box shows the outer boundary of the urban land use. (b) The relationship between the mean UHII of all urban grid cells, $\overline{\Delta T'}$, and the log urban size (L_U) is given in black squares; $\overline{\Delta T'} = 0.58 (\log L_U) + 1.6$. A comparison with Oke's (1973) relationship between urban size (converted from population) and maximum UHII for European cities is shown in black triangles; $\overline{\Delta T} = 1.75 (\log L_U) + 2.92$.

Figure 5.4. Directional time-mean UHII ($\overline{\Delta T^{(\theta)}}$) calculated as the rotated mean of the N, S, E and W wind direction UHII fields for the

16-km urban size. The black arrow represents the mean wind direction (wind flow $< 5 \text{ m s}^{-1}$). The black box shows the outer boundary of the urban land use.

Figure 5.5. Rotated time-mean UHAI field ($\overline{T_{UHA}^{(\theta)}}$) for each idealised urban size (L_U). The black rectangle in each plot represents the urban outline, and black arrow the wind direction wind flow $< 5 \text{ m s}^{-1}$. 122

Figure 5.6. (a) Horizontal transects through the rotated time mean directional UHAI fields ($\overline{T_{UHA}^{(\theta)}}$) for each urban size (shown in Figure 5.5). (b) The negative and positive UHAI transects from Figure 5.6a were combined to show the total UHAI contribution. Spline interpolation is used to smooth each UHAI transect, with the most noticeable effect for the peak UHAI. The vertical lines in a corresponding line type represent the urban boundary for each size. 124

Figure 5.7. (a) The relationship between urban size (L_U) and peak UHAI distance from the urban centre (D_{MAX}). The equation of the line is given at (4). (b) Relationship between log urban size (L_U) and 127

peak UHAI ($\overline{T_{UHA MAX}^{(\theta)}}$). The equation of the line is given at (5). (c) Decomposed UHAI transects (the original transects are shown in Figure 5.6b). (d) Log mean of the collapsed UHAI transects found in Figure 5.7c shown in dots. The equation of the Fourier line is given at (6).

Figure 5.8. UHAI statistical model output for $L_U = 2, 4, 8$ and 16 km are shown solid lines and the original modelled output in dashed lines. 128

List of Tables

Chapter 2

Table 2.1. Station metadata. Local Climate Zones (LCZ) are assigned using the classification by Stewart and Oke (2012). Urban fraction is calculated as the mean pattern within a 1-km radius of each station.	25
---	----

Chapter 3

Table 3.1. Welch two sample t -test between $\overline{T_{UHA}^{(\theta)}(i)}$ for urban and rural wind sectors where the urban sectors correspond to θ with building fraction > 0.1 and the rural sectors to θ with building fraction < 0.1 . The mean of all urban sectors is shown as $\overline{T_{UHA}^{(urban)}}$ and for rural sectors $\overline{T_{UHA}^{(rural)}}$.	66
Table 3.2. Stations where the UHA signal does not exhibit a relationship with upwind building fraction with explanations provided through a visual station analysis.	68
Table 3.3. Pearson's correlation coefficient between the mean UHA signal ($\overline{T_{UHA}^{(\theta)}(i)}$) and upwind building fraction arcs at increasing distances from stations.	71

Chapter 4

Table 4.1. Calculated building morphology parameters: building height (H) quartiles (Q), building width (W_B), street width (W_S) and urban fraction (ufrac).	84
--	----

Table 4.2. WRF simulation periods, run for each urban and rural case. Meteorological data for the mean of each period were taken from Coleshill weather station (located in the centre of domain 4: Latitude 52.4801, Longitude -1.69072). 85

Table 4.3. Station metadata and evaluation statistics. The following abbreviations are used: BUCL (Birmingham Urban Climate Laboratory), MO (Met Office), RMSE (Root Mean Square Error), r (Pearson's Correlation Coefficient), MBE (Mean Bias Error) and n (number of hourly observations). The locations of the stations are shown in Figure 4.1b. 87

Table 4.3. Number of simulation hours and characteristics in each wind direction group. 94

Chapter 5

Table 5.1. WRF simulation periods, run for each urban and rural case. 110

List of Abbreviations

Atmospheric Boundary Layer	ABL
British Atmospheric Data Centre	BADC
Birmingham Urban Climate Laboratory	BUCL
Building Effect Parameterization	BEP
Corine Land Cover	CLC
Internal Boundary Layer	IBL
Local Climate Zones	LCZ
Mean Bias Error	MBE
Met Office	MO
Moderate-resolution Imaging Spectroradiometer	MODIS
Normalized Difference Vegetation Index	NDVI
Office for National Statistics	ONS
Ordnance Survey	OS
Regional Heat Advection	RHA
Root Mean Square Error	RMSE
Urban Boundary Layer	UBL
Urban Canopy Layer	UCL
Urban Fraction	Ufrac
United Nations	UN
UK Climate Projections 2009	UKCP09
Urban Heat Advection	UHA

Urban Heat Advection Intensity	UHAI
Urban Heat Island	UHI
Urban Heat Island Intensity	UHII
United States Geological Survey	USGS
Urban Zones to characterize Energy partitioning	UZE
Weather Research and Forecasting Model	WRF
Wind Group	WG
World Meteorological Organization	WMO

Chapter 1.

Background

1.1. Introduction

Urban areas are now home to over half the world's population, and this is set to increase rapidly in the near future (UN, 2014). Understanding how large-scale anthropogenic changes to the Earth's land surface impact local climate is fundamental, especially when developing adaptation strategies. Cities are well known to be considerably warmer than their surroundings, however little consideration has been given to how heat is advected outwards. This may impact upon areas traditionally viewed as free from urbanisation, and to the accuracy of temperature records used to assess climate. Combined with social and economic challenges already present in cities and rising global temperatures, there is an ever-increasing risk from excess heat, particularly to health and infrastructure. This Chapter provides an overview of urban climate and the aims of this thesis. A formal literature review is not provided in this thesis as specific literature is presented within each main Chapter.

The urban heat island (UHI), first noted in the early 19th Century (Howard, 1833), is characterised as the temperature difference between urban and rural environments. The "island" is synonymous with the urban environment or zone of influence the urban area has on its surroundings (Lowry, 1977). Urban areas effectively modify the local climate through un-natural changes to surface properties. The largest urban heat island intensities (UHII, i.e. maximum difference) are found at night (several hours after sunset) under clear skies and calm winds, i.e. reduced turbulent mixing exists under these conditions. Atmospheric stability classes (e.g. Pasquill and Smith, 1983) are often used to group the UHII by prevailing conditions (Lee, 1975; Kruger and Emmanuel, 2013). The UHII is largest in the most urbanised areas and generally

decreases with distance outwards (this can depend on building materials, geometry and anthropogenic heat release). Features such as temperature cliffs are found at marked land-use boundaries and cool spots can develop in parks. The variety of air temperatures has within the urban environment lead to the creation of “local climate zones” as a means of UHI classification (Stewart and Oke, 2012).

The main factors contributing to UHI development are (Oke, 1987): reduced sky view factors, i.e. trapped outgoing long-wave radiation; changes to building thermal (increased heat capacities and conductivities) and radiative (albedo and emissivity) properties; decreased evapotranspiration due to a lack of vegetation, (less latent heat cooling); anthropogenic heat from buildings, vehicles and people; increased surface areas (short-wave absorption); reduced wind speeds (increased surface roughness) can decrease turbulent heat loss; and increased absorption and re-emission of long-wave radiation due to air pollution. These processes modify the UHI across a broad range scales. Regional synoptic weather can influence a city’s peak UHI (i.e. cloud cover and wind speed) whereas shading from buildings or trees can introduce large temperature differences across a single street canyon. During the daytime urban areas can also exhibit urban cool islands (Yang et al., 2017). These are typically less pronounced and are due to urban areas taking longer to warm than rural areas at sunrise (i.e. increased surface areas).

The resulting UHI, up to 10°C for large cities (e.g. London: Chandler, 1965), is related to the logarithm of city size (Oke, 1973). This can be quantified using several techniques: (i) surface air temperature observations (e.g. Unwin, 1980; Jauregui, 1997); (ii) transects conducted using vehicles (e.g. Unger et al., 2010; Smith et al.,

2011); (iii) remote sensing (e.g. Voogt and Oke, 2003; Tomlinson et al., 2012), and (iv) numerical modelling (e.g. Loridian et al., 2013; Chen et al., 2014). Fixed air temperature observations have the advantage of capturing long temporal records, however they are unable to easily show the spatial nature of the UHI. This is because studies often only use a two-station approach. Whilst transects, modelling and remote sensing can fill this spatial void, they are typically only able to capture short time periods. Furthermore, satellites only capture the surface, skin temperature, not air temperature. Therefore, combinations of these techniques are often used to assess the UHI (Tomlinson et al., 2013). The use of high-density urban meteorological networks (e.g. Basara et al., 2010; Warren et al., 2017) to explore UHI features, whilst desirable, is less common. This is due to siting and maintenance challenges within urban environments (Muller et al., 2013; Chapman et al., 2014).

The UHI impacts are particularly notable during heatwaves, which are set to become an increasingly regular feature of UK climate before the end of the century (UKCP09). Urban areas are particularly at risk as they are unable to cool down as efficiently as their surroundings at night. This may lead to heat-health (Patz et al., 2005) and infrastructure risks (Chapman et al., 2013). The UHI was estimated to account for approximately 50 % of the excess mortality in the West Midlands region of the UK during the August 2003 heatwave (Heaviside et al., 2016). The same heatwave also led to as many as 70 000 excess deaths throughout Europe (Robine et al., 2008). To offset UHI impacts, mitigation strategies are available and in some cases already implemented. These are based on increasing a cities reflectivity (albedo) and moisture availability (i.e. vegetation) for latent heat cooling. Santamouris's (2014) review suggested that green roofs may lower the mean air temperature by 0.3°C for every 0.1

increase in albedo. Green roofs have the additional benefit of improving biodiversity in urban areas (Oberndorfer et al., 2007). However, to mitigate the UHI on any notable scale this would require citywide UHI planning. Conversely, in cold climates the UHI may be beneficial, i.e. reduced energy consumption and winter mortality from excess cold. Secondary UHI impacts include increased downwind precipitation and thunderstorm development (Bornstein and Lin, 1999), and the development of local circulations, similar in mechanism to sea breezes (Haeger-Eugensson and Holmer, 1999; Hidalgo et al., 2008; Ryu et al., 2013). The same synoptic conditions favourable to the UHI development can lead to poor air quality in cities (Lai and Cheng, 2009). More widely, the sum of UHIs from cities worldwide have been shown to warm global surface temperatures (Kalnay and Cai, 2003). As such, considerable effort has been given to understanding the UHI phenomenon. However, only a handful of studies consider how the spatial UHI pattern is modified dynamically.

Aside from physical and thermodynamic changes to surface properties (e.g. albedo and emissivity), urban environments cause notable perturbations to the atmospheric boundary layer. Urban boundary layers are generally deeper and less stable when compared to their surrounding rural boundary layers, due to warmer and drier and rougher conditions from the underlying urban surface (Oke, 1987). The urban boundary layer can be subdivided into several elements. The first part, the roughness sublayer, extends from the surface to roughly 2 -5 times building heights and the lower portion contains the urban canopy layer (Rotach, 1995). Within this zone, air movement around individual elements cause large heterogeneities in horizontal and vertical turbulence and flows (Giometto et al., 2016). Above the roughness sublayer lies the inertial sublayer, where turbulence becomes homogeneous and fluxes do not

vary significantly (Barlow, 2014). The remainder of the urban boundary layer (approximately 90 %) contains the mixed layer (or residual at night) where properties towards the top are unaffected by the surface and are similar in appearance to the rural boundary layer.

In addition to an increased sensible heat flux rising from the urban canopy layer, under calm conditions, the difference in air temperatures between urban and rural areas causes convergent flows near the surface. This convergence will lead to vertical flows above the urban canopy and divergence aloft (Hidalgo et al., 2010). The resulting UHI thermal dome will increase the boundary-layer height compared to rural surroundings (Pal et al., 2012), and therefore vertical dispersion of heat or pollutants (Du et al., 2013). The resulting urban boundary-layer structures have been captured in observations (Bornstein and Johnson, 1977; Hildebrand and Ackerman, 1984; Oke, 1995; Hidalgo et al., 2010) and reproduced by numerical weather prediction (NWP) models (Miao et al., 2009; Fan et al., 2011). For NWP, parameterisations are needed, particularly at mesoscales, because of the sub-grid nature of boundary-layer processes, e.g. turbulent eddies. Reviews of how boundary-layer heat, mass and momentum exchanges are parameterised in NWPs can be found in Stull (1988) and Stensrud (2007). Within NWPs, often multiple boundary-layer parameterisations of turbulent fluxes are available (e.g. local or non-local schemes) based on different interpretations of processes and properties (Cuchiara et al., 2014). These parameterisations represent the wide range of boundary-layer knowledge and interactions with synoptic flows (Fan et al., 2011).

Horizontal winds in the near-surface boundary layer, flowing over rural then urban areas will encounter disparities in surface properties, thus impacting heat flux, moisture and momentum profiles. The overall effect of the horizontal winds are to modify the UHI dome into a plume (see Figure 3.1). Whilst the vertical extent of the urban heat dome is well quantified, knowledge about the horizontal extent is relatively limited due to lack of three dimensional observations. Limited upper air studies have shown plumes can extend up to 15 km downwind (Dirks 1974; Ackerman et al., 1978; Wong and Dirks 1978), also shown in modelling where plumes can extend 2 to 3 times the urban area diameter downwind (Fan et al., 2017). Downwind of the city, the step change back to rural land use, will modify the lower portion of the urban plume as heat flux and temperature profiles adjust back to a rural equilibrium. It is in this region, the downwind rural surface where this thesis explores the change in local temperature caused by advection.

Large-scale wind flows are largely responsible for the transport of atmospheric properties, known as advection, within the boundary layer. The temperature at a fixed point can be expressed as the rate of change of local temperature plus the three-dimensional contribution through advection, Equation 1. This equation forms the basis of the schemes used to represent advection numerically, albeit on a discrete set of grid points and with time integration. For example, WRF uses the third-order Runge-Kutta scheme (Skamarock et al. 2008) due to its efficiency.

$$\frac{dT}{dt} = \frac{\partial T}{\partial t} + \left(u \frac{\partial T}{\partial x} + v \frac{\partial T}{\partial y} + w \frac{\partial T}{\partial z} \right) \quad (1)$$

The advection term on the right-hand side of Equation 1 matches the conceptualisation of rural warming downwind of the UHI by Lowry (1977). Illustrated in Figure 1.1, a given urban area exerts a certain influence on its surroundings and this is dependent upon weather type (or wind direction). According to Lowry's (1977) conceptualisation the temperature at a given location is a function of heat created locally (i.e. influenced by the underlying land use and topography) and heat advected from upwind sources. Within the boundary layer, wind may advect heat downwind through a combination of processes. Firstly within the urban canopy layer (surface to roof level), heat is advected horizontally along street canyons between buildings. Secondly, heat rising above the urban canopy in the urban plume can be mixed downwards (after being advected downwind) by turbulent eddies to the surface level. These same urban heat advection (UHA) processes will transport air pollutants downwind (Ryu et al., 2013). All UHA results presented in this thesis refers to the change in local temperature caused by advection, denoted ΔT , not the physical process (i.e. temperature flux).

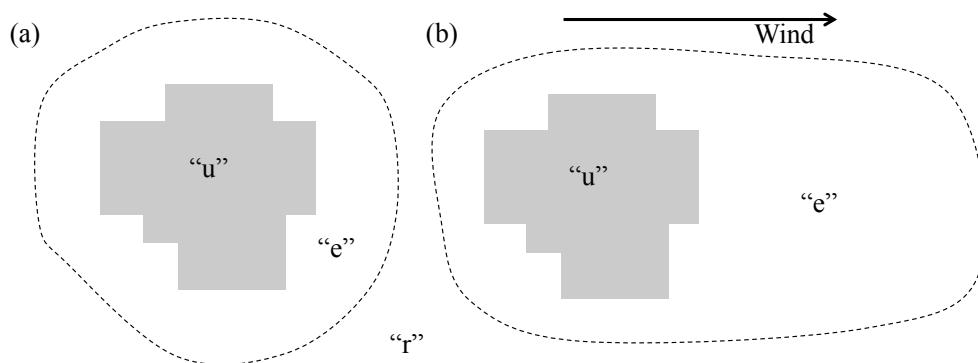


Figure 1.1. Hypothetical influence of an urban area “u” on the surrounding environment “e” for: (a) where all wind directions are considered, and (b) for a single wind direction. “r” indicates rural. Adapted from Lowry (1977).

The resulting downwind surface air temperature warming has already been noted in observations. Chandler (1965) located the highest UHIs northeast of central London, explained by the prevailing south-westerly winds. Similarly, the spatial UHI field in both Szeged and Debrecen, Hungary were determined by the prevailing wind direction (Unger et al., 2010). Brandsma et al. (2003) found observations downwind from towns to contain approximately 1°C warming and findings have also been made in Baltimore, U.S. (Zhang et al., 2011) and in the Suzhou–Wuxi area, China (Zhang and Chen, 2014). Sea breezes can interact with the UHI and advect warm air inland, e.g. New York, U.S. (Gedzelman et al., 2003) and Osaka-Kyoto, Japan (Takane et al., 2013). Numerical modelling has shown the UHI in London (Bohnenstengel et al., 2011, Chemel and Sokhi, 2012) and Birmingham (Heaviside et al., 2015) to be displaced downwind. However, two limitations emerge from these studies. Firstly, a lack of urban meteorological networks prevent advection being evaluated at a high spatial and temporal resolution. Secondly, advection is not always explicitly decomposed, i.e. separated from the background UHI field.

A methodology to decompose these terms, revolving around this concept was developed by Heaviside et al. (2015). Using numerical modelling the dynamic nature of the UHI was reproduced, and the UHA separated as an individual component. The UHA methodology (described in detail in Chapter 2 and refined in Chapters 3 – 5) effectively calculates a time-mean UHI field for: (i) where all wind directions are considered; and (ii) where only a single wind direction is considered. Subtracting one from the other leaves the UHA field, free from any locally generated heat. Using this approach, Heaviside et al. (2015) modelled downwind warming up to 2.5°C from

Birmingham. However, as discussed in Chapter 4, the modelled UHA extent was overestimated as regional influences were not accounted for.

Although boundary-layer processes are well understood, there is a lack of horizontal quantification of surface level UHA. Considering over half the world's population are urban dwellers, and that UHA may extend into the immediate rural surroundings, this presents an ever-increasing impact on society. This is especially compounded when the combined effects of UHA and climate change on vulnerable citizens are considered. Contrarily, climate change could lead to a global reduction in conditions ideal for UHI development (McCarthy et al., 2010). Whilst the UHI effect is recognised to bias long-term climate records (Kalnay and Cai 2003, Parker and Horton 2005, Wickham et al., 2013), UHA reaching rural stations is not considered. The “circle of influence” around observations may explain this oversight, as it is currently thought to extend only 0.5 km (Oke, 2006). This distance is considerably smaller than typical urban scales. Therefore (detailed in Section 1.2), the purpose of this thesis is to provide an accurate quantification of UHA thus addressing a lack of knowledge in this field.

1.2. Overview of thesis data

Several state-of-the-art data sources are drawn upon in this thesis, a combination of land use and meteorological observations, outlined below. The exact use of each dataset is detailed in the methodology for each Chapter. Although the best available data was selected in this thesis, caution should be taken when interpreting results, arising from challenges in appropriately categorising highly-heterogeneous land

surfaces. For example, choice of the rural reference for UHI and UHA calculations may impact results. Additionally, model configurations represent surface conditions using generalised parameters that, whilst applicable for the resolution of the simulation, may not be directly comparable to the local, point observational scale.

High Density Measurements within the Urban Environment (HiTemp) – Data from an array of 25 Vaisala automatic weather stations located across Birmingham is used. The network is unique in its siting of the weather stations within the city, a challenge, that allows for spatial quantification of UHA in Chapter 2.

Met Office – Combined with the HiTemp network, four additional stations provide a spatial coverage across Birmingham at approximately 3 km² resolution. Additionally, access to the vast network (~200) of Met Office weather and climate stations around the UK allows for quantifying UHA from small urban areas in Chapter 3.

Normalized Difference Vegetation Index– A remotely sensed product, calculated as the difference between red and near-infrared light. This approximates vegetation density for a given area, and the inverse is used in this thesis to approximate urban fraction. This is a product commonly used in UHI studies (Chen et al., 2006), and allows categorisation of upwind urban fraction in Chapter 2, and input to the WRF model in Chapter 4.

Ordnance Survey VectorMap – Outlines of all individual buildings in the UK are used in Chapter 3, where land-use products such as NDVI are at resolutions too coarse to

support the analysis. This product is also used to calculate urban model parameters (e.g. height to width ratio) specific to Birmingham in Chapter 4.

Corine Land Cover – High resolution land-use covering Europe is used in Chapter 4 to update the default land use configuration in the WRF model. Corine allows three urban categories to be created, a significant improvement over the default model land use.

1.3. Thesis aim and objectives

Although the dynamic nature of the UHI has been acknowledged, little research into separating UHA from background temperatures has been conducted. Therefore, a significant research gap exists, important to address because UHA can impact on environments away from urban areas and to the accuracy of long-term climate records. The overall aim of this thesis is to quantify the effects of UHA. To support this aim, four specific objectives forming the main Chapters were created:

Chapter 2: Evaluate an existing UHA methodology and demonstrate the significance of UHA using a high-density urban observation network;

Chapter 3: Adapt the UHA methodology for wider use at any weather station and find if even small urban areas have a significant effect;

Chapter 4: Refine modelling limitations in the UHA methodology and remove regional heating effects using the Weather Research and Forecasting (WRF) model;

Chapter 5: Simplify complex UHA patterns arising from heterogeneous land use by through WRF semi-idealised modelling, and develop a simple statistical prediction model from the results.

An illustrative framework is provided in Figure 1.2 to demonstrate how each objective fits within the overall context of this thesis. Four main Chapters are presented in this thesis (2 – 5) that combine both observational analysis and numerical modelling. Chapters 2 and 3 apply and adapt an existing UHA methodology to air-temperature observations at two different urban scales. Chapter 1 analyses the newly available high-density urban observational network called BUCL (Birmingham Urban Climate Laboratory: Warren et al., 2017), located in Birmingham UK. Due to the novelty of this dataset, the city is adopted as the focal region of this thesis. Chapter 3 expands the UHA insight Chapter 2 provides by modifying the UHA methodology for use at any weather station. In particular, the UHA effect from small urban areas ($\sim 1 \text{ km}^2$), where UHIs still exist (Linden et al., 2015), are considered. This analysis is important because climate stations classified as “rural” are usually located near some form of settlement that may cause unwanted observational biases.

Chapter 4 uses the WRF numerical modelling to replicate the UHI field in Birmingham. The simulations are evaluated at a high spatial resolution ($\sim 3 \text{ km}^2$) using the BUCL network. UHA is calculated from the model output with a revised methodology to account for regional heat advection. Chapter 5 uses semi-idealised

WRF modelling to address the main issue when quantifying UHA. This is the complexity of urban land use (i.e. a given location may be influenced by UHA from multiple upwind sources). Chapter 5 models hypothetical, square cities varying in size and thus allowing UHA complexity to be reduced. The relationship between urban size and UHAI is examined and a simple statistical model to predict UHA without the need for computationally expensive models is developed. The final Chapter, 6, contains a synthesis of the main Chapters, limitations and overall conclusions.

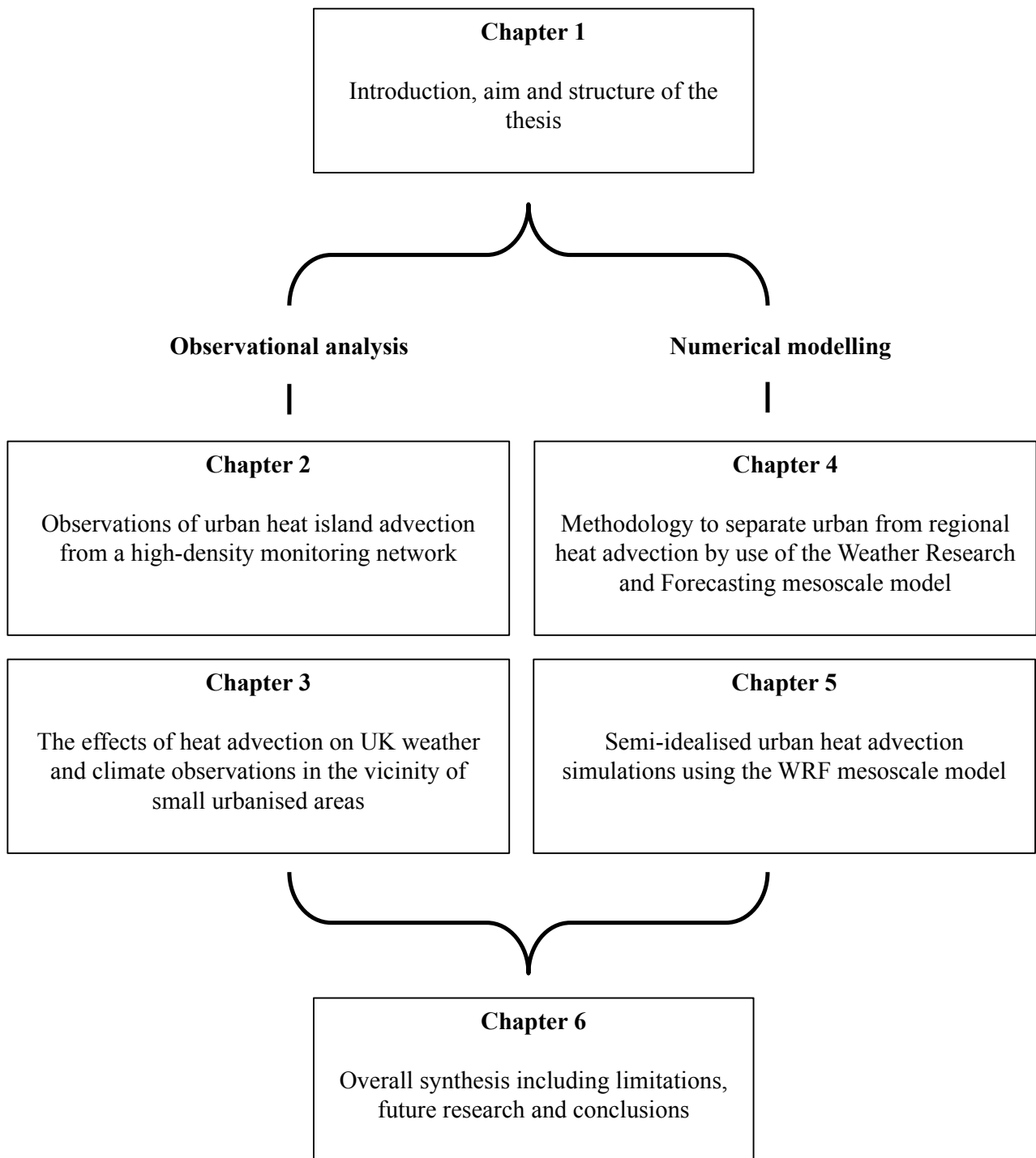


Figure 1.2. Overview of thesis structure.

Chapter 2.

Observations of urban heat island advection from a high-density monitoring network

This Chapter was published as:

Bassett, R., Cai, X., Chapman, L., Heaviside, C., Thornes, J.E., Muller, C.L., Young, D.T., Warren, E.L. (2016) ‘Observations of urban heat island advection from a high-density monitoring network’, *Quarterly Journal of the Royal Meteorological Society*, 142, pp. 2434–2441. doi:10.1002/qj.2836.

RB envisioned and conducted the data analyses, and wrote the paper. XC helped develop the concept. CLN, DTY and ELW collected the data. All contributed to proofing the manuscript.

2.1. Abstract

With 69% of the world's population predicted to live in cities by 2050, modification to local climates, in particular Urban Heat Islands, have become a well studied phenomenon. However, few studies have considered how horizontal winds modify the spatial pattern in a process named Urban Heat Advection (UHA) and this is most likely due to a lack of highly spatially resolved observational data. For the first time, this study separates the two-dimensional advection-induced UHI component, including its pattern and intensity, from the locally-heated UHI component using a unique dataset of urban canopy temperatures from 29 weather stations (3-km resolution) recorded over 20 months in Birmingham, UK. The results show that the mean contribution of UHA to the warming of areas downwind of the city can be up to 1.2°C. Using the inverse Normalized Difference Vegetation Index as a proxy for urban fraction, an upwind distance at which the urban fraction has the strongest correlation with UHA was demonstrated to be between 4 – 12 km. Overall, these findings suggest that urban planning and risk management needs to additionally consider UHA. However, more fundamentally, it highlights the importance of careful interpretation of long term meteorological records taken near cities when they are used to assess global warming.

2.2. Introduction

It is well documented that urban conurbations are warmer than their rural surroundings (Arnfield, 2003; Stewart, 2011). The resulting phenomenon, known as the urban heat island (UHI), develops through the absorption of energy within the built environment during the day, and subsequent release at night. The structure and UHI intensity (UHII) are controlled by the city form and are a direct result of anthropogenic modifications to the surface energy balance (Oke, 1973; Oke, 1982). These changes include: reduced sky view factor (fraction of visible sky from the ground) restricting longwave radiation loss at night; different thermal and reflective properties from construction materials; reduced evapotranspiration due to less vegetation; lower wind speeds (increased surface roughness); and anthropogenic heat from buildings, people and vehicles. Cities typically exhibit spatial variations in UHII that can be broadly classified into Local Climate Zones (LCZ), which are effectively determined by land use (Stewart and Oke, 2012). Alternatively, land cover products, for example vegetation indices derived from remote sensing, can be used to assess UHII (Chen et al., 2006). The largest UHIIs are generally found in the central business districts under clear skies and calm winds, whereas more turbulent conditions increase mixing and weaken UHIIs.

The significance of the UHI effect becomes increasingly apparent by studying interactions with the health and wellbeing of the local population. For example, in England and Wales, 81.5% of the population are urbanised (ONS, 2013) and with cities unable to cool down as efficiently as their surroundings, there is a growing heat-health and infrastructure risk (Grimmond et al., 2010; Thornes, 2015). UHI impacts

are further compounded during heatwave events. It is estimated that the 2003 summer heatwave led to as many as 70,000 excess deaths throughout Europe (Robine et al., 2008), 2,000 of which were in England (Johnson et al., 2005). Climate projections (e.g. UKCP09: <http://ukclimateprojections.metoffice.gov.uk/>) indicate that heatwaves will become an increasingly regular feature of the UK climate before the end of the century, underlining the need for increased mitigative action to protect vulnerable populations and critical infrastructure (Chapman et al., 2013). Until recently, a lack of external influence has left urban planning to habitually follow historical architecture, based on local climate and culture (Grimmond et al., 2010). However, with a changing climate, historical designs may no longer be adequate to cope with an increase in excess heat, particularly during heatwaves. In response cities are progressively developing adaptation strategies to cope with the effects of excess heat on health and infrastructure. However to efficiently target strategies and resources (e.g. green infrastructure), a complete picture of how UHIs develop temporally and spatially is needed.

Lowry (1977) conceptually proposed that the “environ” or area of urban influence on surrounding rural temperatures is not stationary and is in fact determined by weather type. Despite the abundance of studies into the UHI effect (Arnfield, 2003; Stewart, 2011) and the impact of urbanisation on climate (Kalnay and Cai, 2003; Zhou et al., 2004), few studies have considered (or assume it not to be significant) how horizontal winds modify the urban environ through the advection induced UHI component - a process named Urban Heat Advection (UHA).

Oke (1976) highlighted the distinction between processes in the urban canopy layer (UCL) and urban boundary layer (UBL). The UCL extends from the surface to the mean building roof level and within the UCL, canopy-scale processes will influence local UHI values significantly. Whilst winds could effectively move or advect heat (and moisture) horizontally within the UCL (from micro- to neighbourhood-scale), other UHA processes may occur in the UBL (from neighbourhood- to city-scale). Heat released from urban facets (building surfaces, roads etc.) is transferred (through the turbulent roughness sub-layer) from the UCL into the UBL aloft. The buoyant, rising air (forming a thermal dome) over the urban environment at a city scale creates a pressure field that draws in rural air (Barlow, 2014). This can lead to 3D circulations in the form of surface convergence over the city and divergence aloft (Bornstein and Johnson, 1977; Hildebrand and Ackerman, 1983; Hidalgo et al., 2010). If a horizontal wind is present, and prevails over local circulations, a thermal plume from the UCL becomes vertically mixed and subsequently advected downwind (Clarke, 1969; Oke, 1982). Observations during the METROMEX field campaign indicated that advection modulates downwind sensible heat fluxes (Ching et al., 1983; Godowitch et al., 1987) and urban plumes were shown to typically extend 10 – 15 km downwind (Dirks, 1974; Wong and Dirks, 1978). Between the neighbourhood and city scales, the heterogeneous nature of urban environments acts to create a series of overlapping local internal boundary layers (Garratt, 1990; Barlow, 2014). Over a warmer UCL, heat will be transferred upward from the UCL to the UBL, whereas over a cooler UCL, downward heat flux is likely to occur. However, little is known about the mechanisms of the two processes, particularly the latter, i.e. how much heat from these urban plumes are mixed downwards into the UCL to warm the air underneath. Furthermore the vertical scale of the UBL varies diurnally. A well-developed UBL

during the day (1–2 km) will allow plumes to spread high into the UBL. However at night the UBL becomes typically limited to a few hundred meters at night, capped by stable air above. On this basis at night, heat will not be dispersed vertically as far from the UCL at night as possible during the day.

Prior investigations into UHA have mostly been attempted based on temperature data collected from two related methodologies: mobile sensors traversed along (Brandsma and Wolters, 2012; Unger et al., 2010) and fixed sensors at weather stations in the region (Chandler, 1965; Brandsma et al., 2003; Haeger-Eugensson and Holmer, 1999; Gedzelman, 2003; Takane et al., 2013). In addition to presenting the spatial patterns of UHI, not UHA, a limitation of these methodologies is a general inability to demonstrate the high-resolution two-dimensional structure of UHA with any statistical confidence due to either temporal or spatial limitations of the chosen approach. Typically, the method of using mobile sensors along transects suffers from short duration of measurement, whereas the method of using fixed sensors at stations is constrained by the small number of stations. For example the METROMEX campaign demonstrated wind modifications to the UHI (Ackerman et al., 1978); however the UHA signals were weak due to the coarse spatial resolution (horizontal resolution of about 13 km) and because not all observations were within the UCL. Given these constraints, recent attempts to quantify UHA have focussed on modelling approaches to enable the simulation of spatial dimensions that observations have, to date, been unable to capture (e.g. Bohnenstengel et al., 2011; Chemel and Sokhi, 2012, Heaviside et al., 2015; Zhang et al., 2009). Remote sensing techniques have also been increasingly used to capture the spatial nature of surface UHI (Tomlinson et

al., 2012; Tomlinson et al., 2013). However, satellite derived surface UHIs are not always directly comparable with UCL air temperature UHI (Azevedo et al., 2016).

Fundamentally, a lack of high quality dense urban networks has restricted the study of UHA features (Muller et al., 2013), largely due to the difficulty and cost of siting and maintaining urban networks (Chapman et al., 2014). This paucity of data has resulted in previous observational studies relying on a transect approach and modelling approaches limited by a lack of evaluation data. To overcome this challenge this paper presents the two-dimensional pattern and intensity of the advection-induced UHI component, UHA, under various wind speeds and directions at the city scale using a new high-resolution urban meteorological observational dataset. In doing so, a quantification of UHA is achieved which can be used strategically to mitigate heat impacts of upwind local climate on downwind populations. It also enables a critical view of whether rural reference stations commonly used in UHI studies are truly representative of the background climate due to possible contamination by UHA, which has potential implications on the accuracy of temperature records used for analyses of global warming.

2.3. Methods and Background

2.3.1. Study Area and Data

A new network of automatic weather stations – the Birmingham Urban Climate Laboratory (BUCL) has been installed across Birmingham (52.5°N, 1.9°W, Figure 2.1), the UK's second largest city with 1.1 million inhabitants, specifically to study city scale weather processes using stations within the UCL. The BUCL network consists of two arrays of weather monitoring equipment and this study utilises data from the coarse array of 25 automatic weather stations (Vaisala WXT520, accurate to $\pm 0.3^{\circ}\text{C}$ at 20°C ; Vaisala, 2012) that records minute averages of air temperature, relative humidity, atmospheric pressure, wind speed and direction, and precipitation at 3 m above ground. Guidelines on siting instruments in urban areas (Oke, 2006) were adhered to where possible when the network was installed with most stations sited within school grounds. A full description of the network can be found in Chapman et al., (2014) and is further documented via a new urban metadata protocol devised during the deployment (Muller et al, 2013). Observations are also taken from four UK Met Office weather stations accessed through the British Atmospheric Data Centre: Paradise Circus, Winterbourne, Elmdon and Coleshill. In total 29 stations provide coverage across Birmingham at approximately 3-km resolution (Table 2.1.; Figure 2.1). To represent an unobstructed synoptic flow, wind data are taken from Coleshill, at a height of 10 m, due to its location outside the city. Data for this study were obtained from 1st January 2013 to 1st September 2014. The network and data undergo a rigorous process of quality assurance and control. Full descriptors of the data quality

assurance procedures are documented in Warren et al. (2016) complete with repository links directly to the data and associated metadata.

In addition to the meteorological data, the normalized difference vegetation index (NDVI), a readily available MODIS product already used in UHI studies (e.g. Chen et al., 2006), is used to indicate urban fraction across Birmingham. The mean NDVI is calculated from averaging a 250 m resolution January and July 2014 (16 day composite) image to account for seasonality in leaf coverage. From herein the NDVI data, normalised to between 0 (rural) and 1 (urban), is referred to as urban fraction (Ufrac).

Table 2.1. Station metadata. Local Climate Zones (LCZ) are assigned using the classification by Stewart and Oke (2012). Urban fraction is calculated as the mean pattern within a 1-km radius of each station.

Station	Network	Latitude	Longitude	Altitude (m)	Urban fraction (1-km radius)	LCZ
W001	BUCL	52.57	-1.84	119	0.36	Scattered Trees
W002	BUCL	52.39	-2.06	187	0.23	Scattered Trees
W003	BUCL	52.54	-1.96	104	0.38	Scattered Trees
W004	BUCL	52.37	-1.92	202	0.16	Scattered Trees
W005	BUCL	52.44	-1.86	158	0.49	Open Low Rise
W006	BUCL	52.50	-1.92	132	0.60	Open Low Rise
W007	BUCL	52.49	-1.90	134	0.83	Compact Mid Rise
W008	BUCL	52.44	-1.97	168	0.45	Open Low Rise
W009	BUCL	52.47	-1.86	123	0.70	Compact Mid Rise
W010	BUCL	52.48	-1.93	157	0.61	Open Low Rise
W011	BUCL	52.39	-2.00	190	0.51	Open Low Rise
W012	BUCL	52.42	-1.91	134	0.50	Open Low Rise
W013	BUCL	52.47	-1.90	125	0.82	Compact Mid Rise
W014	BUCL	52.42	-1.84	141	0.50	Open Low Rise
W015	BUCL	52.51	-1.83	98	0.68	Heavy industry
W016	BUCL	52.45	-1.82	130	0.53	Open Low Rise
W017	BUCL	52.48	-1.79	101	0.52	Open Low Rise
W018	BUCL	52.49	-1.81	100	0.48	Open Low Rise
W019	BUCL	52.50	-1.87	110	0.74	Open Mid Rise
W020	BUCL	52.53	-1.85	140	0.55	Open Low Rise
W021	BUCL	52.56	-1.89	173	0.51	Open Low Rise
W022	BUCL	52.41	-1.95	150	0.47	Open Low Rise
W023	BUCL	52.56	-1.79	122	0.32	Open Low Rise
W026	BUCL	52.46	-1.93	150	0.41	Open Low Rise
W027	BUCL	52.44	-1.89	158	0.49	Open Low Rise
Coleshill	Met Office	52.48	-1.69	96	0.39	Scattered Trees
Elmdon	Met Office	52.45	-1.74	96	0.61	Open Mid Rise
Paradise Circus	Met Office	52.48	-1.90	139	0.90	Compact High Rise
Winterbourne	Met Office	52.46	-1.93	140	0.40	Open Low Rise

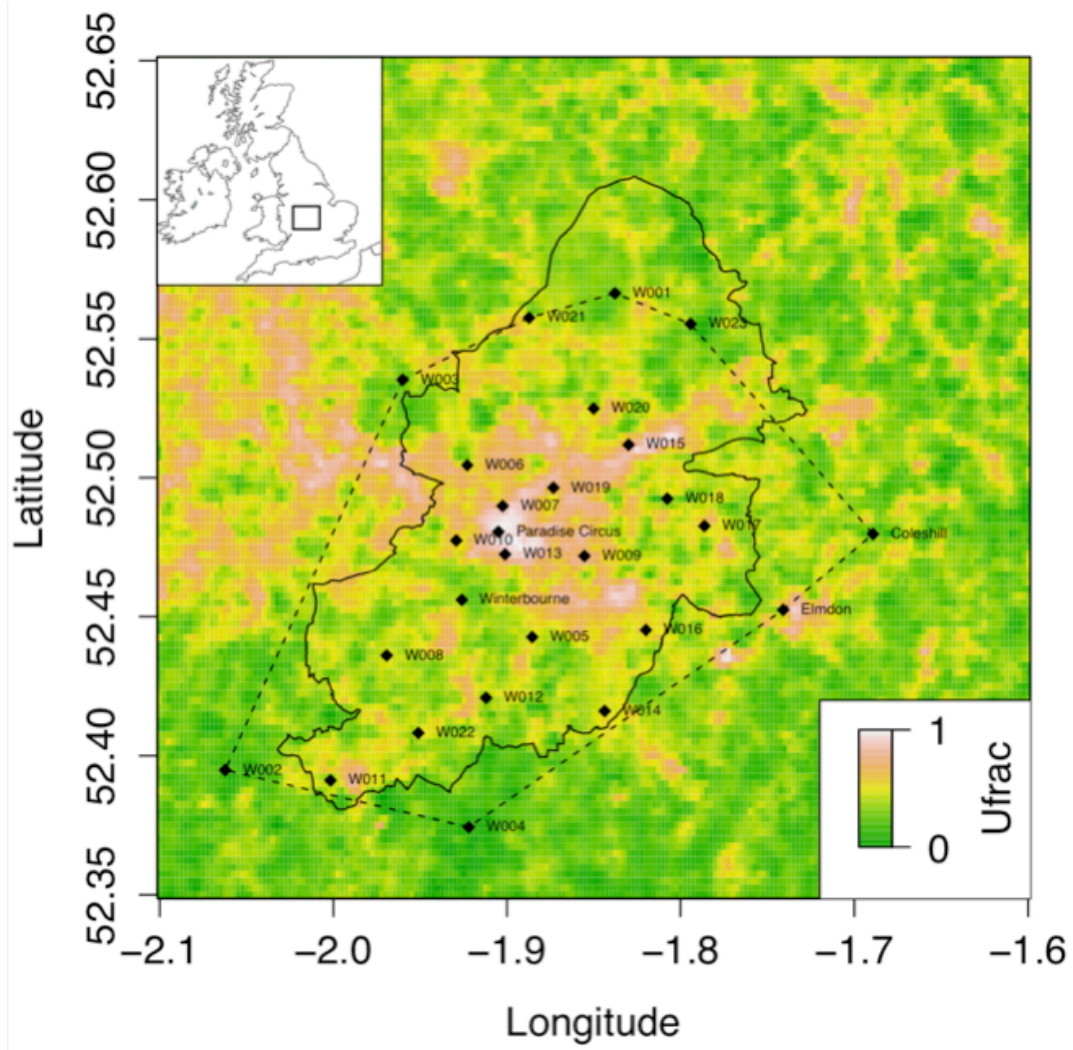


Figure 2.1. Study area and location of BUCL stations, and urban fraction (Ufrac): ranging from 0 (rural) to 1 (urban). Birmingham's administrative region is outlined with a solid border. The dashed border indicates the outer boundary of observations.

2.3.2. Urban Heat Island

UHII is traditionally calculated by taking the temperature difference between an urban and a rural reference station (Arnfield, 2003; Stewart, 2010). However, this approach is challenged by the fact that rural reference stations near cities may be influenced by UHA if they are located within the urban environ as demonstrated conceptually by

Lowry (1977) and directly in the region of study through modelling (Heaviside et al., 2015). To minimise this influence by UHA, a new concept of ‘inverse UHI’ is introduced, which adopts temperatures at a central urban station (T_u) as reference. The Met Office station at Paradise Circus is chosen to represent the central urban station (T_u) due to its location within the centre of Birmingham and is the station where the highest temperatures have been identified in previous studies (Heaviside et al., 2015; Tomlinson et al., 2012; 2013). The hourly temperature difference (ΔT_{i-u}) between each station in the network (T_i , where i denotes the i -th station) and the central urban station (T_u) is calculated for the data period (Equation 1):

$$\Delta T_{i-u} = T_i - T_u. \quad (1)$$

The value of this temperature difference (ΔT_{i-u}) will be mostly negative as the central urban station (T_u) is likely to be higher than other stations in the network (T_i). Temperature data are split equally into three wind speed groups, WG1 ($< 2 \text{ m s}^{-1}$), WG2 ($2 - 3 \text{ m s}^{-1}$) and WG3 ($> 3 \text{ m s}^{-1}$). Only night-time observations (based on daily sunset and sunrise times) with low cloud cover ($< 4/8$ oktas) are included, to focus on conditions most favourable for strong UHI development. Classifying by wind speed, cloud cover and night-time, groups the data into conditions of similar stability (neutral and stable) as per Pasquill-Gifford stability classes (Pasquill and Smith, 1983, Tomlinson et al., 2012). The mean temperature difference within each wind speed group is taken ($\overline{\Delta T_{i-u}}$). The assumption is made that the mean difference between the i -th station and central urban station (T_u) remains constant within these stability classifications, thereby compensating for some stations not being temporally homogeneous. In order to interpret the intensity of the mean temperature difference

$\overline{(\Delta T_{i-u})}$ as the positive UHII, the minimum temperature difference in each wind speed group is subtracted from each station. The resulting positive UHII is denoted by $\overline{\Delta T^+}$.

2.3.3. Urban Heat Advection

As discussed in section 1, the environ (or area) of influence exerted by a city on its surroundings varies with prevailing conditions. Lowry's (1977) working model (Equation 2) states the temperature (T, or other element) at a given station x , time t , and weather type x is a sum of the background temperature (B), and deviation caused by landscape (L, e.g. relief) and urban effects (U). If landscape effects are comparable at two given stations (rural and urban), any temperature difference can be attributed to urban effects. However, in practice, a given rural station may be influenced by the urban environ under particular weather type (or wind direction), and therefore the temperature difference is not an accurate reflection on UHII. Lowry's (1977) model is therefore unable to distinguish between urban effects, i.e. heat created locally or advected from upwind. As such, Lowry's (1977) concept should be enhanced through separating urban effects (U) at a given location into contributing terms: local UHI, and additional UHA (Equation 3). Separating these terms however is complicated by the fact that observed data combines information on both processes.

$$T_{i,t,x} = B_{i,t,x} + L_{i,t,x} + U_{i,t,x} \quad (2)$$

$$T_{i,t,x} = B_{i,t,x} + L_{i,t,x} + (UHI_{i,t,x} + UHA_{i,t,x}) \quad (3)$$

In order to separate UHA from UHI, a methodology used in WRF modelling of the August 2003 heatwave (Heaviside et al., 2015) is adapted for the BUCL observation network. Here, the time-mean temperature field is subtracted from the averaged modelled field for each of four specified wind directions at 90 degree intervals (θ : northeast (NE), southeast (SE), southwest (SW) and northwest (NW)). A hypothetical example is presented in Figure 2.2, whereby this methodology decomposes the UHI into the time-mean component (predominantly dependent of local land surface) and a horizontally advected component. To calculate the mean UHA intensity (UHAI) at the i -th station in the BUCL network, $\overline{T_{UHA(i)}^{(\theta)}}$, the temperature field $\overline{\Delta T_{i-u}}$ across all wind directions is subtracted from the mean temperature difference for a given wind direction sector (θ), $\overline{\Delta T_{i-u}^{(\theta)}}$, shown in Equation 2. An example calculation is presented in Figure 2.3a. To account for any directional biases within the data, the temperature field across all wind directions $\overline{\Delta T_{i-u}}$ used in Equation 4 is calculated by taking the mean of the mean temperature difference of each wind sector, $\overline{\Delta T_{i-u}^{(\theta)}}$, Equation 5.

$$\overline{T_{UHA(i)}^{(\theta)}} = \overline{\Delta T_{i-u}^{(\theta)}} - \overline{\Delta T_{i-u}} \quad (4)$$

$$\overline{\Delta T_{i-u}} = \frac{(\overline{\Delta T_{i-u}^{(NE)}} + \overline{\Delta T_{i-u}^{(SE)}} + \overline{\Delta T_{i-u}^{(NW)}} + \overline{\Delta T_{i-u}^{(SW)}})}{4} \quad (5)$$

By calculating the mean UHAI for a given wind sector, $\overline{T_{UHA(i)}^{(\theta)}}$, the positive value is interpreted as half the advection-induced UHI component and negative value is half the advection-induced UHI component from the opposing wind direction (Figure 2.2,

illustration [C]). As such UHAI can be interpreted as the difference between these two values (n.b. upwind and downwind values will swap with opposing wind directions), and free from background, landscape and UHI effects. Whilst this approach distinguishes between each component in Lowry's (1977) model, it is unable to determine the process and scale at which UHA occurs (i.e. horizontally through the UCL or downwards mixing from the thermal plume), as vertical observations are not available.

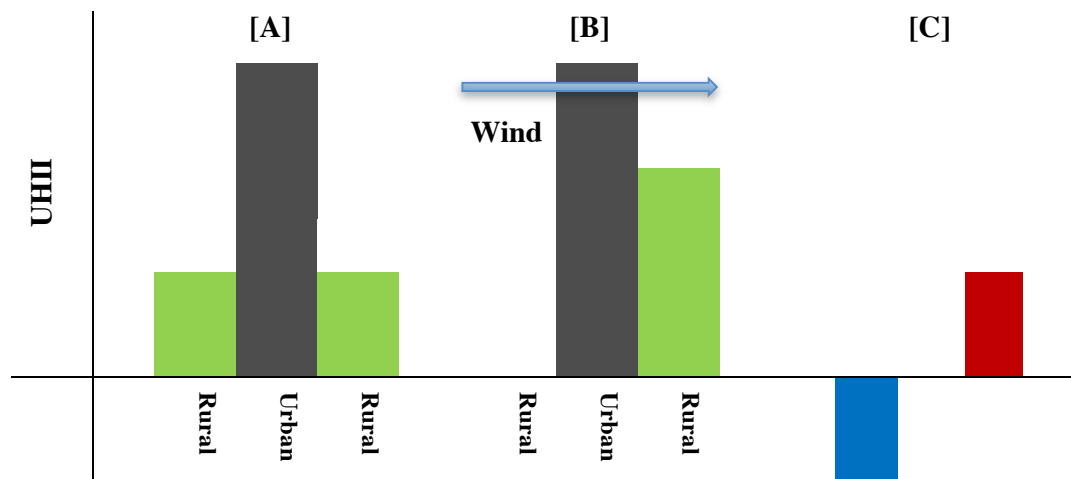


Figure 2.2. Hypothetical advection calculation (adapted from Heaviside et al., 2015). Illustration [A] signifies a typical time-mean UHII, assuming that the advection-induced warming is symmetric with respect to two wind directions under the same wind speed and stability group. Therefore, both rural columns will be warmed and the intensity of the positive bar over the right rural area in [A] is effectively a half of the UHII due to advection in [B]. Illustration [B] considers a single wind direction, left to right, and this hypothetically means no heat is transferred upwind from the urban to left rural column (n.b. the rural background temperature, created by local land use, does not decrease). Illustration [C] is derived by subtracting [A] from [B], i.e. removing the locally heated UHI component (the middle positive bar) and separating

the advection-induced component. The negative value in [C] is linked to UHA from the opposing wind direction. The difference between positive and negative bars in [C] is interpreted as the UHA signal.

2.3.4. Urban Heat Advection distance

To investigate the spatial scale at which UHA occurs, concentric annuli (*ann*) at 3-km intervals extending 0 – 3, 4 – 6, 7 – 9, 10 – 12 and 13 – 15 km from each station (*i*) are overlaid onto the Ufrac data (Figure 2.3). Within each of the five annuli, the mean urban fraction is calculated, referred to as $Ufrac_{(i,d)}^{(ann)}$, where *d* is the index of the annuli (i.e. *d*=1: 0 – 3 km; *d*=2: 4 – 6 km; ... *d*=5: 13 – 15 km). Each annulus is further split by the four wind direction sectors (*θ*) to create four arcs, and for each *θ*, the mean urban fraction is calculated, referred to as $Ufrac_{(i,d)}^{(θ)}$. A similar methodology used to calculate the mean UHAI for a given wind sector ($\overline{T_{UHA}^{(θ)}(i)}$) is then applied to the Ufrac data. Namely, at a given station *i* and distance *d*, the Ufrac annuli $Ufrac_{(i,d)}^{(ann)}$ is subtracted from the Ufrac arc $Ufrac_{(i,d)}^{(θ)}$ (Equation 6):

$$\overline{\Delta Ufrac_{(i,d)}^{(θ)}} = \overline{Ufrac_{(i,d)}^{(θ)}} - \overline{Ufrac_{(i,d)}^{(ann)}} \quad (6)$$

This quantity, $\overline{\Delta Ufrac_{(i,d)}^{(θ)}}$, reflects the directional inhomogeneity, or variability of urban land use, of the *d*-th annulus, i.e. whether the urban fraction value in a given direction is higher or lower than the mean of all directions. A hypothetical calculation is shown in Figure 2.3a. In order to generate statistically meaningful correlations

between UHAI and directional variability of upwind urban fractions, stations in the network with little Ufrac variation between arcs (< 0.1 range) are excluded from the analysis. Whilst the station data are grouped for similar stability, there are still differences in the mean UHII and UHAI for each wind direction explained by meteorological differences within wind groups that cannot be accounted for. For example the data are categorised into less than 4/8 oktas, however within this group winds from the SE may have higher percentage of completely clear skies. Finally, to account for directional differences, normalised UHII and UHAI values for each wind direction are taken.

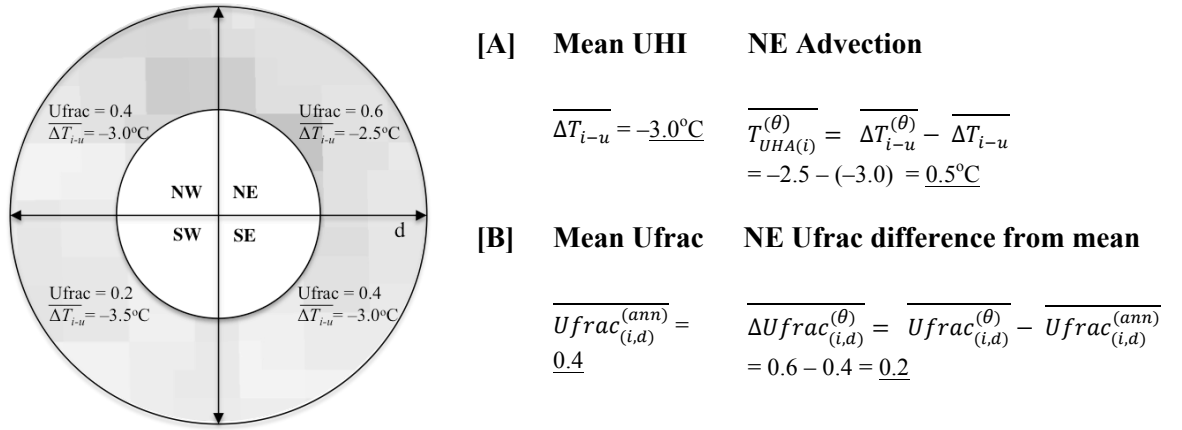


Figure 2.3. Hypothetical explanation of how [A] UHAI ($\overline{T_{UHA(i)}^{(\theta)}}$) and [B] Ufrac difference from the mean ($\overline{\Delta Ufrac_{(i,d)}^{(\theta)}}$) are calculated under a NE wind for a given station (i) located in the centre of the crosshairs. The temperature difference ($\overline{\Delta T_{i-u}^{(\theta)}}$) has a smaller intensity from the NE (more urbanised sector), i.e. the actual temperature is closer to the urban reference, than SW (less urbanised sector).

2.4. Results and Discussion

2.4.1. Urban Heat Island

Ordinary kriging (R ‘kriging’ package version 1.1) is used to interpolate the positive UHII ($\overline{\Delta T^+}$) for each wind speed group (Figure 2.4). Interpolation predicts temperatures at unmeasured locations using weighted averages from surrounding stations. Kriging-based approaches to spatial interpolation have been used in several UHI studies (e.g. Knight et al., 2010; Szymanowski and Kryza 2009; Unger et al., 2010; Azevedo et al., 2016). As per Knight et al., (2010) the analysis is confined to the outer boundary of observations and only used for visualisation. A large mean night-time UHII under low cloud cover up to 4.3°C is observed across the region in WG1. Cool spots are found to the north of the city (see top of Figure 2.4 WG1), that corresponds to Sutton Park (a large semi-rural park on the periphery of the city), and directly to the south in notably green urban areas within the city. Both areas are approximately 2°C cooler and are marked by "temperature cliffs": a sharp change in temperatures over short distances. A decrease in the maximum UHII is found when wind speed increases (WG2: 3.0°C and WG3: 1.3°C) and spatially the heat becomes more confined to the city centre. The observed UHII spatial pattern is found to be similar to satellite and modeling research in Birmingham (Heaviside et al., 2015; Tomlinson et al., 2012; 2013). However UHIIs vary between these methodologies due to inherent differences between surface and UCL temperatures.

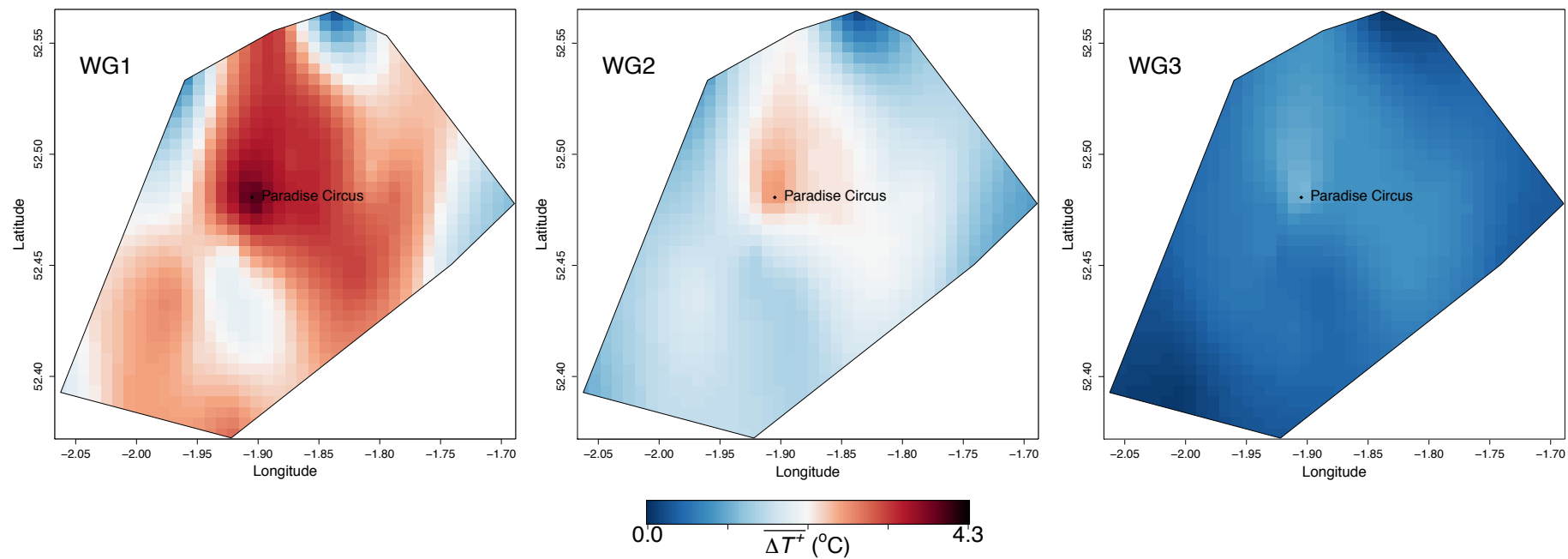


Figure 2.4. Spatial interpolation (kriging) of the nocturnal positive UHI ($\overline{\Delta T^+}$) under low cloud cover in three wind speed groups: WG1 ($< 2 \text{ m s}^{-1}$), WG2 ($2 - 3 \text{ m s}^{-1}$) and WG3 ($> 3 \text{ m s}^{-1}$). The analysis is limited to the outer boundary of observations.

2.4.2. Urban Heat Advection

The resulting mean UHAI ($\overline{T_{UHA(i)}^{(\theta)}}$) is shown spatially for each wind speed group and sector in Figure 2.5. The results show that a significant upwind, downwind temperature difference of up to 1.2°C exists across Birmingham (WG2). The NE and SW cases show a clear downwind warming, present in each wind group, with a transition from a positive to negative warming located over the city centre. The NW case has warming and SE cooling present over the whole domain, in all wind groups. Whilst warming is still most pronounced downwind in the NW case, the cross-domain warming could be accounted for by urbanisation northwest of Birmingham (see Ufrac in Figure 2.1). Additionally as the analysis is confined around the city, there are limitations with kriging or any spatial interpolation technique at the edge of a domain. Spatially the results have demonstrated the urban influence, through UHA, to extend outside the city limits. In effect the observed UHA patterns match the hypothetical calculation (Figure 2.2) and substantiate Lowry's (1977) dynamic urban environ zone.

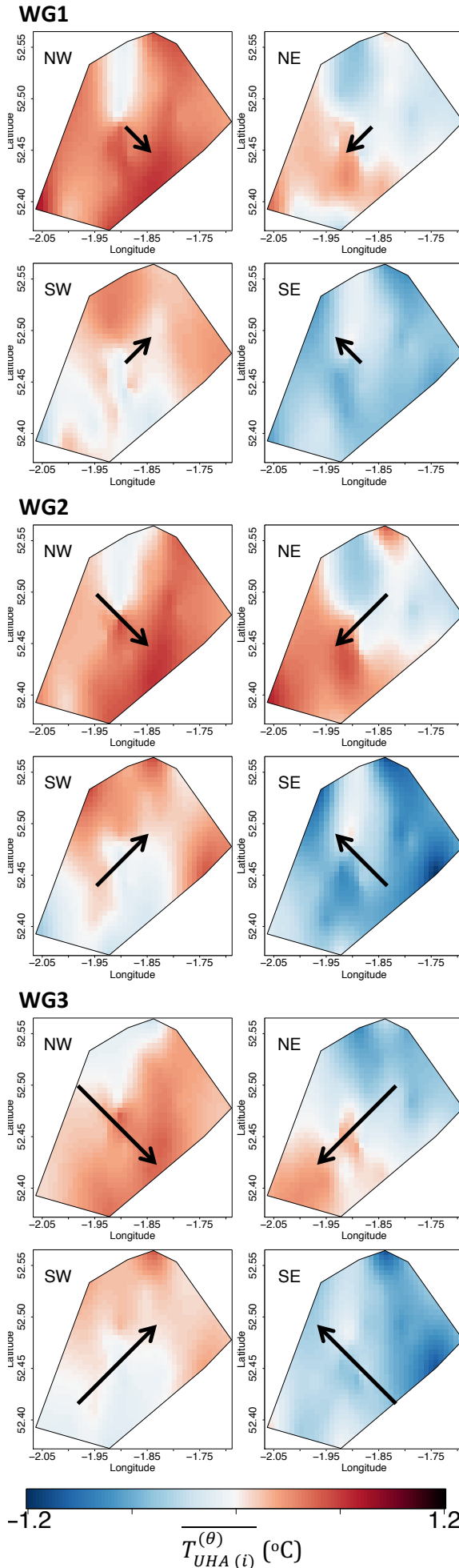


Figure 2.5. Spatial interpolation (kriging) of UHAI $\overline{T_{UHA(i)}^{(\theta)}}$ in three wind speed groups: WG1 ($< 2 \text{ m s}^{-1}$), WG2 ($2 - 3 \text{ m s}^{-1}$) and WG3 ($> 3 \text{ m s}^{-1}$). Within each wind speed group, each box represents a wind direction sector (θ : NW, NE, SE, SW).

In order to quantify the mean UHAI across all stations, the data are split into two groups of stations that are considered to be upwind or downwind of the city centre. The SW and NE wind sectors, as indicated in Figure 2.1, are used for this analysis due to the increased number of stations in this direction across the city (the administrative outline of the city). This allows for the analysis of UHA to contain both urban and rural stations that would not be possible in the other direction. The calculated mean UHAI ($\overline{T_{UHA(i)}^{(\theta)}}$) at each station in the SW and NE groups are combined (i.e. both groups show positive UHA downwind) for each wind speed group (Figure 2.6). For WG1 a mean UHAI across all stations of 0.2°C is observed. As wind speeds increase (WG2) the mean UHAI rises to 0.4°C. A further increase in wind speed (WG3) reduces mean UHAI to 0.3°C. It is also found that for WG2, UHAI reaches 0.5°C or higher at 25% of stations, up to a maximum of 1.2°C. A maximum UHAI occurring in WG2 could be explained by a reduced capability to advect heat with lower wind speeds, and less heat to advect from a smaller UHII at high wind speeds. This finding is similar to Brandsma et al. (2003), who found peak UHAI to occur at medium wind speeds between 2.2 and 3.9 m s⁻¹.

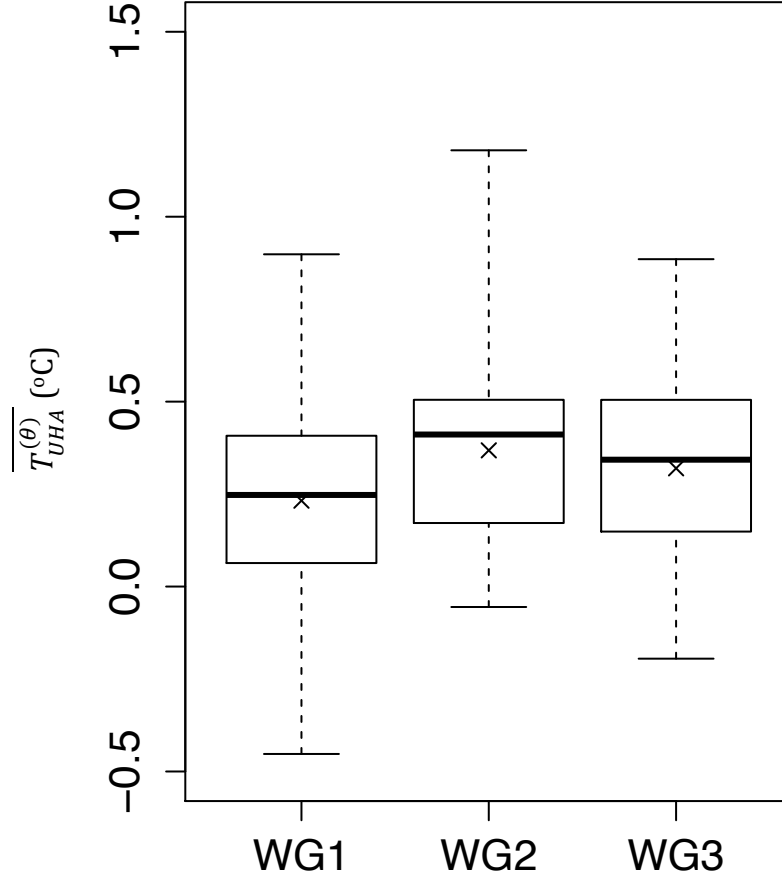


Figure 2.6. UHAI Box-and-whisker plot ($\overline{T_{UHA}^{(\theta)}}$) using SW and NE wind sectors, in three wind speed groups: WG1 ($< 2 \text{ m s}^{-1}$), WG2 ($2 - 3 \text{ m s}^{-1}$) and WG3 ($> 3 \text{ m s}^{-1}$). The x marker signifies the mean.

The results show that UHA is a significant phenomenon present in the UCL and is not limited to a thermal plume in the UBL (Clarke, 1969; Dirks, 1974; Wong and Dirks, 1978; Oke, 1982). As such this analysis shows that the temperature of a given location is significantly affected by adjacent urban fraction. Additionally, because the UHA components presented in Figures 2.5 and 2.6 are temporally averaged over 20 months, it is suggested that UHAI could be higher under certain meteorological conditions, for example a heatwave (Heaviside et al., 2015). To place this additional downwind warming in context, a degree temperature difference has the potential to

increase mortality by 2 % for every degree rise over 17.7°C in the West Midlands (Hajat et al., 2014; Heaviside et al., 2016).

However whilst UHA is successfully separated from the UHI signal and quantified for Birmingham, these observations are unable to differentiate UHA processes. Further work is needed to explore whether winds move heat horizontally through the UCL, or if urban heat is mixed into the UBL, and then a proportion brought back to the UCL downwind.

2.4.3. Urban Heat Advection distance

In order to show the relationship between urban fraction the two urban effects UHI and UHA, Pearson's correlation coefficient is firstly conducted across all stations between the Ufrac annuli $\overline{Ufrac_{(i,d)}^{(ann)}}$ and normalised UHI $\overline{(\Delta T_{i-u})}$, ($i=1, \dots, N_{station}$; $d=1$: 0 – 3 km; $d=2$: 4 – 6 km; ... $d=5$: 13 – 15 km) Figure 2.7a. The strongest relation is found at the 0 – 3 km urban fraction range in all wind speed groups. The strength of the correlation is shown to decline quickly thereafter with distance. For WG1 and WG2 groups the correlation is only significant at the 0.01 level at 0 – 3 km distance. Correlations significant at the 0.01 level extend to 7 – 9 km under WG3. These results indicate that the UHI at each site is strongly related to the local land use up to 3 km for WG1 and WG2 and 9 km for WG3. This is in line with our prior understanding that (excluding meteorological factors) UHIs are predominantly controlled by local land use.

To determine the distance from which the additional UHA term may influence temperature at a station, the same correlation analysis is conducted between the Ufrac arcs ($\overline{\Delta Ufrac^{(\theta)}_{(i,d)}}$) and mean UHAI ($\overline{T^{(\theta)}_{UHA(i)}}$), Figure 2.7b. In this analysis data from all wind sectors (θ) are combined. No correlations significant at the 0.01 level are found closest to the stations (0 – 3 km) in any wind speed groups. This corresponds to how UHA has been defined (see Figure 2.2) and confirms that the local UHII has been effectively removed. The correlation strength increases and is significant to the 0.01 level for all wind speed groups at distances 4-6 km from the stations. This indicates the UHA distance at which Ufrac begins to influence UHA. For WG1, correlations are strongest at 4-9 km from the stations, i.e. UHA advection from distant sources will be diminished. For WG2, the highest correlation is at 7 – 9 km and it remains high until 10 – 12 km. For WG3, the highest correlation is shifted to 13 – 15 km, i.e. increased wind speed transports heat further. As such each wind speed group has its own characteristic UHA distance, the higher the wind speed, the larger the distance. With peak UHAI observed in WG2, the UHA distance analysis shows that the downwind UCL warming from the city in this group will be experienced in rural areas up to 12-km away. These distances are calculated based on the mean UHAI pattern, therefore on an individual night these distance would be variable. For example modelling the UHI of a significantly larger city, London, has shown UHA can extend as far as 40-km downwind (Bohnenstengel et al., 2011).

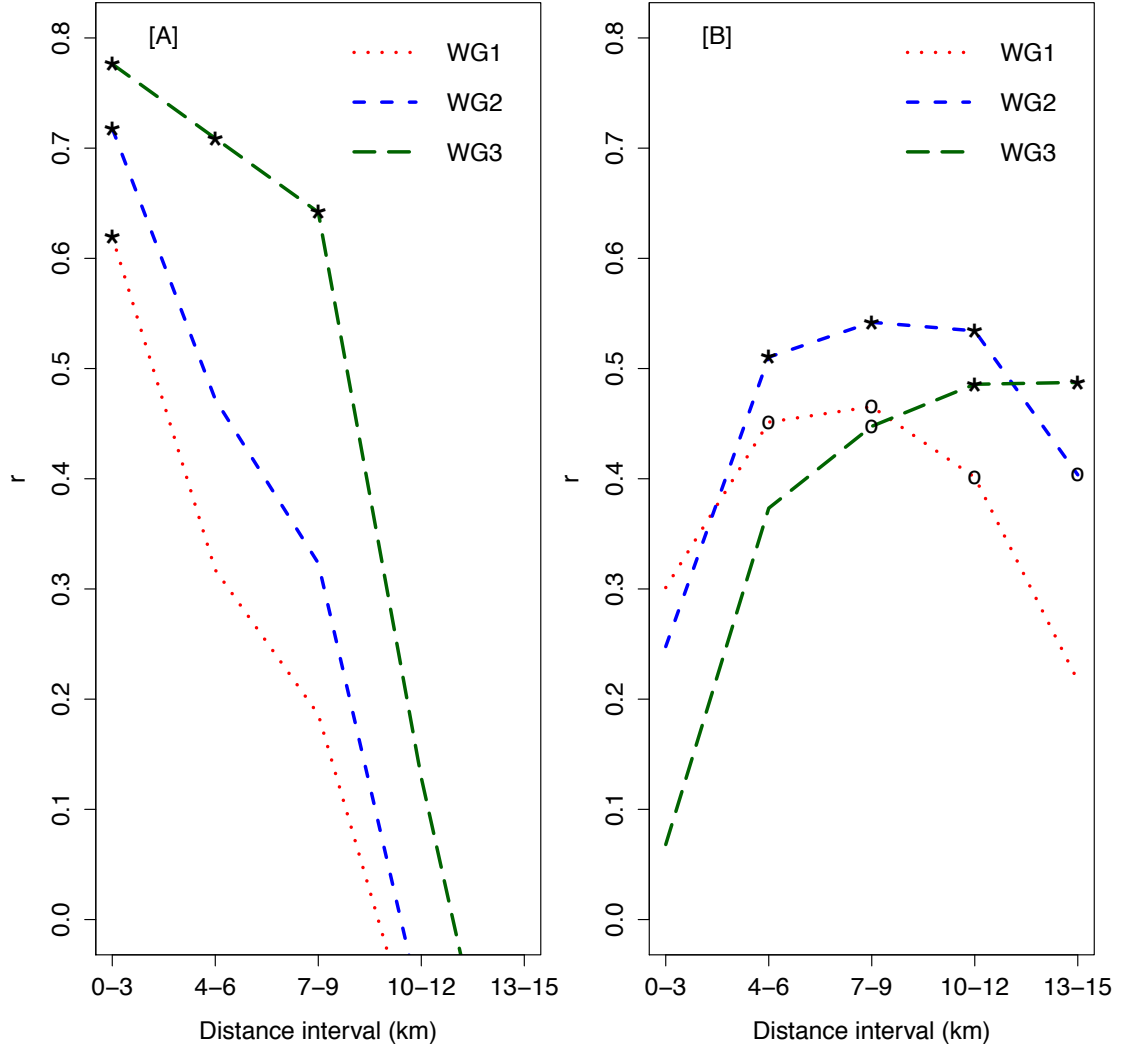


Figure 2.7. Pearson's correlation coefficient (r) between [A] UHI (ΔT_{i-u}) and Ufrac annuli ($Ufrac_{(i,d)}^{(ann)}$), [B] UHAI ($T_{UHA(i)}^{(\theta)}$) and Ufrac arcs ($\Delta Ufrac_{(i,d)}^{(\theta)}$) at 3-km intervals from the stations. * correlation is significant at the 0.01 level.

2.5. Conclusions

The complex nature of urban environments provides intrinsic challenges in quantifying UHA. To address this, a new high-density network of urban weather stations (BUCL) in Birmingham has been used to quantify both UHI and UHA at a sub-city scale. The unique spatial and temporal aspects of this dataset has shown

Birmingham to exhibit a large mean nocturnal UHII of up to 4.3°C under low wind speeds and clear skies over 20 consecutive months.

Overall, using the novel methodology outlined, a clear spatial pattern of long-term averaged UHAI (the advection-induced UHI component separated from the locally-heated UHI component) is found across the city, with a maximum UHII of 1.18°C. The peak UHAI influence is found under the medium-wind group (WG2), with a mean UHAI signal of 0.4°C, and with 25% of stations experiencing between 0.5°C and 1.2°C. The maximum UHAI found in WG2 rather than WG1 (the low-wind group) could be explained by a reduced capacity to advect heat for WG1. For the high-wind group (WG3), however, conditions associated with large UHI development are reduced, thus leaving little urban heat available for advection. Whilst these observations establish that UHA in the UCL is a significant phenomenon, the processes at which heat is transported (i.e. horizontally through the UCL or mixed downwards from the urban plume) cannot be identified in this study. However the correlation methodology based on urban fraction data are able to show that the total UHI component at a given location is a construct of the urban heat created by local land use and heat advected from upstream sources, with distance dependant on wind speed. With distances over 10 km at which the advection signal is still present, this has considerable implications not only for long-term climate records taken near cities, but for adapting cities and protecting vulnerable citizens in a changing climate.

Although UHA has previously been difficult to quantify and is not always considered in UHI studies due to the lack of urban meteorological observations, this paper has successfully demonstrated UHA to be a substantial and noteworthy urban climate

process. The unique methodology developed in this paper (i.e. use of urban reference temperatures and techniques to isolate UHA only previously used in mesoscale modelling approaches) can be readily adapted to other urban networks worldwide.

Chapter 3.

The effects of heat advection on UK weather and climate observations in the vicinity of small urbanised areas

This Chapter was published as:

Bassett, R., Cai, X., Chapman, L., Heaviside, C., Thornes, J.E. (2017) ‘The effects of heat advection on UK weather and climate observations in the vicinity of small urbanised areas’, *Boundary-Layer Meteorology*. doi:10.1007/s10546-017-0263-0.

RB envisioned and conducted the data analyses, and wrote the paper. XC helped develop the concept. All contributed to proofing the manuscript.

3.1. Abstract

Weather and climate networks traditionally follow rigorous siting guidelines, with individual stations located away from frost hollows, trees or urban areas. However, the diverse nature of the UK landscape suggests that the feasibility of siting stations that are truly representative of regional climate and free from distorting local effects is increasingly difficult. Whilst the urban heat island is a well-studied phenomenon and usually accounted for, the effect of warm urban air advected downwind is rarely considered, particularly at rural stations adjacent to urban areas. Until recently, urban heat advection (UHA) was viewed as an urban boundary-layer process through the formation of an urban plume that rises above the surface as it is advected. However, these dynamic UHA effects are shown to also have an impact on surface observations. Results show a significant difference in temperatures anomalies ($p < 0.001$) between observations taken downwind of urban and rural areas. For example, UHA from small urbanised areas ($\sim 1 \text{ km}^2$) under low cloud cover and wind speeds of $2 - 3 \text{ m s}^{-1}$ is found to increase mean nocturnal air temperatures by 0.6°C at a horizontal distance of 0.5 km. Fundamentally, these UHA results highlight the importance of careful interpretation of long-term temperature data taken near small urban areas.

3.2. Introduction

3.2.1. Background

Average global air temperatures increased by 0.9°C between 1880 and 2012 (IPCC, 2014). Concurrently, rapid urbanisation continues to take place with 54 % of the world's population now residing in urban areas (higher in developed countries, e.g. 82 % in the UK; United Nations, 2014). Attempts to quantify the contribution of increasing urbanisation to the rise in global temperatures show that the effect is typically an order of magnitude less than overall warming due to increasing greenhouse gas concentrations (e.g. $0.05^{\circ}\text{C century}^{-1}$, Jones et al., 1990; $0.27^{\circ}\text{C century}^{-1}$, Kalnay and Cai 2003; $0.05^{\circ}\text{C century}^{-1}$, Zhou et al., 2004).

Urban fabric alters the local surface energy balance, resulting in heat storage during the day, and heat release at night. The resulting nocturnal warming, known as the urban heat island (UHI), can be locally several times larger than the observed global warming over the last century. For example, in the UK, UHI intensities (UHII, the maximum low-level temperature difference between the urban and rural areas) up to 9°C have been found in London (Kolokotroni and Giridharan, 2008) and 10°C in Manchester (Smith et al., 2011). The UHII for a given urban area is approximately related to city size (Oke, 1973) and varies with atmospheric stability (Azevedo et al., 2016). Indeed, even small urban areas (populations $10^3 - 10^4$), can still generate UHIIs in excess of 1°C (Oke, 1973; Ivajišić et al., 2014; Linden et al., 2015). However, absolute maximum air-temperature variations are not always captured due to the challenges associated with locating stations within the urban environment

(Chapman et al., 2015; Stewart, 2011). Furthermore, UHI effects are not confined to temperature. The UHI has been shown to modify low-level flow (Bornstein and Johnson, 1977) and increase precipitation downwind (Ackerman et al., 1978). The UHI can also have a specific impact on public health and infrastructure. For example, Heaviside et al. (2016) attributed approximately 50 % of the heat-related mortality in the West Midlands, UK during the August 2003 European heatwave to the UHI.

Official weather and climate networks follow rigorous siting guidelines of the World Meteorological Organization (WMO, 2008) so as to avoid undue local effects on observations (i.e. locating stations away from frost hollows, trees or urban areas). Using the classification developed by the WMO to assess the exposure of surface observations, the most representative stations are defined as those located more than 0.1 km from any anthropogenic heat sources (WMO, 2008). However, Oke (2006) suggested that the actual source area affecting screen-level observations may extend up to 0.5 km. Whilst there remains no consensus in the literature with respect to source areas, indeed Parker (2006) disputed whether urban influences are present in the data at all, the heterogeneous nature of the UK landscape suggests that the search for representative stations away from the influence of urbanisation is becoming increasingly difficult. However, despite these uncertainties, the majority of UHI studies only consider immediate station characteristics (up to 0.1 km, WMO, 2008) and not always more distant source areas. As such, this paper sets out a methodology for exploring the role of urban heat advection (UHA) in contaminating the climate signal at weather stations located in proximity to urban areas.

3.2.2. Urban Heat Advection

Although UHI effects are generally well understood (see Arnfield, 2003, Stewart, 2011 for extensive reviews), the process of UHA is rarely considered. UHA is the horizontal transport of heat originating from urban areas, and was conceptually considered by Lowry (1977) regarding rural weather stations contaminated by warm urban air known as an “urban environ”. To understand UHA processes, the UHI can be categorized by its vertical extent into an “urban canopy layer (UCL) UHI” and “urban boundary-layer (UBL) UHI” (Oke, 1976). The UCL and UBL structure is illustrated in Figure 3.1a, adapted from Oke (1976). Within the urban canopy-layer UHI (from ground to roof level) airflow effectively advects heat horizontally through street-canyon networks (Figure 3.1b), as demonstrated by Belcher et al. (2015) using a street-network model. In contrast, the urban boundary-layer UHI (above roof level) is heated from the air below, and is affected by local to mesoscale processes. Warm, buoyant urban air forms a thermal dome that is advected horizontally if airflow is present (Figure 3.1a). UBL observations have shown elevated urban thermal plumes to typically extend 10-15 km downwind of an urban area (Dirks, 1974; Wong and Dirks, 1978). A step change in surface properties, from urban to rural, modifies the lower part of the urban plume as heat flux and temperature profiles adapt to the rural conditions, via the internal boundary layer (IBL). The near-surface air within the IBL in the downwind proximity to the city or town is in equilibrium with the dynamical and thermal forcings at the following interfaces: (i) the local rural surface (predominately via vertical turbulent mixing), (ii) the urban plume above the IBL (predominately via vertical turbulent mixing), and (iii) the leading edge of the IBL at the downwind edge of the urban area (predominately via horizontal advection). These

processes are illustrated in Figure 3.1b, noting that the effects of upwind urban land use are not limited to temperature. Significant relationships have been shown to exist between upwind urban land use and turbulent heat fluxes (Rooney, 2001; Rooney et al., 2005; Barlow et al., 2008).

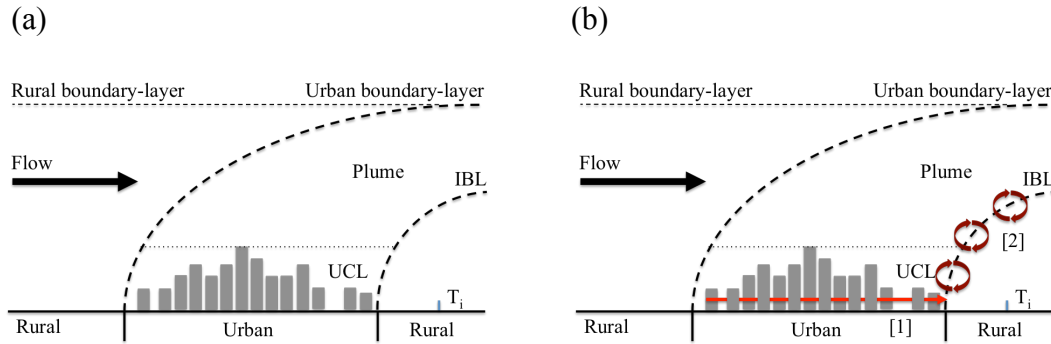


Figure 3.1. (a) Urban boundary-layer structure and urban plume (after Oke, 1976). (b) Adapted urban plume to show UHA processes: [1] horizontally through the UCL, and [2] horizontal and vertical heat mixing from the urban plume shown through hypothetical eddies.

Whilst spatial UHI studies exist and some acknowledge UHA (e.g. Klyzik and Fortuniak, 1999; Bohnenstengel et al., 2011; Azevedo et al., 2016), they do not explicitly separate UHA from the UHI signal (i.e. (i) the locally generated UHI component with intensity dependent upon underlying land use, and (ii) the UHA that is generated from upwind urban land use). To decompose these components a methodology was developed by Heaviside et al. (2015) that used a time-mean 2-m air-temperature field created from mesoscale modelling to deduce UHA. This methodology was subsequently adapted for use with observations from a high-density urban observation network (Birmingham Urban Climate Laboratory, Warren et al., 2016) where a significant UHA signal was found and linked to the upwind normalized

difference vegetation index, a proxy for urban fraction, at city scale (Chapter 2). Whilst this methodology is able to demonstrate UHA, there remain several identifiable research gaps: (i) UHA effects on global temperature series are rarely considered, (ii) the extent of UHA arising from small urban areas is unknown, and (iii) station metadata do not include source areas, i.e. proximity of rural stations to urban areas. Therefore, the aim of our study is to develop previous UHA methodologies (Brandsma et al., 2003; Heaviside et al., 2015; Chapter 2) in order to quantify the influence of UHA on the UK Met Office weather and climate observation network from small urban areas.

3.3. Methods and Background

3.3.1. Building fraction data

Categorized land-cover products (Stathopoulou and Cartalis, 2006), vegetation indices (Chen et al. 2006) or local climate zones (Stewart and Oke, 2012) are frequently used to link the UHII to local land use. However, the resolution of such products is generally too coarse to study small-scale UHA features. As such, building fractions calculated from Ordnance Survey 1:10000 VectorMap data are used (a dataset that contains outlines of all individual buildings in the UK: see Figure 3.2a for examples of the data at selected Met Office stations). The Ordnance Survey data were aggregated to 30-degree sectors within a 0.5-km radius to create a “directional building fraction” for each station (Figure 3.2b). Based on Oke (2006), a 0.5-km radius was initially selected to represent the circle of influence for screen-level temperatures (a distance that has also been adopted for classifying local climate

zones: Stewart and Oke, 2012). Whilst the building-fraction methodology presented could be used as a simple means to provide enhanced urban metadata for station networks, it should be noted that the calculated building fraction will underestimate the actual urban fraction because only building footprint areas are available in the dataset (and not all other paved surfaces). This limitation should not significantly affect the outcome of a correlation analysis in Section 3.4 since an approximate proportionality between building fraction and urban fraction was assumed. However, this may not be the case in all urban areas worldwide, e.g. extensive paved areas in U.S. cities.

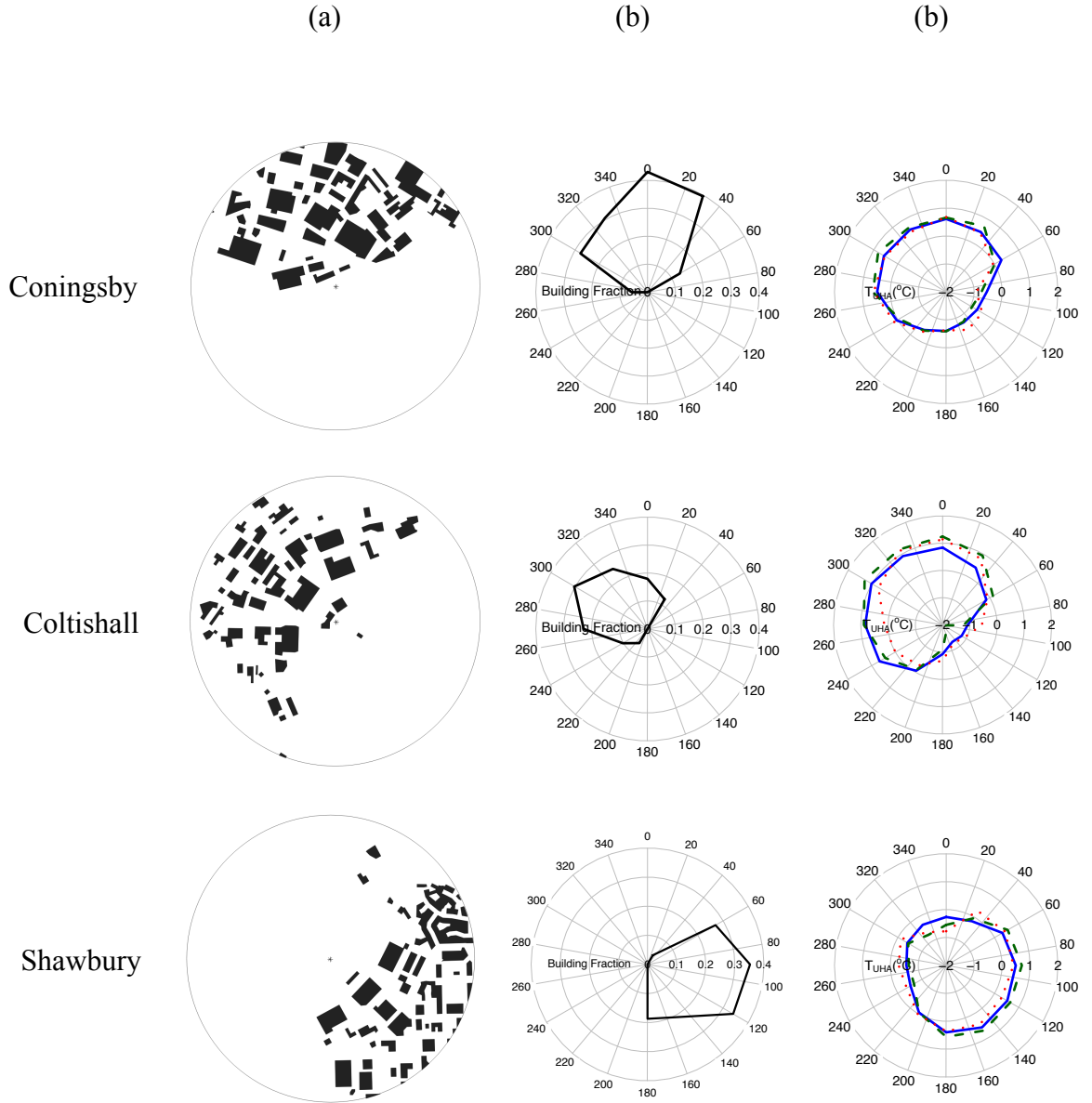


Figure 3.2. (a) Ordnance Survey VectorMap building data in a 0.5-km radius around the Met Office station at Coningsby, Coltishall and Shawbury (centre stars). (b) Building fraction at 30-degree arcs extending 0.5 km from each station. (c) Mean UHAI for the wind sector θ and station i ($T_{UHA}^{(\theta)}(i)$, defined in detail below) in three wind-speed groups (WG1, solid blue line: $< 2 \text{ m s}^{-1}$, WG2, dashed green line: $2 - 3 \text{ m s}^{-1}$, WG3, dotted red line: $> 3 \text{ m s}^{-1}$).

3.3.2. Selection of stations

The UK Met Office station network consists of approximately 200 operational weather and climate stations (Met Office, 2016), where the exposure of each station is chosen to represent the weather and climate of a wide area (≈ 40 -km spacing). Data from this network were accessed through the Met Office Integrated Data Archive System that provides land-surface observations from 1853 to present (Met Office, 2012). Air temperature (accurate to 0.1°C) was measured at 1.25 m above ground using thermometers located inside Stevenson screens, while wind data were collected at 10 m above ground (speed accurate to 0.51 m s^{-1} and direction within 5 degrees). Only stations with 1-hr temperature and wind records covering a year or more were selected for further analysis. Next, digital elevation data from the Shuttle Radar Topography Mission (Reuter et al., 2007) were used to determine the local topography at each station. As in Kalnay and Cai (2003), albeit more conservative, our study only used stations located at altitudes less than 300 m. Additionally, stations with a significant local topography change ($> 150 \text{ m}$ in a 1-km radius) and stations located near coasts ($< 5 \text{ km}$) were excluded from the analysis. Although, sea breezes can extend beyond this distance, the analysis was limited to nighttime (see Section 3.3.4), therefore limiting any coastal effects. Overall, these measures were taken as an attempt to exclude unwanted advective warming or cooling.

For the remaining stations that satisfied these conditions, there was a need to identify specific sites prone to UHA for detailed analysis. Building on Lowry (1977), it was assumed that only stations within the urban environ will be influenced by UHA under a given wind sector. To identify these stations a two-stage approach was taken.

Firstly, the building fraction data were used to automatically exclude from the analysis: (i) rural stations with no local urbanisation in the surrounding area (0.5-km radius), and (ii) urban stations (i.e. the land-use pattern would be too complex to separate local effects). Secondly, a visual check using satellite imagery was used to confirm the automatic station classification was correct (satellite imagery and urban fraction is presented in the Appendix). This visual check highlighted further stations that needed to be excluded from the analysis that were either surrounded by larger scale urban features or were next to other external heat sources or sinks, e.g. lakes or coal power stations. Overall, 42 stations were identified with available 1-hr temperature data at locations that could be considered at a high risk of UHA (Figure 3.3). Typically, sites were located adjacent to a village or small town with an area of approximately 1 km². Many sites in the analysis were weather stations located near small airfields, a consequence of the historical link between aviation and meteorology.

3.3.3. UK baseline temperature

The temperature data across all available stations were not temporally homogeneous (stations may be re-sited or closed over time). To ensure reliable comparisons across stations when UHA was calculated, a consistent baseline temperature series was required. The baseline covered a 30-year analysis period from 1985 – 2015 at a 1-hr resolution. In the spatial domain, ideally, one ‘pure rural’ station (i.e. no surrounding urban heat sources) close enough to each of these 42 stations would be sufficient, but close scrutiny of the stations demonstrated that this was rarely available. In total, just seven suitable rural stations were found that had continuous temperature data (greater

than 99 % data capture) over the 30-year analysis period (Figure 3.3). By adjusting for altitude (range of 20 to 145 m) using the environmental lapse rate ($6.0^{\circ}\text{C km}^{-1}$), the dominant control for mean temperature across the 30-year period was latitude ($R^2 = 0.93$). Based upon this, two different baseline temperature series were constructed from the data of the seven stations: (i) the mean temperature of these seven stations for each hour over the 30-year time period, denoted by $T_B(t)$, and (ii) latitude-dependent 1-hr data over the 30-year time period, denoted by $T_B(t, y)$. It will be demonstrated later in Section 3.3.4 that for the UHA analysis, use of the two types of baseline temperature series is identical under a reasonable assumption for the functional form of $T_B(t, y)$. Thus, $T_B(t)$ was adopted, which is a function of time (t) and independent of location. It was also acknowledged that whilst stations used in the baseline were considered rural, they could have contained unavoidable UHA influences. However, any impacts on results were limited by taking the mean of several stations to create the baseline. In order to check the representivity of the baseline, a comparison was made with ECMWF ERA-Interim (Balsamo et al., 2015) re-analysis temperature data. A grid point (52.125,-1.625) in the middle of the seven stations was chosen for the comparison, with data taken at 6-hr intervals. At midnight (0000 UTC) the ECMWF reanalysis was found to strongly correlate with the baseline temperature series over the 30-year period ($R = 0.99$, mean squared error = 0.4°C). Example data from individual months are presented in Figure 3.4 where it was evident that the baseline temperature series and ECMWF reanalysis follow the same trend. This provided evidence of the suitability for interpreting this baseline as a background climate for later use in the UHA calculation.

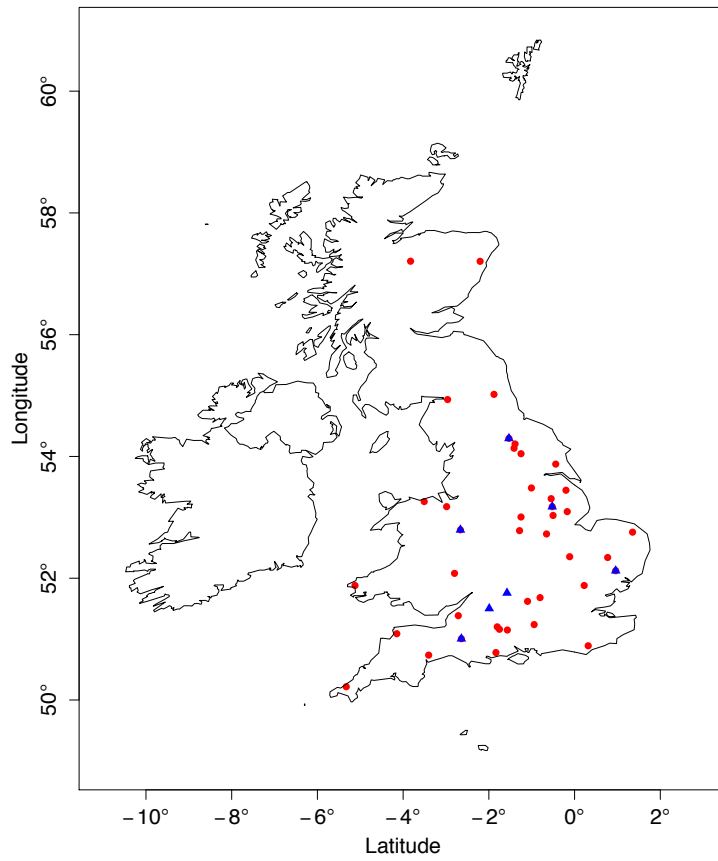


Figure 3.3. Stations used for the baseline temperature series (blue triangles) and advection analysis (red dots).

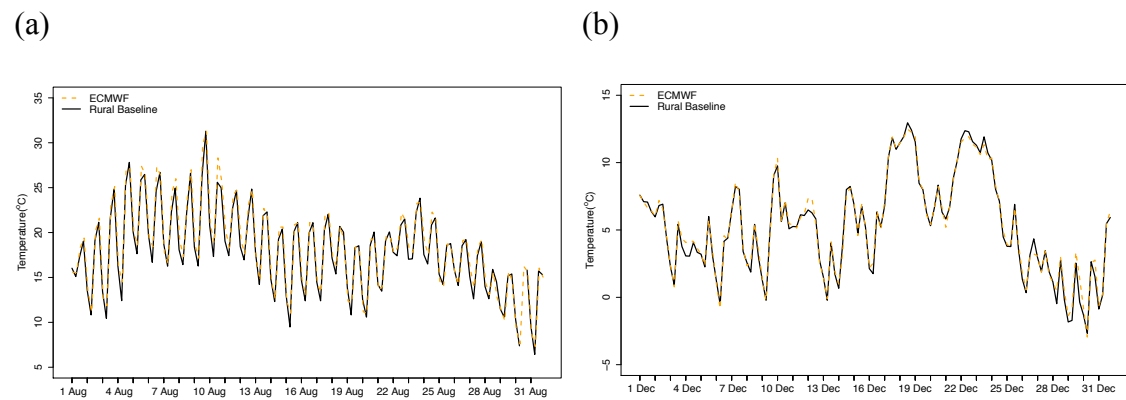


Figure 3.4. ECMWF ERA-Interim comparison with the baseline temperature series: (a) August 2003, and (b) December 2014.

3.3.4. Urban heat advection

This section demonstrates that the use of a location-independent 1-hr rural baseline, $T_B(t_n)$, in the UHA analysis is justifiable, where t_n denotes the n -th hour, and subscript B denotes ‘baseline’. As indicated in Section 3.3.3, analysis of the data from the seven rural stations’ showed that the dominant control in the spatial domain (longitude, latitude, altitude, or x, y, z) for temperature was latitude ($R^2 = 0.93$). It is thus evident to assume a latitude-dependent baseline temperature time series, or even in a much more general sense, a location-dependent baseline temperature time series, $T_{B,i}(t_n, x_i, y_i)$, which can be decomposed into two terms,

$$T_{B,i}(t_n, x_i, y_i) = T_B(t_n) + T'_B(x_i, y_i), \quad (1)$$

where subscript i denotes the i -th station, x_i and y_i are the longitudinal and latitudinal coordinates of the i -th station. $T'_B(x_i, y_i)$ represents regional-scale variability of $T_{B,i}$ (by definition it is an offset of $T_{B,i}$ from T_B), and was a function of location only. Analysis of the temperature data at the seven stations showed that the offset of $T_{B,i}(t_n, x_i, y_i)$ from $T_B(t_n)$ were strongly dependent on latitude, y_i (Section 3.3.4), and this provides evidence to support the assumption (Equation 1). However, this assumption does not include other effects that could become apparent with larger latitude changes, i.e. sunrise / sunset times.

The following demonstrates that use of a hypothetical location-independent $T_B(t_n)$ and location-dependent baseline temperature time series $T_{B,i}(t_n, x_i, y_i)$ satisfying (Equation 1), yielded identical results for the directional UHA analysis described in

Chapter 2. By denoting the observed temperature data at the i -th station as $T_i(t_n)$, the increases in temperature at this site relative to the two baseline temperatures,

$T_{B,i}(t_n, x_i, y_i)$ and $T_B(t_n)$, are,

$$\Delta_{B,i}T_i = T_i(t_n) - T_{B,i}(t_n, x_i, y_i), \quad (2)$$

and

$$\Delta_B T_i = T_i(t_n) - T_B(t_n), \quad (3)$$

respectively. Equations 1-3 can be combined to obtain,

$$\Delta_{B,i}T_i = \Delta_B T_i - T'_B(x_i, y_i). \quad (4)$$

Applying the directional UHA analysis (Chapter 2), firstly the all-hour-mean (i.e. all wind directions included) warming increment, $\overline{\Delta_{B,i}T_i}$, from Equation 4 was obtained,

$$\overline{\Delta_{B,i}T_i} = \overline{\Delta_B T_i} - T'_B(x_i, y_i). \quad (5)$$

Then the mean warming increment was calculated for one direction sector, θ (a 30-degree interval), from Equation 4,

$$\overline{\Delta_{B,i}T_i^\theta} = \overline{\Delta_B T_i^\theta} - T'_B(x_i, y_i). \quad (6)$$

Finally, the all-hour-mean warming increment, $\overline{\Delta_{B,i}T_i}$, was subtracted from $\overline{\Delta_{B,i}T_i^\theta}$ to give the mean UHA intensity (UHAI) for the wind sector,

$$\overline{T_{UHA(i)}^{(\theta)}} = \overline{\Delta_{B,i}T_i^\theta} - \overline{\Delta_{B,i}T_i}. \quad (7)$$

Following the substitutions of Equations 5 and 6 into 7, this provides,

$$\overline{T_{UHA(i)}^{(\theta)}} = \overline{\Delta_B T_i^\theta} - \overline{\Delta_B T_i}. \quad (8)$$

The interpretation of the notations in Equations 7 and 8 was that Equation 7 calculates the mean UHAI for the wind sector θ using location-dependent baseline temperature time series, $T_{B,i}(t_n, x_i, y_i)$, whereas Equation 8 calculates the same quantity using location-independent baseline temperature time series, $T_B(t_n)$. Thus, this demonstrates that the use of $T_B(t_n)$ and use of $T_{B,i}(t_n, x_i, y_i)$ yield identical results for the directional UHAI analysis; the condition is that assumption (Equation 1) holds.

Through prior UHA studies (Heaviside et al., 2015; Chapter 2), a positive mean UHAI value ($\overline{T_{UHA(i)}^{(\theta)}}$) is expected if a given station is located downwind of an urban area. Due to the way $\overline{T_{UHA(i)}^{(\theta)}}$ is defined, negative results indicate that the temperature in a given wind sector is less than the all-hour mean. In reality, a range of air-mass types have different stability conditions, which would affect the results. To account for directional stability inhomogeneity, data corresponding to nighttime (from sunset to sunrise) and low cloud cover (< 5 oktas) conditions were selected. Additionally the

data were classified into three wind-speed groups (WG1: $< 2 \text{ m s}^{-1}$, WG2: $2 - 3 \text{ m s}^{-1}$, WG3 $> 3 \text{ m s}^{-1}$). These categories, applied to all results, represent the Pasquill-Gifford stability (Pasquill and Smith, 1983) conditions from neutral to stable, where conditions have been shown to favour large UHIs (Tomlinson et al., 2012; Azevedo et al., 2016).

3.4. Results and discussion

3.4.1. Case studies

In order to demonstrate the methodology, three case studies are presented for the Met Office stations at Coningsby, Coltishall and Shawbury (Figure 3.2). Each station is consistent with the criteria for identifying stations suitable for analysis: flat terrain, inland from the coastline and a simple urban pattern in a single direction (Figure 3.2a). The calculated upwind building fraction at 30-degree intervals extending to 0.5 km from the station for each station is presented in Figure 3.2b. The mean directional temperature anomaly or UHAI ($\overline{T_{UHA(i)}^{(\theta)}}$) for each case study (Figure 3.2c) indicates a bias in the same direction as the urban area next to the station. At each station a clear relationship is found in all wind-speed groups whereby $\overline{T_{UHA(i)}^{(\theta)}}$ is linked to the upwind urban fraction. At Shawbury, the difference between the mean $\overline{T_{UHA(i)}^{(\theta)}}$ for all urban sectors (i.e. for θ with building fraction > 0.1) and for all rural sectors (θ with building fraction < 0.1) is 1.1°C . For Coningsby and Coltishall, the mean $\overline{T_{UHA(i)}^{(\theta)}}$ for all urban sectors is up to 1°C and 2°C greater than rural sectors respectively. A scatterplot showing the relationship between the upwind building fraction and

temperature anomaly at these stations is presented in Figure 3.5. Whilst these UHAI values seem large, mesoscale modelling, albeit on a different scale, has shown similar values of UHAI to be plausible (Heaviside et al., 2015).

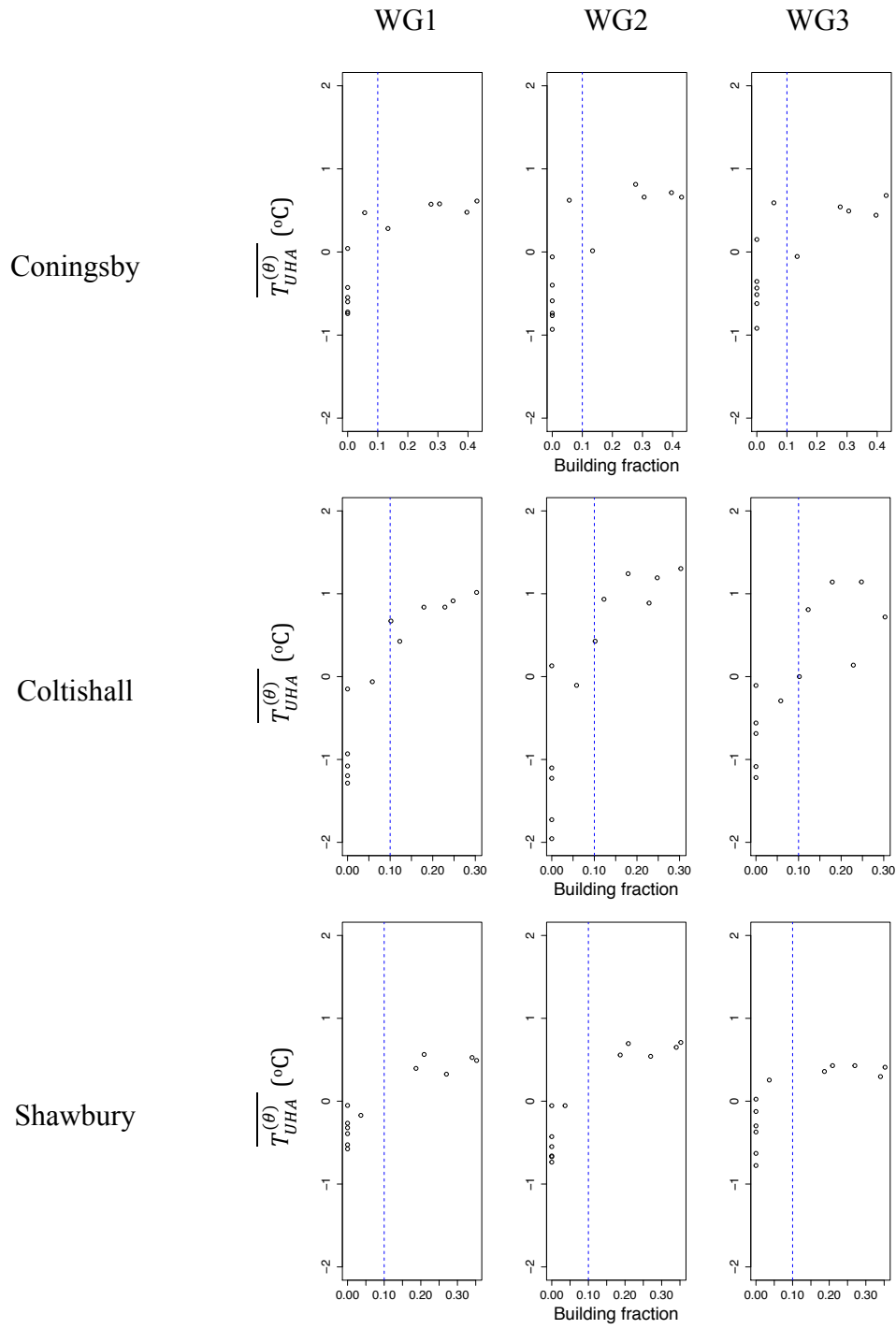


Figure 3.5. The relationship between 0.5-km upwind building fraction and mean UHAI ($\overline{T_{UHA}^{(\theta)}}$) in three wind-speed groups at Coningsby, Coltishall and Shawbury weather stations (WG1: $< 2 \text{ m s}^{-1}$, WG2: $2 - 3 \text{ m s}^{-1}$, WG3: $> 3 \text{ m s}^{-1}$).

3.4.2. Urban heat advection

The analysis was then re-scaled to include each station (42 total). Figure 3.6 shows the relationship between upwind building fraction and the UHAI ($\overline{T_{UHA}^{(\theta)}(i)}$) across all stations, including the mean UHAI and standard deviations over 0.1 building fraction intervals. The mean UHAI incrementally increases with each increase in building fraction, from zero to 0.3, before generally reaching a plateau, likely caused by fewer data points available at dense urban areas (for this reason the mean and standard deviation are not shown at building fraction intervals > 0.4).

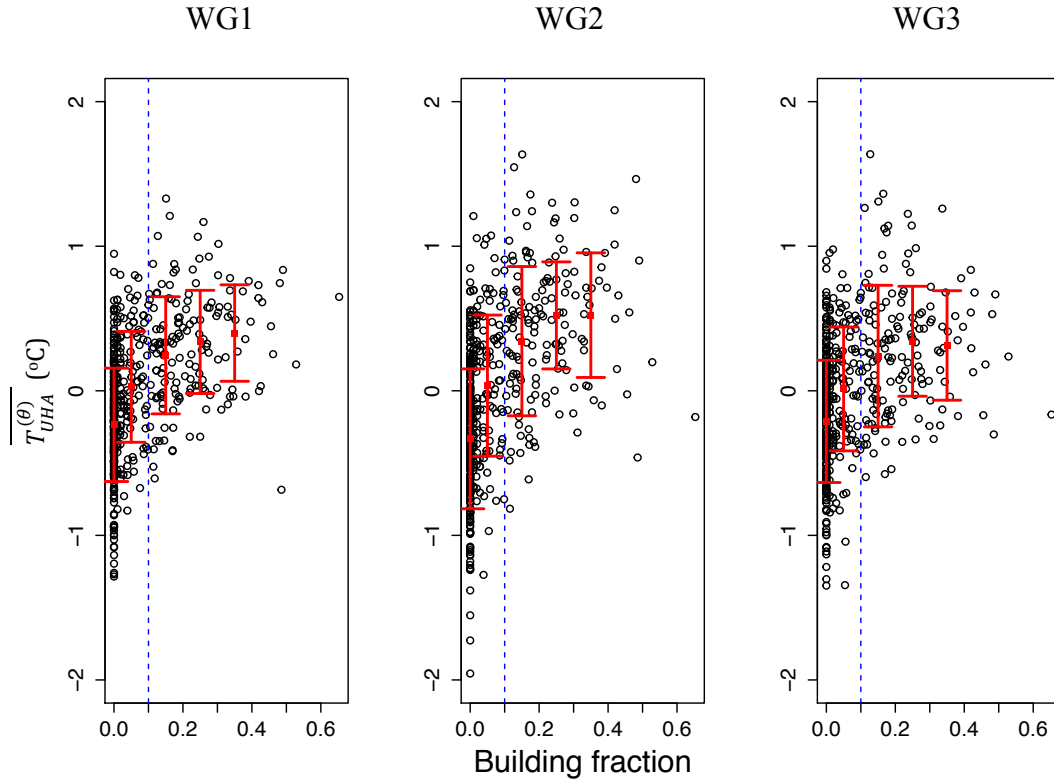


Figure 3.6. The relationship between upwind building fraction and the mean UHAI ($\overline{T_{UHA}^{(\theta)}(i)}$) across all stations in three wind-speed groups (WG1: $< 2 \text{ m s}^{-1}$, WG2: $2 - 3 \text{ m s}^{-1}$, WG3: $> 3 \text{ m s}^{-1}$). The red square indicates the mean UHAI at urban fractions: 0,

0 - 0.1, 0.1 - 0.2, 0.2 - 0.3, 0.3 - 0.4. The vertical lines either side of the mean represent \pm one standard deviation. The dashed blue line at the 0.1 building fractions indicates the urban, rural separation used for statistical analysis in 3.1.

To test the significance of UHA ($\overline{T_{UHA(i)}^{(\theta)}}$) differences between wind sectors, the data are split into two groups by their upwind building fractions (for θ in the urban sectors, building fraction > 0.1 and θ in the rural sectors, building fraction < 0.1). The distribution of the UHA for urban sectors is presented in Figure 3.7. These groups contain 154 and 350 values of $\overline{T_{UHA(i)}^{(\theta)}}$ respectively. A null hypothesis is created stating that: “there is no significant difference between the temperature anomaly caused by urban and non-urban wind sectors”. The data are tested for consistency with a normal distribution (skewness between -1 and 1) and Welch’s two-sample t -test is conducted to determine whether there is a significant difference between means. The results of the t -test are summarized in Table 3.1. For each wind-speed group, a significance (p) value < 0.001 is calculated, thus the null hypothesis can be rejected. It can be concluded that increased temperatures for the airflow from urban sectors, relative to the flow from rural sectors, are due to the change in upwind characteristics from rural to urban. The difference between the mean of all urban sectors ($\overline{T_{UHA}^{(urban)}}$) and the mean of all rural sectors ($\overline{T_{UHA}^{(rural)}}$) shows that the effect of upwind urban sectors contributes to a mean air-temperature increase of 0.6°C under low cloud cover at night (WG2). Whilst this warming may not be considered large, it is important to note these are averaged effects and therefore may be larger on individual nights at given stations. Indeed, already the case studies presented in Section 3.4.1 have demonstrated that a significantly larger UHAI is possible. A

distance analysis is conducted in the next section to confirm whether this 0.5-km radius used is appropriate. Of 42 stations analysed, 32 % of the wind sectors are considered urban (> 0.1 building fraction), and assuming equal distribution of airflow in all wind directions, the overall mean nocturnal warming under low cloud cover is therefore 0.1°C , 0.2°C and 0.2°C , in WG1, WG2 and WG3 respectively.

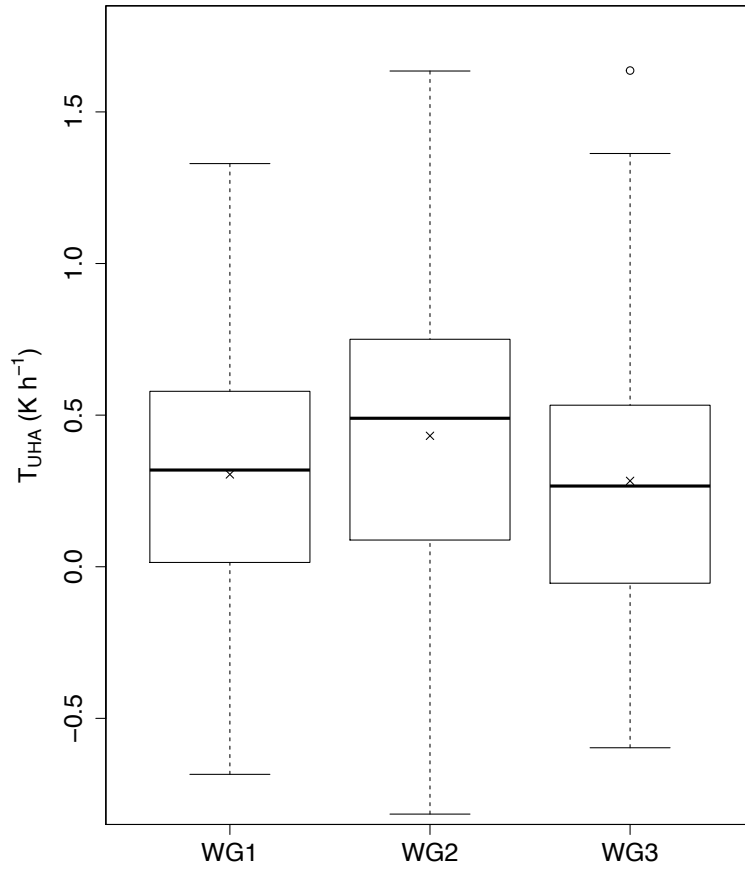


Figure 3.7. Box-and-whisker plot for $\overline{T_{UHA}^{(\theta)}}$ where building fractions > 0.1 for WG1, WG2 and WG3. The x marker signifies the mean and whiskers 1.5 IQR.

Table 3.1. Welch’s two-sample t -test between $\overline{T_{UHA}^{(\theta)}(i)}$ for urban and rural wind sectors where the urban sectors correspond to θ with building fraction > 0.1 and the rural sectors to θ with building fraction < 0.1 . The mean of all urban sectors is shown as $\overline{T_{UHA}^{(urban)}}$ and for rural sectors as $\overline{T_{UHA}^{(rural)}}$.

	t-value	degrees of freedom	p-value	$\overline{T_{UHA}^{(rural)}}$ (°C)	$\overline{T_{UHA}^{(urban)}}$ (°C)	$\overline{T_{UHA}^{(urban)}} - \overline{T_{UHA}^{(rural)}}$ (°C)
WG1	11.5	306.2	< 0.001	-0.13	0.30	0.43
WG2	13.5	312.3	< 0.001	-0.19	0.43	0.62
WG3	9.7	291.8	< 0.001	-0.13	0.28	0.41

A large degree of scatter is found within the data (Figure 3.6). Indeed, relating an upwind land-use parameter to a meteorological observation is not straightforward. The scatter in the UHAI signals may be attributed to the building-fraction methodology: (i) building fraction represents building coverage, or roof area and not the total urban fraction, (ii) the size and complexity of each adjacent urban sector differs, and (iii) the form and function of each building is not considered. This makes analysis challenging because for given wind category, no two stations necessarily have the same upwind urban land use. In addition, if there are two stations with the same building fraction profiles, flow and turbulent characteristics within allocated groups may differ due to other unaccounted local or regional factors. The location of the buildings within the 0.5-km wind sector may also differ between two stations that are classified with identical 30-degree upwind building fractions. Whilst the use of Ordnance Survey building data has its limitations, this sub-km analysis is not possible with coarser resolution products typically used to classify the UHI (e.g. satellite data).

Whilst the overall pattern shows a significant UHA effect, and most stations exhibit a pattern similar to that presented in the case studies (Figure 3.2), a handful of stations within the dataset do not follow this trend. These discrepancies can be readily explained (Table 3.2) when interpreting satellite imagery for the given station (Appendix). In addition, the mean UHAI signal at several stations only contains a relationship with building fraction in one or two of the wind-speed groups. This may be explained by station specific characteristics that are not accounted for, through simply classification of the data using urban fraction and stability conditions. The explanations provided highlight the previously discussed limitations in the building-fraction methodology, as opposed to a lack of a UHA signal. The methodology also does not account for changes in urbanisation over the 30-year analysis period since building fraction was calculated at a fixed point in time. Additionally, all paved surfaces that could generate UHA are not presently accounted for and the distance at which each station is located from the urban areas varies. There is also a large range of (negative) UHAI values associated with rural (zero building fraction) directions. The methodology is presently unable to determine vegetation type (e.g. open fields or forests) or other external heat sources that could account for these differences. Vegetation could also help explain UHA scatter for upwind urban directions.

Table 3.2. Stations where the UHA signal does not exhibit a relationship with upwind building fraction with explanations provided through a visual station analysis.

Station (ID)	Explanation
Binkbrook (394)	The station closed in 1992. The adjoining land use has since changed from an airfield to industrial estate. Therefore the calculated building fraction is different during the observation period.
Herstmonceux (811)	Tall hedges surround the station on two sides, and slight elevation changes present nearby.
Larkhill (888)	There is a visual link between the land use and UHAI pattern, however this is not reflected in the building fraction data. For example south-west of the station there is a large area of paved surfaces. Additionally this station could have two UHA sources, therefore the pattern is less clear.
Bristol / Lulsgate (18912)	The UHAI pattern relates to satellite imagery, however similarly to Larkhill the building fraction does not capture a large portion of paved surfaces, in particular the airport car park.

Under the same conditions (WG2, nighttime and cloud cover < 5 oktas) that a mean difference between urban and rural wind sectors ($\overline{T_{UHA}^{(urban)}} - \overline{T_{UHA}^{(rural)}}$) of 0.6°C is found, Chapter 2 found a mean UHAI signal of 0.4°C for Birmingham, UK. This was calculated by taking the mean UHAI signal from a network of urban canopy stations

downwind of the city centre. Whilst the mean UHAI found is greater than that found in Birmingham (a city several orders of magnitude larger in size than the urbanised areas in this study), conducting UHA analysis within a large city has several limitations: (i) the mean observed signal will be weakened by UHA in opposing directions, (ii) a central urban reference station was used for the UHA calculation that could itself be influenced by local heat advection, and (iii) stations downwind of the central business district could be encircled by suburban land use (although analysis was still possible because certain upwind sectors, i.e. towards the city centre, contained higher urban fractions). By only analysing stations with a clear distinction between urban and rural wind sectors, this could explain the higher observed UHAI effect from small urbanised areas than that found in Chapter 2. The results also indicate the highest UHAI to be present under medium wind speeds (WG2: $2 - 3 \text{ m s}^{-1}$), which is consistent with other UHA studies (Brandsma et al., 2003; Chapter 2). At low wind speeds (WG1), whilst the UHI is most pronounced, there is little potential to transport heat. At high wind speeds (WG3) heat transport is increased, however the UHI is least pronounced. Therefore a balance between these factors occurs under medium wind speeds (WG2) leading to the highest UHAI values. However even under WG1, air travels further than the distance between the station and urban boundary at the 1-hr time scale.

3.4.3. Urban heat-advection footprint

The results presented in Section 3.4.2 use a fixed building fraction distance of 0.5 km, as the suggested circle of influence on screen-level temperatures (Oke, 2006). However UHA signals have previously been found at greater distances downwind

(Brandsma et al., 2003; Chapter 2). To test the 0.5-km circle of influence, the methodology used to calculate building fraction is extended for 30-degree arcs extending: 0.5 – 1 km, 1 – 2 km and 2 – 3 km from each station. The building fraction calculated at these distances can be visualised as arcs, and do not contain the information from preceding (smaller) distances. Pearson’s correlation coefficient is calculated between the directional building fraction and the mean UHAI signal $\overline{(T_{UHA(i)}^{(\theta)})}$ at these distances, with results presented in Table 3.3. The correlation coefficient is shown to weaken with increased distance from the stations. Whilst the results support Oke’s (2006) circle of influence with the strongest correlation coefficients found at 0.5 km, the UHAI footprint or distance is not directly comparable to other studies because different urban sizes are analysed. Only the UHA effect from villages and small towns are considered, whereas Brandsma et al. (2003) and Chapter 2 analysed temperature observations from large towns and cities. As such Brandsma et al. (2003) found distances in the order of several kilometres and Chapter 2 found evidence for UHA at distances > 10 km. As observations from urban areas of different sizes are analysed the processes and scale of UHA transport will differ considerably. Thus, the peak UHAI correlation with upwind distance of 0.5 km may be an artefact of the length scale of buildings adjacent to the stations. Therefore, further work is needed to explore UHA, perhaps in the form of downwind transects from urban areas of different sizes and complexities.

Table 3.3. Pearson’s correlation coefficient between the mean UHAI signal ($\overline{T_{UHA(i)}^{(\theta)}}$) and upwind building fraction arcs at increasing distances from stations.

	0.5 km	0.5 – 1 km	1 – 2 km	2 – 3 km
WG1	0.46	0.30	0.15	0.19
WG2	0.49	0.32	0.17	0.17
WG3	0.38	0.23	0.17	0.14

3.5. Conclusions

Whilst the effects of large urbanisation on station temperature data have previously been noted, urban heat advection, particularly from small urban areas, has rarely been considered. In total, 42 stations from the UK Met Office network were identified as having an adjacent urban area (approximately 1 km² size) in a single wind sector. The stations are typically located at airfields due to historical associations between aviation and meteorology, although these selected stations should not be considered an exclusive list of those likely to be influenced by UHA. Station data with surrounding urban land use in all directions, near coasts or in areas of high terrain, were not analysed. In these cases station data could also be affected by UHA but the effect would be difficult to determine. In addition 1-hr data were required, and with a large percentage of UK stations capturing only daily data, this limits the numbers of stations available for analysis.

Overall, the results demonstrate that even small urban areas ($\sim 1 \text{ km}^2$) exert a significant warming on their surroundings. An increase in air temperature between rural and urban upwind sectors of up to 0.6°C was found at night under low cloud

cover and wind speeds of $2 - 3 \text{ m s}^{-1}$. This warming is larger than found in previous UHA observation studies. The warming presented due to UHA is the mean pattern, and so may be larger on individual nights or at given stations (e.g. a 1.1°C difference at Shawbury). A degree of spread in UHAI values between stations were found (see Figure 3.7.) and, indeed, several stations do not show any association between the UHAI and upstream building fraction. This may be associated with limitations in the building-fraction methodology, i.e. it does not represent the total urban fraction. However, for stations that do not follow the overall trend, a visual analysis using satellite imagery is often able to explain differences. The distance or circle of influence at which UHA has the greatest effect was also tested finding building fraction within a 0.5-km distance to have the greatest influence on temperatures. This distance is in line with previous theory (Oke 2006) but does not match previous UHA studies that find greater distances (Brandsma et al. 2003, Chapter 2). However, these studies are not directly comparable because of scale and siting differences.

Station temperature data are crucial to comprehending trends in weather and climate. Although rigorous observational standards exist, our results question the representativeness of station siting, particularly for nighttime minimum temperatures taken near urban areas. Out of the 42 Met Office stations analysed, 33 remain operational and therefore potentially contain a UHA bias. The traditional UHI methodology of calculating the temperature difference between an urban and rural station may also be scrutinized. The results demonstrate that a downwind rural reference station, even in an area outside of the main urban areas, may be influenced by local UHA, and so underestimating the total UHI effect.

Chapter 4.

Methodology to separate urban from regional heat advection by use of the Weather Research and Forecasting mesoscale model

This Chapter was published as:

Bassett, R., Cai, X., Chapman, L., Heaviside, C., Thornes, J.E. (2017) ‘Methodology to separate urban from regional heat advection by use of the Weather Research and Forecasting mesoscale model’, *Quarterly Journal of the Royal Meteorological Society*, 143: 2016–2024. doi:10.1002/qj.3062.

RB envisioned and conducted the data analyses, and wrote the paper. XC helped develop the concept. All contributed to proofing the manuscript.

4.1. Abstract

Recent studies have identified the significance of urban heat advection (UHA) as the process whereby heat, originally generated through urban modifications to the Earth's surface, is transported downwind of urban areas. Current techniques to separate UHA from local heat signals do not exclude the additional potential impacts of regional heat advection (RHA). For example, large-scale coastal effects, in addition to latitude and longitude variations, could cause downwind temperature gradients to exist. In this study, the numerical Weather Research and Forecasting (WRF) model coupled with the Building Effect Parameterization (BEP) urban scheme is used to simulate meteorological fields for Birmingham, UK, at a high horizontal resolution (1 km²). The model is run over six case studies to provide over 1600 hours of simulations (called “urban-case”), and evaluated using a unique high resolution dataset from 32 weather stations across Birmingham. The UHA component is decomposed from RHA by conducting a second set of simulations (called “rural-case”), where all urban land use is replaced with vegetation. Simulated directional “rural-case” time-mean temperature fields, that show RHA, are then subtracted from the equivalent “urban-case” time-mean fields. This effectively separates UHA from RHA and shows that a significant portion of heat, previously attributed to UHA in mesoscale modelling, is found due to RHA. Using the new methodology, a UHA intensity up to 1.9°C is found largely confined to within, and several kilometres downwind of, the urban areas. These UHA effects highlight the importance of using wind direction segmentation when determining local climate.

4.2. Introduction

Anthropogenic warming in towns and cities at night is known as the urban heat island (UHI) effect and is recognised worldwide. Urban areas make profound changes to surface properties that contribute to a nocturnal warming that can exceed 10°C in UK conurbations compared to surrounding rural areas (Smith et al., 2011). Modifications which affect local temperatures include: (i) reduced albedo (ii) lack of vegetation, (iii) increased roughness, (iv) larger surface area, (v) heat fluxes from buildings and vehicles, and (vi) building geometries (i.e. radiation trapping in urban canyons). The UHI intensity (UHII) (difference between urban and background rural temperature) is determined by the urban configuration and local meteorology. UHIs are most pronounced under anticyclonic conditions where calm winds and clear skies emphasise the differential heating and cooling rates between urban and rural areas.

Urban conurbations are now home to over half the world's population, higher still in heavily urbanised countries such as the UK: 81.5% (ONS, 2013). The combined effects of excess heat and rising global temperatures means there is an ever-increasing risk to health and public services. Prolonged high temperatures can have adverse effects on human health, particularly amongst vulnerable citizens. Indeed, the severe August 2003 European heatwave is thought to be responsible for up to 70 000 excess deaths (Robine et al., 2008). Heat-health effects during heatwaves are likely to be exacerbated in urban areas where temperatures are further warmed by the UHI. It has been estimated that the UHI effect contributed to around 50% of the excess mortality in the West Midlands region of the UK, during the August 2003 heatwave (Heaviside

et al., 2016). Nonetheless UHIs also present a winter trade-off, e.g. reduced heating requirements (Mavrogianni et al., 2011; Li et al., 2012).

To quantify Birmingham's UHI, the UK's second most populous city (1.1 million inhabitants), several approaches have been taken: (i) remote sensing (Tomlinson et al., 2012; Azevedo et al., 2016), (ii) modelling (Heaviside et al., 2015), and (iii) observations (Unwin, 1980; Johnson 1985; Chapman et al., 2014; Chapter 2). Urban observations, often a challenge within urban environments, have recently become available in the form of a newly installed high-density network of automatic weather stations – BUCL (Birmingham Urban Climate Laboratory, Warren et al., 2016). In addition to determining the static UHI pattern, these observations have also allowed detection of urban heat advection (UHA), i.e. the heat spread from urban areas to surroundings. UHA, or the advection induced UHI component, is thought to occur through either: (i) horizontal heat advection within the urban canopy layer, or (ii) horizontal advection of warm air in the urban boundary layer and then mixed downwards. Whilst UHA has been conceptualised for a number of years (Lowry, 1977) and quantification attempts have been made (Brandsma et al., 2003) it is a common limitation of recent UHI studies to confine results to cities and not consider momentum effects. This is in part due to the majority of UHI studies using a small number of fixed weather stations which are unable to capture how the UHI is advected by wind. However wind direction segmentation has been used to study downwind impacts of UHI on thunderstorm generation (Dou et al., 2015).

A methodology to isolate the UHA intensity (UHAI) was first put forward by Heaviside et al., (2015) using mesoscale modelling. UHA was calculated by removing

the time-mean UHI field from the UHI field associated with a given wind direction, since the temperature at a given location is a function of background temperature (i.e. regional), local effects (i.e. topography and land use) and that advected from upwind sources (i.e. UHA). The methodology effectively separates the temperature created locally from that advected. A key feature of this methodology is that it only needs temperature values at the same height across the area (with a reasonable spatial resolution) as the main input; thus it can also be used to analyse observational datasets. Using this approach Heaviside et al., (2015) found an upwind / downwind temperature difference of approximately 2.5°C in the region around Birmingham during the period of the heatwave in August 2003. This concept was recently adapted further and expanded to cover 20 months of data from the high-density BUC network where a mean downwind warming of up to 1.2°C was found (Chapter 2). However neither of these studies considers the potential impacts of any additional regional heat advection (RHA). Whilst Birmingham is the most land-locked city in the U.K., large-scale coastal effects, in addition to latitude and longitude changes, could cause downwind temperature gradients to exist. These effects are not excluded in the current interpretation of the UHA signal.

This study uses the WRF (Weather Research and Forecasting) non-hydrostatic mesoscale model. WRF has a large range of applications and can be coupled with several urban parameterisation schemes of varying complexity. WRF has already been extensively tested in the urban environment (Loridian et al., 2013; Heaviside et al., 2015) as well as being used to demonstrate how wind can spread heat horizontally (Chemel and Sokhi et al., 2012; Takane et al., 2013). A discussion of the boundary layer, advection and model parameterisations are provided in Chapter 1. However,

high-resolution observation networks, necessary for model evaluation, have not always been available. This is largely due to the challenges and associated cost of network maintenance within cities (Chapman et al., 2014). The BUCL observation network addresses this issue in Birmingham and allows model evaluation to be conducted across a broad range of urban land use types within the urban canopy layer.

By demonstrating the suitability of WRF in reproducing the UHI characteristics in Birmingham, the overall aim of this study is to create a new methodology that removes any RHA effects that were not previously accounted for. This approach, along with wind direction segmentation, will subsequently isolate the mean spatial UHA pattern. By developing this tested UHA modelling approach in Birmingham, it is anticipated that it can be applied in other cities worldwide, especially where high-density urban observations are not available. This insight into UHA will be particularly useful to help city planners combat the effects of excess heat on health and infrastructure. The results for Birmingham and potential application to other cities could also be used to assess the location of long-term climate records and whether UHA bias corrections need to be made.

4.3. Methodology

4.3.1. WRF modelling framework

WRF (Skamarock et al., 2008; version 3.8) was configured to run using four one-way nested domains (Figure 4.1a) at 3:1 grid ratios centred over Birmingham. The coarse, outer domain 1 extends across northwest Europe at 27-km grid spacing. The fine, inner domain 4 covers an area of 91 x 91 km at 1-km resolution. Model time-step was set to 120 s in the outer domain with a 3:1 ratio for the inner domains and hourly output was taken. The NCEP (National Center for Environmental Prediction) FNL (Final) Operational Model Global Tropospheric Analyses data at $1 \times 1^\circ$ horizontal and six-hourly temporal resolution is used for initial and lateral boundary conditions. This NCEP data product is widely used in high-resolution WRF urban studies (Loridian et al., 2013).

The model was set up for longwave radiation using the Rapid Radiative Transfer Model (RRTM; Mlawer et al., 1997). The Goddard (Chou et al., 1994) scheme was selected for shortwave radiation as it was shown to have the best representation of air temperatures, despite a positive shortwave radiation bias (Loridian et al., 2013). This combination of RRTM and Goddard schemes is commonly used in WRF studies (Lee et al., 2011; Flagg and Taylor, 2011). The Noah land surface model (Tewari et al., 2004) that has four vertical soil levels was used for natural rural surfaces and this was coupled with the multilayer Building Energy Parameterization (BEP; Martilli, 2002) for urban surfaces. Energy fluxes are partitioned between the two models using a tiled approach based on urban fraction. This allows a single grid cell to represent surface

heterogeneity and therefore improves model performance (Li et al., 2013), where previously only the dominant land-use category was used. The BEP scheme calculates the horizontal and vertical urban impact on wind, temperatures and turbulent kinetic energy (Martilli et al., 2002). Additionally, through an array of 3D buildings, radiation trapping and differential heating caused by shading in urban canyons are calculated. The BEP scheme has been extensively tested in urban environments (Salamanca et al., 2011; Chemel and Sokhi 2012; Liao et al., 2014; Gutiérrez et al., 2015; Heaviside et al., 2015). However, BEP as a standalone model only considers anthropogenic heat fluxes (AHF) through constant internal building temperatures during simulations. Finally the Bougeault-Lacarrère (1989) planetary boundary layer parameterisation scheme is used because it is designed for use with the BEP urban canopy model.

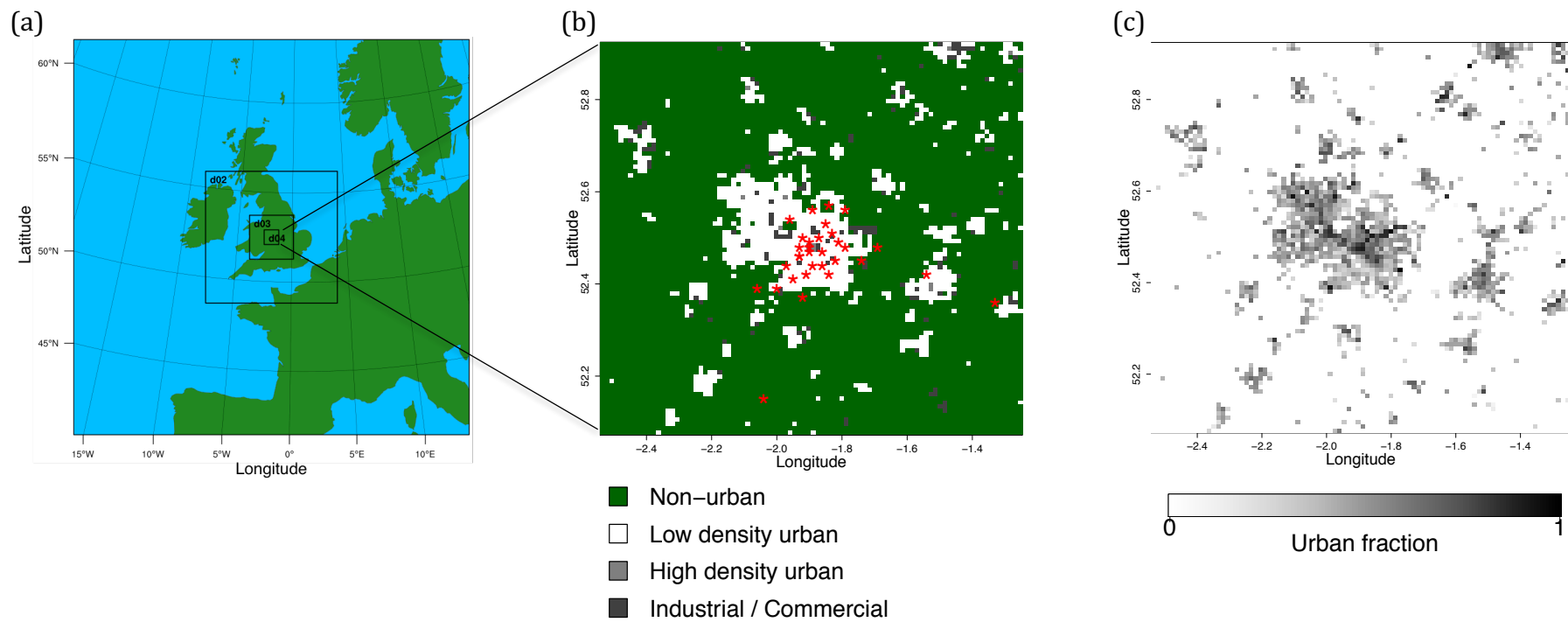


Figure 4.1. (a) Nested configuration of WRF domains at 27, 9, 3 and 1-km resolutions. (b) Domain 4 land use adapted from Corine land cover. The red stars are the location of the observation BUCL and Met Office stations in the region. (c) Domain 4 urban fraction created using a NDVI image taken in July 2013.

4.3.2. Land use and urban canopy parameters

The US Geological Survey (USGS) 24-category land-use data was used for the outer 3 domains. Corine Land Cover 2012 (CLC, 100 m spatial resolution) was used for the inner domain and reclassified for rural land-use categories using equivalencies defined by Pineda et al. (2004). The CLC urban land-use categories were refined into three urban land classes used by the BEP parameterisation: (i) low intensity residential (CLC: Discontinuous urban fabric; Road and rail networks and associated land; Construction sites), (ii) high density residential (CLC: Continuous urban fabric) and (iii) commercial (CLC: Industrial or commercial units). The remaining CLC urban categories (e.g. green urban areas) were assigned to the USGS category Dryland Cropland and Pasture. Satellite imagery checks showed these categories to be largely vegetated. Furthermore, these “urban” categories do not occupy large surface areas and therefore it would not be significant when viewed at a 1-km WRF model resolution. The resulting land use using the dominant category for each 1 x 1 km grid square for the inner domain 4 is shown in Figure 4.1b.

A 250 m resolution Normalized Vegetation Difference Index (NDVI) image was used to calculate gridded urban fraction for the inner domain (Figure 4.1c). This use of NDVI as a proxy for urban fraction (normalised to between 0 (rural) and 1 (urban)) uses the same approach as Chapter 2. An NDVI image from July 2013 was used to represent urban fraction. The default WRF-BEP model is configured using generalised urban parameters. However, these are not specific to the study region and BEP specifically requires 3D building and street geometry distributions for each urban land-use category. To provide this level of detail, 3D Ordnance Survey (OS)

building data is used. The OS data contains building height and areas for individual buildings across most urban regions in the UK. For each of the three BEP land-use classes in Birmingham, the mean building widths and building heights are calculated using the OS data (Table 4.1).

However, street width calculations are less straightforward. The OS building data effectively contains two sets of information: (i) total building area and (ii) total area. The totals and means can be calculated for each urban land-use class. Subtracting the total building area from the total area leaves the total non-building area. However, if the mean street width is calculated from total non-building area (weighted by the total number of buildings in that category), this would over-estimate street widths, i.e. widths would be calculated in areas containing green space. Therefore, the urban fraction is used to weight the total area in each urban land-use category to that only covered by urban surfaces, and allows for a more accurate calculation of street widths. Street widths are important because a sub-tiling approach is implemented whereby BEP calculates fluxes in urban areas, and the remaining portion of a given grid cell is calculated by the Noah land surface model. The remaining thermal and radiative parameters used in BEP are taken from Urban Zones to characterize Energy partitioning (UZE: Loridian and Grimmond, 2012; Loridian et al., 2013). Whilst UZE parameters are created for London it is assumed that the building stock between Birmingham and London, located approximately 100 miles apart, does not vary considerably.

Table 4.1. Calculated building morphology parameters: building height (H) quartiles (Q), building width (W_B), street width (W_S) and urban fraction (ufrac).

	Q1 & 2 H (m)	Q3 H (m)	Q4 H (m)	W_B (m)	W_S (m)	Ufrac (0 – 1)
Low intensity residential	5.1	8.5	11.0	7.3	11.1	0.43
High density residential	6.2	10.3	16.5	13.4	14.4	0.74
Industry / commercial	5.0	8.2	9.7	17.9	28.8	0.58

4.3.3. WRF simulations

In total, six simulations covering a total of 67 days were run across Summer 2013 (Table 4.2.). The case studies were chosen because they contain periods of stable weather conditions that are favourable to UHI development. For each simulation period a second run (called “rural-case”, in contrast to “urban-case” for the first run) is conducted whereby the urban land use across all domains is replaced with USGS category Dryland Cropland and Pasture. A similar approach, albeit using urban and pre-urban land use, was used by Comarazamy et al. 2013. The rural-case simulation is used as part of the calculation to separate UHA from RHA described in Section 4.4. The first 12 h of each simulation are disregarded to account for model spin-up. The hourly model output for night-time hours (2100 – 0500 UTC) and low wind speeds ($< 5 \text{ m s}^{-1}$) are chosen for the analysis. Additionally, using the WRF output variable QCLOUD (column liquid water content) simulation hours where the sky is overcast (8 Oktas) are excluded. This filtering (leaving 450 h data) is conducted to limit the analysis to weather conditions that are favourable to UHI and hence UHA development.

Table 4.2. WRF simulation periods, run for each urban and rural case.

Meteorological data for the mean of each period were taken from Coleshill weather station (located in the centre of domain 4: Latitude 52.4801, Longitude -1.69072).

	Temperature (°C)	Wind speed (m s⁻¹)	Relative humidity (%)	Cloud cover (oktas)	Sea-level pressure (mb)
2013					
30 April - 08 May	10.9	3	67.6	2.7	1018.7
30 May - 08 June	12.3	3.5	73.9	3.5	1023.9
02 July - 23 July	18.7	2.4	71.7	2.7	1023.3
25 August - 06 September	16.2	2.6	76.9	4	1020.4
2014					
13 May - 20 May	16.2	2.6	76.9	4	1020.4
20 July - 27 July	19.6	2.8	71.7	2.9	1018.3
Mean	15.6	2.8	73.1	3.3	1020.8

4.3.4. Surface observation networks

Observations for the model evaluation are taken from two observation networks: (i) BUCL, installed in 2013 and (ii) Met Office MIDAS surface station network. The BUCL network contains 25 automatic weather stations (Vaisala WXT520, accuracy of $\pm 0.3^{\circ}\text{C}$ at 20°C : Vaisala, 2012) located across Birmingham. The high-density, urban nature of the BUCL network was specifically designed to study urban climate features. Within Birmingham the network has approximately one WXT station per 3-km^2 area with observations taken at 3 m above ground across a range of different land-use types. A full description of the network, including calibration and quality control checks can be found in Chapman et al. (2014) and Warren et al. (2016). The BUCL network is supplemented by surface observations at 7 Met Office stations, accessed through the British Atmospheric Data Centre (BADC). A full list of the

stations used in this study can be found in Table 4.3 and spatial distribution shown in Figure 4.1b. To assess model performance, the mean of the nearest four modelled grid cells in domain 4 to each observation, inverse weighted by distance, was calculated. For comparisons, three statistical measures were used: (i) Pearson's Correlation Coefficient (r), (ii) Mean Bias Error (MBE), and (iii) Root Mean Square Error (RMSE). The evaluation was conducted using all model hours over the six urban simulations.

Table 4.3. Station metadata and evaluation statistics. The following abbreviations are used: BUCL (Birmingham Urban Climate Laboratory), MO (Met Office), RMSE (Root Mean Square Error), r (Pearson’s Correlation Coefficient), MBE (Mean Bias Error) and n (number of hourly observations). The locations of the stations are shown in Figure 4.1b.

Station	Network	Latitude	Longitude	Altitude (m)	RMSE (°C)	r	MBE (°C)	n
W001	BUCL	52.57	-1.84	119	2.39	0.94	-1.23	1394
W002	BUCL	52.39	-2.06	187	1.92	0.93	-0.64	1233
W003	BUCL	52.54	-1.96	104	2.10	0.94	-0.73	1394
W004	BUCL	52.37	-1.92	202	2.13	0.92	-0.71	1069
W005	BUCL	52.44	-1.86	158	1.95	0.94	-0.53	828
W006	BUCL	52.50	-1.92	132	1.62	0.95	-0.27	1390
W007	BUCL	52.49	-1.90	134	1.65	0.95	-0.09	1257
W008	BUCL	52.44	-1.97	168	1.56	0.95	-0.03	1415
W009	BUCL	52.47	-1.86	123	1.71	0.93	-0.08	1103
W010	BUCL	52.48	-1.93	157	1.33	0.95	-0.46	587
W011	BUCL	52.39	-2.00	190	1.75	0.93	0.03	1085
W012	BUCL	52.42	-1.91	134	1.46	0.95	-0.65	429
W013	BUCL	52.47	-1.90	125	1.37	0.96	0.32	316
W014	BUCL	52.42	-1.84	141	1.62	0.94	-0.05	1048
W015	BUCL	52.51	-1.83	98	1.32	0.96	0.05	316
W016	BUCL	52.45	-1.82	130	1.26	0.95	-0.14	587
W017	BUCL	52.48	-1.79	101	1.59	0.94	-0.08	886
W018	BUCL	52.49	-1.81	100	1.68	0.93	-0.10	882
W019	BUCL	52.50	-1.87	110	1.38	0.96	-0.30	316
W020	BUCL	52.53	-1.85	140	1.76	0.94	-0.55	1233
W021	BUCL	52.56	-1.89	173	1.36	0.95	-0.52	587
W022	BUCL	52.41	-1.95	150	1.40	0.96	-0.24	316
W023	BUCL	52.56	-1.79	122	1.46	0.96	-0.37	316
W026	BUCL	52.46	-1.93	150	1.83	0.93	-0.44	827
W027	BUCL	52.44	-1.89	158	1.37	0.96	-0.57	581
Church Lawford	MO	52.36	-1.33	107	1.78	0.95	-0.27	1410
Coleshill	MO	52.48	-1.69	96	1.81	0.95	-0.54	1415
Coventry Coundon	MO	52.42	-1.54	119	1.69	0.95	-0.46	1414
Elmdon	MO	52.45	-1.74	96	1.90	0.94	-0.12	1415
Paradise Circus	MO	52.48	-1.90	139	1.71	0.95	0.38	1379
Pershore	MO	52.15	-2.04	35	1.90	0.95	-0.45	1412
Winterbourne	MO	52.46	-1.93	140	1.87	0.95	-0.75	1412

4.3.5. Urban heat advection

Observational studies have demonstrated that horizontal wind flow can transport heat generated by UHIs downwind (Brandsma et al., 2003; Chapters 2 and 3). In order to separate the modelled UHA effect from UHI pattern (Figure 4.2b), a methodology was put forward by Heaviside et al. (2015). Although its first application was for analysis of modelled output, this diagnosis type of methodology, by its nature, has an advantage of being suitable also for analysing measured data (Chapter 2). The key idea of this method is to subtract the time-mean temperature field (all wind directions, $\overline{\Delta T}$) from the time-mean temperature field for a given wind direction ($\overline{\Delta T^{(\theta)}}$, where θ : NE, SE, SW, NW). This effectively separates the advection-induced UHI ($\overline{T_{UHA}^{(\theta)}}$) from the local heating component created by the underlying land use:

$$\overline{T_{UHA}^{(\theta)}} = \overline{\Delta T^{(\theta)}} - \overline{\Delta T} \quad (1)$$

In order to further isolate the local UHA from regional effects, we used a modified procedure, detailed as following. Similar to Heaviside et al. (2015), each simulation hour was categorised into one of four wind directions using the cross-domain-mean 10 m wind direction. Within each wind direction group, the time-mean 2 m temperature field was calculated for both “urban-cases” ($\overline{T_{urban}^{(\theta)}}$) and “rural-cases” ($\overline{T_{rural}^{(\theta)}}$). The time-mean temperature field from all four wind direction groups, shown below in Equation 2, was then taken to create an overall time-mean temperature field for urban-case ($\overline{T_{urban}}$) and rural-case ($\overline{T_{rural}}$) simulations. This approach was used

to account for biases in the number of wind directions in the simulations (see Table 4.3).

$$\overline{T_{urban}} = \frac{\overline{T_{urban}^{NE}} + \overline{T_{urban}^{SE}} + \overline{T_{urban}^{SW}} + \overline{T_{urban}^{NW}}}{4} \quad (2a)$$

$$\overline{T_{rural}} = \frac{\overline{T_{rural}^{NE}} + \overline{T_{rural}^{SE}} + \overline{T_{rural}^{SW}} + \overline{T_{rural}^{NW}}}{4} \quad (2b)$$

To exclude any non-urban advection components from the time-mean UHI pattern ($\overline{\Delta T}$), the rural-case time-mean was subtracted from the urban-case time-mean, indicated in Equation 3. This effectively removed any local or regional heat patterns that are not caused by urbanisation. The same subtraction was then processed for each directional time-mean, shown in Equation 4. The outputs of Equation 3 were then subtracted from Equation 4. The resulting temperature field, $\overline{T_{UHA}^{(\theta)}}$ in Equation 5, was considered the deviation from the time-mean due to horizontal wind advecting heat from urban areas ($\overline{T_{UHA}^{\theta}}$). This field does not contain the RHA effects as these will have been removed by subtraction of the rural-case time-mean.

$$\overline{\Delta T} = \overline{T_{urban}} - \overline{T_{rural}} \quad (3)$$

$$\overline{\Delta T^{(\theta)}} = \overline{T_{urban}^{(\theta)}} - \overline{T_{rural}^{(\theta)}} \quad (4)$$

$$\overline{T_{UHA}^{(\theta)}} = \overline{\Delta T^{(\theta)}} - \overline{\Delta T} \quad (5)$$

Finally, the cross-domain mean value of $\overline{T_{UHA}^{(\theta)}}$ was subtracted from each modelled UHA output to correct for small temperature biases between different wind directions, and therefore allowing comparisons on the same temperature scale (i.e. the resulting fields have a zero value for the domain average). The resulting UHAI ($\overline{T_{UHA}^{(\theta)}}$) therefore represents the departure of temperature from the long-term mean due to advection of the UHI. A negative value indicates cooler than the mean, and a positive value indicates warmer (n.b. these will switch with opposing wind directions).

4.4. Results and discussion

4.4.1. Model evaluation

In order to demonstrate the suitability of using the WRF-BEP model for urban temperature predictions in Birmingham, modelled 2 m hourly air temperatures are evaluated against observations. Overall model performance (presented in Table 4.2) is good with RMSE values obtained for the simulations similar to those found other WRF urban studies (e.g. Liao et al., 2014; Heaviside et al., 2015). Mean RMSE across all stations is 1.68°C and MBE -0.33°C. Differences between observed and simulated temperatures could be explained by inherent challenges assessing point observations against model simulations at 1-km resolution. For example, the local land use surrounding an observation creates its own local climate, where as the model configuration uses coarser land use. Additionally, building geometries and distributions in the model are generalised into three categories, far simpler than the multitude of urban configurations found in reality. For example, the model performs

noticeably worse at station W001 which, on inspection, is located at the edge of Sutton Park (a large semi-rural park on the periphery of the city) and therefore the model does not fully represent the local land use at this station.

4.4.2. Urban Heat Island

UHII is normally calculated by subtracting the temperature at a reference rural weather station from an urban weather station (Stewart, 2011). UHI modelling has the advantage that a rural reference can be effectively provided at every grid point, in this case by use of the “rural-case” simulations where all urban areas have been replaced with vegetation. Two time-mean temperature fields are therefore created using the mean of six urban-case and six rural-case simulations respectively. The temperature difference between the urban-case and rural-case time-mean temperature fields at each grid cell is calculated during night-time hours (2100 – 0500 UTC). The difference between these two time-mean patterns is interpreted as the time-mean UHI field (Figure 4.2a). However, whilst the same wind categorisations for the urban and rural cases are used, a limitation is noted that for the rural-case, removing all urban components (and associated changes in surface roughness) could change wind flows in the domain.

The largest mean UHIIs, up to 2.9°C, are found in the centre of Birmingham. Notable UHIIs are also present in smaller conurbations surrounding Birmingham, for example Coventry. Overall the spatial UHII pattern is consistent with other studies in the region (Tomlinson et al., 2013; Heaviside et al., 2015; Azevedo et al., 2016). It should be noted the pattern in Figure 4.2a is the mean nocturnal pattern and therefore

higher UHIs could be experienced on individual nights. The time-mean UHI field also shows evidence of UHA. This can be seen clearly as the glow in temperatures that extend outwards from Birmingham (Figure 4.2a), which does not show any directional signal.

To illustrate how the spatial time-mean UHI pattern can change with wind direction, the urban-case and rural-case time-means temperature fields are then split by wind direction (θ : NE, SE, SW, NW). This categorisation is based on the cross-domain 10 m wind direction for each simulation hour, following the methodology in Heaviside et al. (2015). Isolating the time-mean UHI by wind direction (Figure 4.2b) shows two notable features: (i) the UHI core shifts downwind of the urban centre for all wind directions, and (ii) the UHI differs between wind directions. Whilst simulations are filtered into night-time hours, wind speeds less than 5 m s^{-1} and excluding periods where the sky is completely overcast, differences still exist within the categories (Table 4.3). For example the mean wind speed is lowest from the SW and highest from the NE. These correspond to the smallest and largest UHIs respectively. Secondly, and similarly to the heat glow shown for the time-mean UHI in Figure 4.2a, evidence of UHA can be seen at the downwind edge of all plots shown in Figure 4.2b. The outwards heat spread from the urban areas appears strongest for the SW and SE cases where the wind speed is lowest, i.e. there is a higher UHI component to be advected. The presence of UHA is further explored in the following section by effectively decomposing the local heating component (UHI) from the advected heat component.

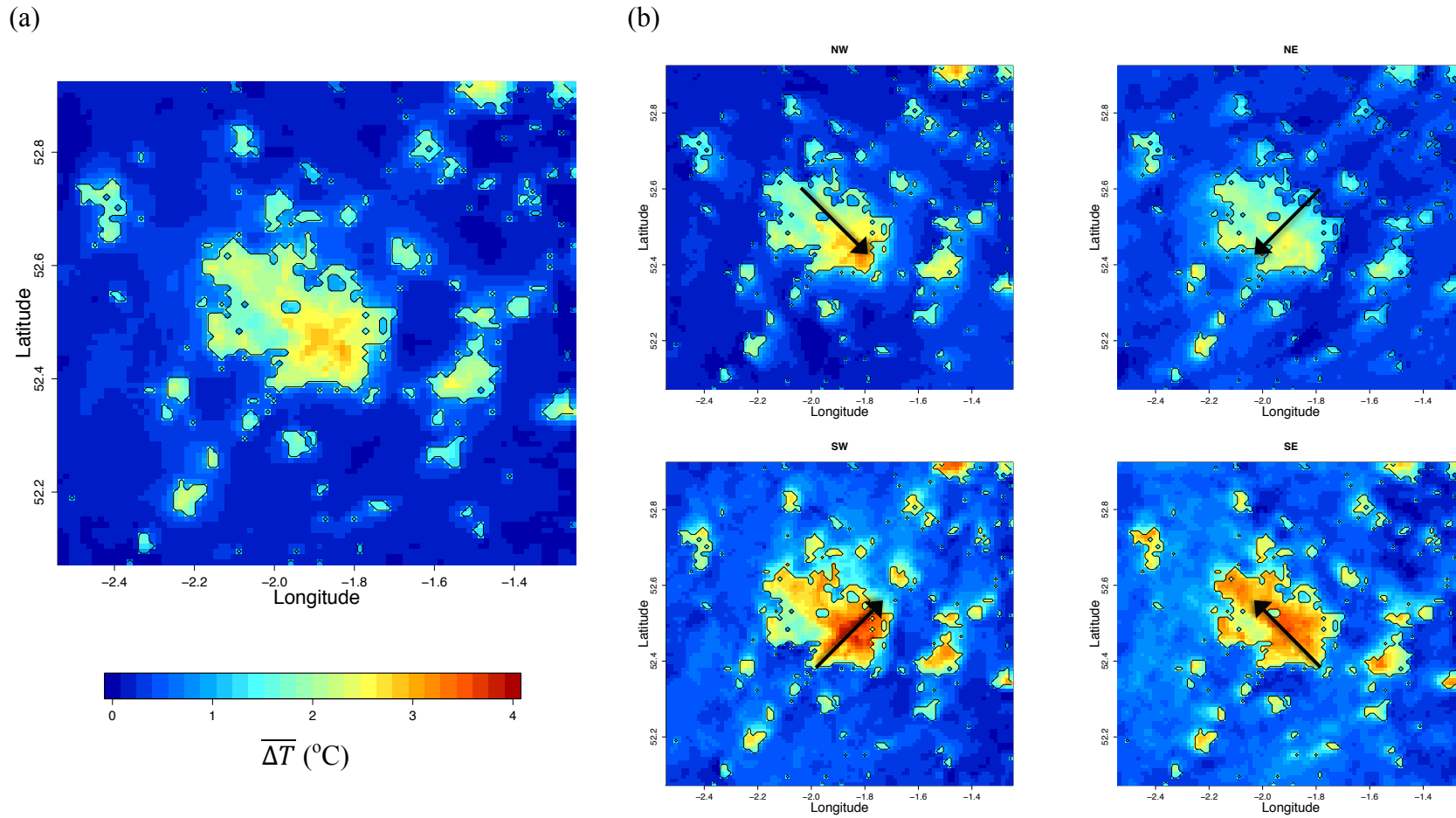


Figure 4.2. (a) Time-mean UHI field ($\overline{\Delta T}$, domain 4). The black lines represent the urban land-use boundaries. (b) Directional time-mean UHI pattern. Each image is the difference between the time-mean urban and time-mean rural-case simulation for a given wind direction (θ : NE, SE, SW, NW).

Table 4.4. Number of simulation hours and characteristics in each wind direction group.

	NE	SE	SW	NW
Simulation hours	156	42	37	215
Mean wind speed (m s^{-1})	3.6	2.4	1.8	2.8
Mean wind direction (deg)	40.6	127.9	237.0	326.3

4.4.3. Urban Heat Advection

The UHAI results using the original methodology put forward by Heaviside et al. (2015) are presented in Figure 4.3a here. The results show that there is an approximate diagonal divide across the domain between downwind warming and upwind cooling. The upwind / downwind temperature differences are slightly smaller than found by Heaviside et al. (2015). This could be due to the 67 nights of mild UHI events in 2013 and 2014 used here instead of 10 days of strong UHI event during the 2003 severe heatwave period used in Heaviside et al. (2015). Whilst this methodology quantifies upwind / downwind temperature differences, at larger scales it fails to account for regional-scale heat advection.

In order to address this issue, the original methodology is improved by subtracting the mean hourly temperature output of “rural-cases” from those of “urban-cases”. The “rural-case” results presented for domain 4 in Figure 4.3b show it is clear that the upwind /downwind temperature difference is present in each wind direction, although at a reduced magnitude to the simulations that contain urbanisation. As there is no urban land use in this “rural-case” simulation, there are still regional advection

processes at play. These RHA results show a similar pattern to the UHA results found by Heaviside et al. (2015), and in this study we propose a modification to refine the methodology in order to separate UHA from RHA (see Section 4.3.5).

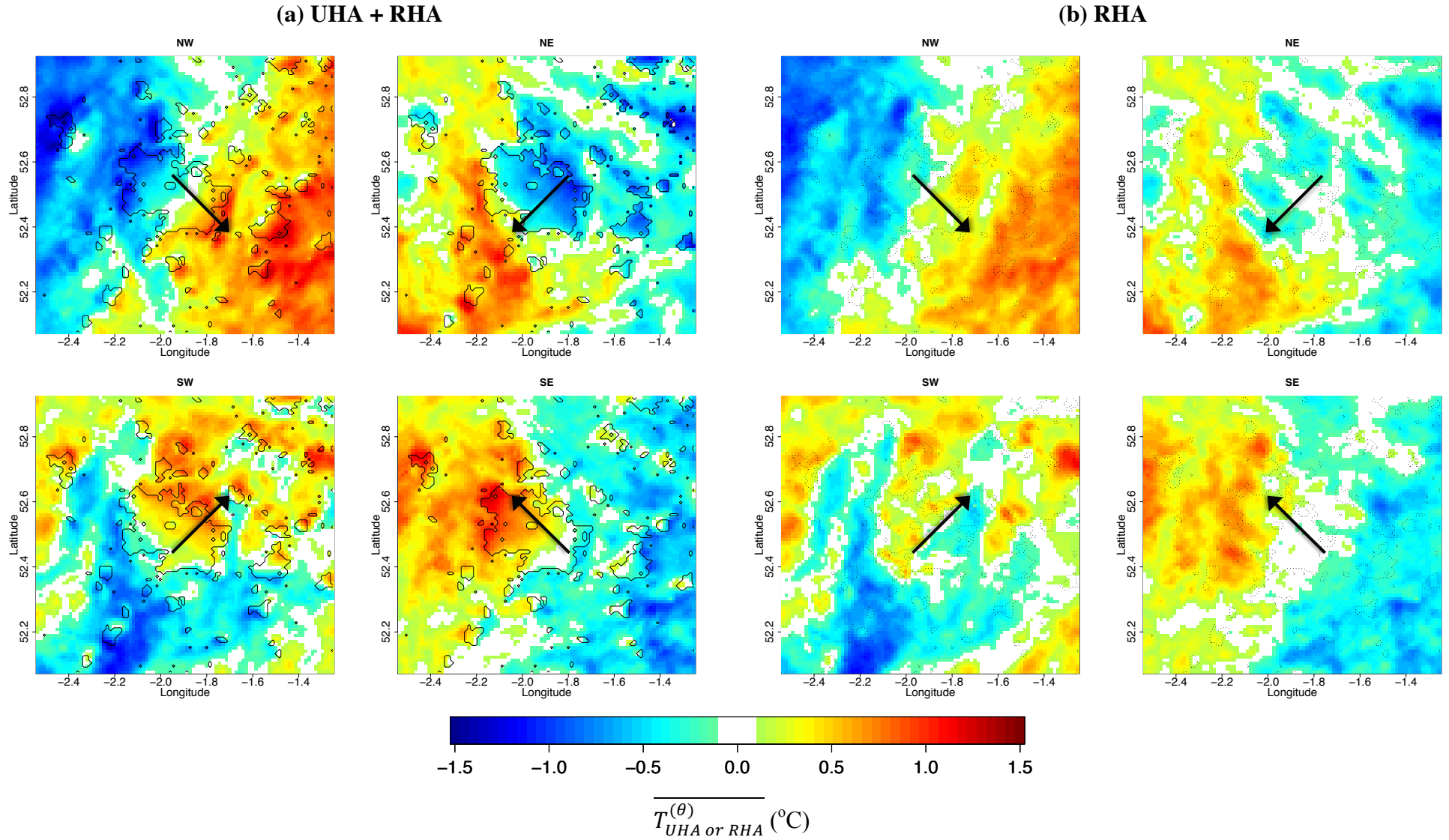


Figure 4.3. (a) Time-mean UHAI ($\overline{T_{UHA}^{(\theta)}}$) effects (domain 4) derived using the methodology from Heaviside et al. (2015). This methodology also contains RHA information. The thin black curves represent the urban land-use boundaries and thick black arrows represent mean wind direction. UHAI values between -0.1 and 0.1 are not displayed because these could be natural temperature fluctuations. (b) Regional heat advection (RHA) effects calculated using the UHA methodology from Heaviside et al. (2015) on the rural-case time-mean simulations only. The dashed black lines represent where the urban areas have been removed.

The UHAI results using the new methodology to separate UHA from RHA are presented in Figure 4.4. In all four wind directions a clear positive UHAI ($\overline{T_{UHA}^{(\theta)}}$) signal of up to 1°C degree is found downwind of the urban areas. The UHA signal is not only restricted to Birmingham, but can be found downwind from smaller urban areas within the domain. A positive UHAI value effectively contains half the advection-induced UHI, whilst negative values are a construct of half the advection-induced UHI from the opposite wind directions. The total UHAI component is therefore the difference between these two values and is calculated using domains with opposing wind direction, i.e. NW-SE and NE-SW. To quantify the UHAI totals, the 75th percentile and the maximum UHAI across the domain are adopted. For the NW-SE direction, these two respective values are 0.5°C and 1.4°C, and for the NE-SW direction, these are 0.6°C and 1.9°C, respectively. The UHA signal is shown to extend up to approximately 8 km on the SW case. However the exact UHA distance is difficult to determine due to the land-use complexity.

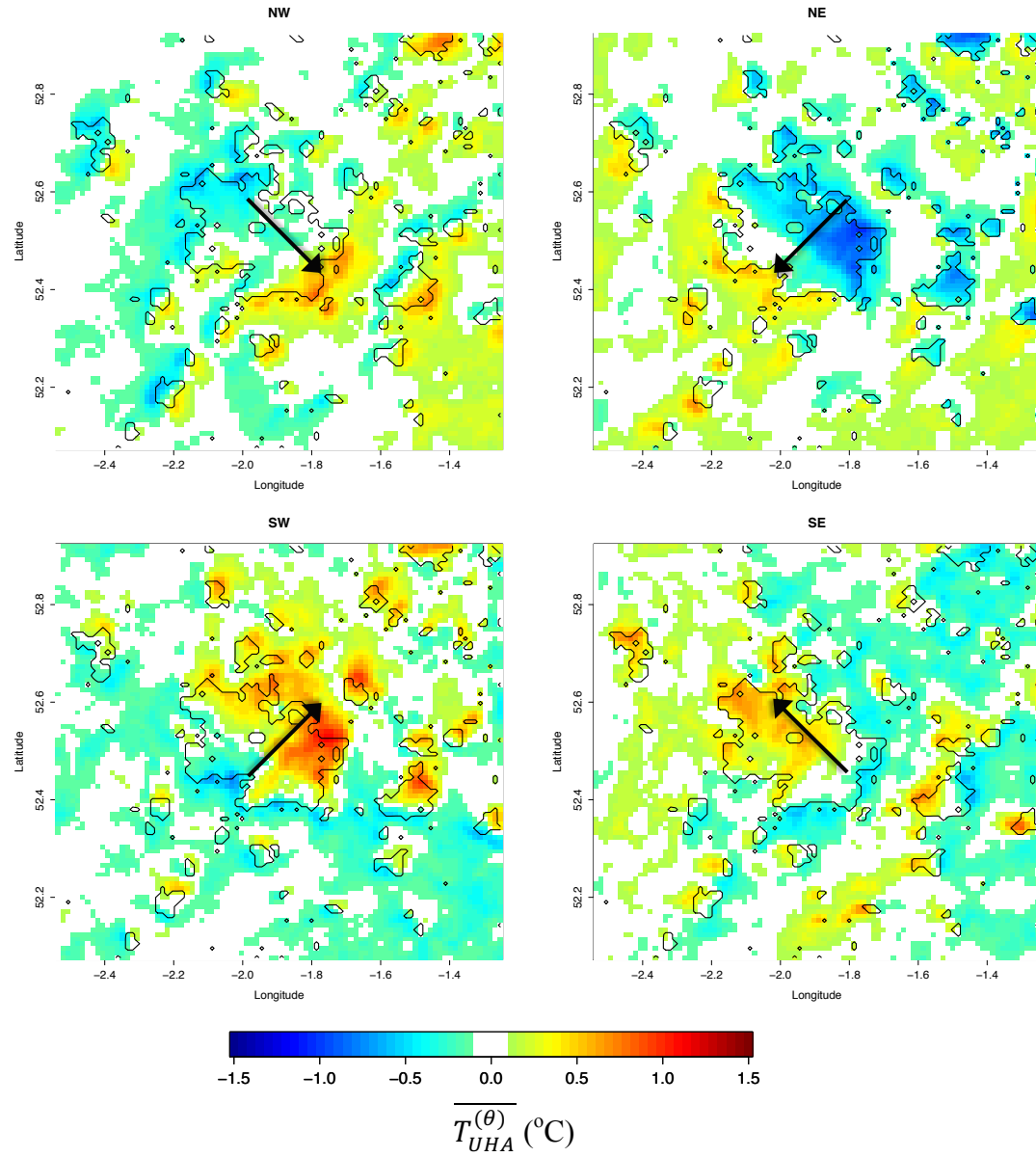


Figure 4.4. Time-mean UHAI ($\overline{T_{UHA}^{(\theta)}}$) effects (domain 4) derived using the new methodology where RHA has been excluded. The black lines represent the urban land-use boundaries and arrows mean wind direction. UHAI values between -0.1 and 0.1 are not displayed because these could be natural temperature fluctuations.

Although taking the mean of six case studies has improved the directional representation of UHA, the resulting UHA pattern is not symmetrical. This may be attributed to unevenly distributed wind conditions across quadrants, as shown in Table 4.4. Although the UHA pattern is calculated using a minimum of 37 nocturnal simulation hours in each direction (Table 4.4), this suggests that longer simulations are still required. However, the present results are an improvement over Heaviside et al. (2015) where RHA was not excluded and UHA was not present in all wind directions due to a limited number of cases in certain directions over the time period studied. If wind and stability conditions were identical across all categories, the methodology would produce an opposite spatial pattern in opposing wind directions. Overall, once RHA effects are removed (Figure 4.4), the UHAI is less extensive than found using the previous methodology (Figure 4.3a). The improved UHA methodology shows UHA to be more confined to immediate rural surroundings and within the urban boundaries. However, to explore the exact UHA contributions from urban areas of different sizes, it is suggested that idealised cases are needed to exclude complex urban land-use patterns.

4.5. Conclusions

Previous attempts to model UHA attempted to separate local and regional effects. Whilst over short distances the RHA effect is not large, when a 91 x 91 km domain is considered it could be easy to confuse this with UHA, especially if the domain is centred over an urban area. Here, an existing methodology is extended to characterise UHA, based on separating the time-mean temperature field across an urban area from temperature fields classified by each of four wind directions. The new methodology

detailed here utilises the temperature output from “rural-case” as well as “urban-case” simulations, which allows us to successfully separate UHA from RHA.

The WRF-BEP model configuration is run over several time periods across the Birmingham region, totalling 67 days. This enabled a time-mean UHI field with sufficient hourly data compared with previous UHA modelling studies to be created. The method applied to the modelling results to isolate the UHA signal involves subtracting a duplicate “rural-case” time-mean simulation in which all urban land-use types are replaced by a vegetation category. UHA effects are shown to be largely confined to within and near the edges of urban areas, but can be extended to approximately 8-km downwind. Overall the total warming caused by UHA, depending upon wind direction, is up to 1.9°C for the simulated periods. The results show UHA is not confined to Birmingham's surroundings but is also present adjacent to small urban areas within the domain.

Whilst this new methodology is an improvement over previous modelling attempts, there are still limitations. For example, as wind direction biases are accounted for in the methodology, wind speed biases within categories still have an effect on results. Although the data are filtered to speeds less than 5 m s⁻¹, there are still differences in speed between wind direction categories. However, there are too few hours of data to allow further classification, even though a total of 67 days simulations are available. This is particularly noticeable in the results because the UHAI at a given location contains information from opposing wind directions. To overcome this, simulations would need to be conducted for longer time periods. It would be expected that increasing the number of simulation hours would reduce these directional biases.

However, this is constrained by computational requirements. Additionally, replacing all urban land-use types directly with a vegetation category may alter wind flows in the domain due to changes in surface roughness. It is also difficult to determine exact UHA contributions with distance from urban areas. This is largely because of the complexity of the urban pattern in the region, and therefore UHA could originate from multiple sources. It is therefore suggested that idealised simulations are needed to simplify the urban pattern. This has the added benefit that wind speeds and directions can be controlled, therefore eliminating any biases.

Despite limitations, this UHA modelling highlights the necessity to consider wind direction when calculating temperatures in or around urban areas. As long as there are an adequate number of simulation hours this methodology can be put into practice using mesoscale modelling on any urban area worldwide. With ever increasing urban populations there is a compelling need to spatially quantify excess heat and its impacts on health and infrastructure. Indeed, urban heat effects can exceed climate projections over the next century. The results could also be extremely useful for siting or correcting long-term temperature measurements taken near cities that do not previously account for UHA biases.

Chapter 5.

Semi-idealised urban heat advection simulations using the WRF mesoscale model

This Chapter has been submitted for publication as:

Bassett, R., Cai, X., Chapman, L., Heaviside, C., Thornes, J.E. (Submitted) ‘Semi-idealised urban heat advection simulations using the WRF mesoscale model’.

RB envisioned and conducted the data analyses, and wrote the paper. XC helped develop the concept. All contributed to proofing the manuscript.

5.1. Abstract

Urban heat advection (UHA) can extend a city's impact on air temperature to the surrounding countryside. This may lead to an intensification of already well-documented UHI impacts on health and infrastructure, and challenge the representativeness of long-term temperature records taken near urban areas. However, previous UHA studies have been unable to accurately quantify UHA due to challenges arising from complex urban land-use patterns. To address this, the numerical Weather Research and Forecasting (WRF) mesoscale model coupled with the Building Energy Parameterization urban canopy scheme is used to simulate meteorological fields for idealised land-use cases. Hypothetical square cities (up to 16 km in size) are simulated using 450 hours of real night-time weather data. A time-mean 2 m temperature field (representing the canopy UHI) shows that the mean UHI intensity (up to 3.6°C) is linearly related to the logarithm of city size. A UHA methodology was then applied to the temperature fields to separate UHA from the UHI, with up to 2.4°C of UHA found downwind of largest city size. For this hypothetical city size, an UHA intensity of 0.5°C is found up to 9-km downwind from the urban boundary. In addition, the UHA-distance profiles along the central horizontal transect for various urban sizes are found to follow a scaling rule as a good approximation. Based on this finding, a UHA model is developed and can be used to estimate UHA without the need for complex, computation-intensive simulations. This UHA model has practical benefits, for example, to estimate UHA effects in areas not currently considered at risk, i.e. outside the traditional UHI concept. The UHA model could also be used to assess the extent of “contamination” of climate records by

nearby urban settlements. The model may also help mitigate heat-health and infrastructure risks, particularly when combined with a changing climate.

5.2. Introduction

The urban heat island (UHI) is a zone (the “island”) of warmer air and surface temperatures caused by differential heating and cooling rates between urban and rural land-use types. Typically, the air temperature in cities can be several degrees warmer than rural surroundings, and up to 10°C in extreme cases (e.g. 7°C Singapore, Chow and Roth, 2006; New York 8°C, Gedzelman et al., 2003; Mexico City 8°C, Jauregui, 1997; Vancouver 10°C, Runnalls and Oke, 2000). The size of this temperature difference, the UHI intensity (UHII), is greatest at night under the conditions of clear skies and calm winds. The UHII is also a function of the logarithm of urban size, demonstrated using population as a proxy for urban size (Oke, 1973). Comparable studies have found similarity in their relationship between the UHII and population, however the slope of this relationship fluctuates (e.g. Park, 1986; Santamouris, 2015). This is due to different city forms (i.e. European versus Asian cities) and observational techniques.

The UHI may benefit society in cold climates, i.e. reduced energy consumption (Santamouris et al., 2001), and negatively impact it during summer due to excess heat. Any adaptation strategies should take both effects into consideration, i.e. mitigating heat without removing the winter benefits. UHI disadvantages include health risks, particularly during heatwaves (Stone et al., 2010; Heaviside et al., 2016); and infrastructure, e.g. railway buckling (Chapman et al., 2013; Ferranti et al., 2016). The

UHI may initiate thunderstorms (Bornstein and Lin, 2000; Dou et al., 2015), and increase precipitation (Shepard et al., 2002; Dixon and Mote, 2003). The UHI can also corrupt long-term climate records (Kalnay and Cai, 2003; Parker and Horton, 2005; Wickham et al., 2013). Therefore, understanding the dynamic, spatial nature of the UHI is particularly important to fully quantify risk due to the UHI. This is compounded by the fact that over half (and set to rise) of the world's population is now urbanised, and many areas are already at risk from a changing climate.

The transport of heat to areas downwind of the UHI by a horizontal wind flow is known as urban heat advection (UHA). Whilst traditional theories suggest that the UHI is dispersed vertically to form an elevated urban plume (Oke, 1982), as supported by downwind airborne observations (Dirks, 1974; Wong and Dirks, 1978), UHA is also present at the near-surface level. This is due to: (i) horizontal heat movement within the urban canopy layer (i.e. below roof level), and (ii) downwind mixing of elevated heat downwards by turbulent eddies. Although surface-level UHA has been hypothesised for a while (Lowry, 1977) and acknowledged in several UHI studies (Brandsma et al., 2003; Brandsma and Wolters, 2012; Unger et al., 2010), UHA is rarely considered as the subject of UHI studies. This is in part due to a lack of spatial information caused by an observational paucity within the urban environment. Challenges associated with siting and maintaining urban meteorological networks are discussed in Muller et al. (2013) and Chapman et al. (2014). Another obstacle is the lack of an effective approach to enable one to separate the UHA from measured UHI data, because the air temperature at a given location is influenced by a combination of locally generated heat (i.e. due to underlying land use, topography and aspect) and the heat transported from upwind sources.

Nevertheless, recent observational (Chapters 2 and 3) and modelling (Heaviside et al., 2015; Chapter 4) studies have overcome some of these challenges by developing and refining a methodology to separate UHA from the background UHI data. Detailed in the methodology, a time-mean temperature field (where all wind directions were considered) represents the background temperature, and a time-mean temperature field (for a chosen wind direction) represents the departure from the background temperature. For a given location with an upwind urban area, the difference between these two fields was attributed to the UHA.

This methodology was successfully tested on a high-density urban observation network where a UHA intensity (UHAI) up to 1.2°C was found for the city of Birmingham, UK (Chapter 2; details of the high-density urban observation network can be found in Warren et al. 2016). The UHA methodology was also shown to hold at a smaller (village) urban scale (Chapter 3). However, although the UHA methodology was suitable to decompose temperatures into local and advected components at a local-scale, it failed to account for regional heat advection (RHA). Due to the island nature of the UK where the methodology was developed, RHA may be particularly pronounced (i.e. large-scale coastal effects). However, for modelling, this was overcome by conducting a second set of rural simulations that effectively removed any RHA effects (Chapter 4).

Whilst previous UHA studies were able to show the significance and general UHA spatial pattern, the exact UHAI was difficult to determine due to the complexity of spatial pattern of urban (and rural) land use. For example, temperature at a given

location may be influenced by multiple upwind UHA sources. Furthermore, UHI processes occur across a range of scales. At smaller scales, shading from buildings or trees could introduce large temperature differences across street canyons that could exceed the UHAI. Additionally, these UHA studies hypothesised a symmetrical pattern between UHAI in opposing wind directions. However, the asymmetric urban land-use patterns used meant the results only partially matched this.

In order to address issues caused by complex urban land use, the non-hydrostatic Weather Research and Forecasting (WRF) model is applied to semi-idealised urban land-use cases (i.e. simplifying the land use but retaining real meteorology). WRF is a community-based model equipped with several urban parameterisations that have been extensively tested on the urban environment (Chen et al., 2011; Loridian et al., 2013). This paper presents the first study of to apply the UHA methodology to simplified, idealised cities. The overall aim is to quantify how both the UHI and UHAI change with urban size. The results will be used to develop a simple statistical model that can be used to estimate UHAI without the need for computationally expensive simulations.

5.3. Methodology

5.3.1. WRF configuration

WRF (Skamarock et al., 2008) v3.8 was configured to run four one-way 60 x 60 km nested domains at 3:1 grid ratios (Figure 5.1a). The model was centred over Birmingham, UK (52.5°N, 1.9°W), a configuration already evaluated in Chapter 4.

The outermost domain covered northwest Europe at 27-km resolution and the innermost domain was set at 1-km resolution. The Rapid Radiative Transfer Model (Mlawer et al., 1997) was selected for longwave and the Goddard (Chou et al., 1994) scheme for shortwave radiation. The Noah (Tewari et al., 2004) land surface model, that has four vertical soil layers, was used to represent natural surfaces, and for urban surfaces the multilayer Building Energy Parameterization scheme (BEP: Martilli, 2002) was employed. For the initial and boundary meteorological conditions, the NCEP (National Center for Environmental Prediction) FNL (Final) Operational Model Global Tropospheric Analyses data at six-hour temporal and one degree horizontal resolution were used.

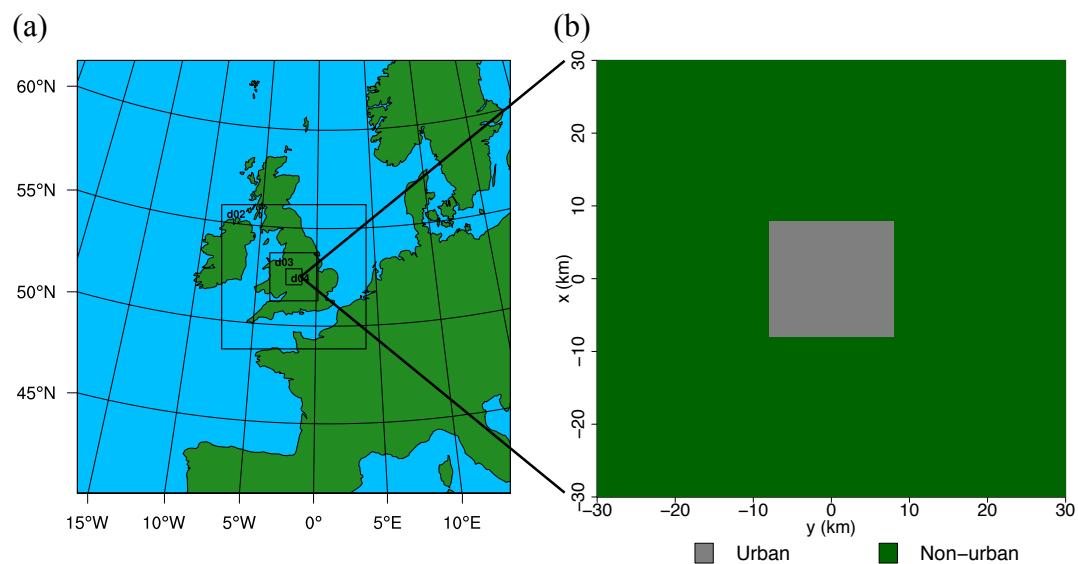


Figure 5.1. (a) WRF domain 1 (the outermost) to 4 (the innermost) configuration. (b) The black square represents the semi-idealised urban land-use (high-density residential) configuration in domain 4 for the 16-km case. The remainder of the domain was filled with the USGS land-use category 2, Dryland Cropland and Pasture.

In order to simplify UHA, the complex urban land use associated with real cases was replaced with a single urban square centred in the innermost domain as shown in

Figure 5.1b. In total, five land-use configurations were created for the innermost domain: the first specifies a rural land use for the entire domain, whereas the others specify a squared urban land use surrounded by rural land use, with urban sizes (L_U) of 2, 4, 8 and 16 km, respectively. An example of the 16-km urban size is presented in Figure 5.1b. Larger urban sizes (e.g. 32 km) were not run because the signals of UHAI could be influenced numerically by the domain size. Whilst the domain size could be extended, this would have impacted significantly on the simulation time. A square land-use configuration was chosen because it would not be possible to create perfect circles using the WRF grid. It is noted that for real cases urban land-use is neither circle nor square and this may have implications when interpreting results. For the urban simulations, the middle BEP urban land-use category, high-density residential, was used. The rural land use was set as “dryland cropland and pasture” in the USGS land-use categories. The urban fraction was set to one for the urban land use and zero for the rural land use. To avoid any undue effects from topography, e.g. katabatic winds, the topography in the inner domain was flattened to sea level. Furthermore, to avoid any sudden step changes at the domain boundaries the topography was also set to 0 m in the other domains. It is expected that the simulations using flattened topography are not completely consistent, particularly in mountainous areas, with the initial conditions for all domains and boundary conditions specified in domain 1 from the NCEP model output. However, this study is focused on the city-scale simulations near Birmingham, UK, where topography is relatively flat. Secondly, the main reason for using nested WRF configuration is to obtain reasonable, if not precise, synoptic weather conditions as the boundary conditions for the innermost domain. Thirdly, the model output for domains 1, 2 and 3 with the flattened topography have shown (not presented here) that the meteorological

fields (temperature, wind and pressure) are spatially smooth and in a dynamical balance after a couple of hours of spin-up time. Compared with simulations that adopt true topography, the key meteorological fields (wind, temperature, humidity and pressure) at the boundary of domain 4 are very little influenced by the flattened topography during the analysis periods.

In total, five time periods were run for the five different WRF-BEP configurations (total of 30 model runs). The time periods (Table 5.1) were selected for having clear and calm weather conditions, favourable for UHI development. To account for model spin-up, the first 12 hours of each simulation were disregarded. Furthermore, night-time hours (2100 – 0500 UTC), were chosen for analysis; in addition, the weather conditions where the sky was completely cloudy (8 Oktas, calculated using the WRF output variable QCLOUD) and wind flows $> 5 \text{ m s}^{-1}$ were excluded from the analysis. This resulted in a total of 450 simulation hours to conduct the UHA analysis, detailed below.

Table 5.1. WRF simulation periods, run for each urban and rural case.

<i>2013</i>
30 April – 08 May
30 May – 08 June
02 September – 23 September
25 August – 06 September
<i>2014</i>
13 May – 20 May
20 July – 27 July

Whilst it was not possible to directly evaluate simulated 2 m temperatures for the semi-idealised cases, the same WRF-BEP configuration has been run for a real urban case and evaluated (Chapter 5). In that paper, the evaluation used a combination of UK Met Office surface observations and data from the Birmingham Urban Climate Laboratory (Warren et al., 2016). A mean Root-Mean-Square-Error (RMSE) of 1.68°C and Mean-Bias-Error (MBE) of -0.33°C across 32 stations (both urban and rural) were found. It was suggested that statistical differences could be due to comparisons between point observations (that may be effected by sub grid scale processes) and the 1-km model resolution.

5.3.2. Urban heat island and advection

Techniques developed through observational (Chapters 2 and 3) and modelling studies (Heaviside et al., 2015) have shown that the temperature at a given location was a combination of: (i) heat generated locally (i.e. determined by the underlying land use) and (ii) heat advected from upstream urban sources. Further analysis in Chapter 4 showed that the derived UHAI results contained regional heat advection (RHA). A methodology to separate UHA from RHA was consequently developed and contained two stages: (Stage I) total urban heat (UHI and UHA) was separated from background regional temperature field (i.e. the rural simulation), and (Stage II) UHA was separated from the UHI. A hypothetical illustration to explain this approach is provided in Figure 5.2 and explained below.

The results of hypothetical urban and (single) rural simulations for the selected 450 hours (see Section 5.3.1 for the details) were analysed to derive various types of time-

mean 2-m air temperature field. For example, for the “rural case”, (i) averaging all 450 hours yields $\overline{T_{rural}}$ where all wind directions were considered; and (ii) averaging for each of four specified wind directions (θ : N, S, E and W) yields $\overline{T_{rural}^{(\theta)}}$. Each simulation hour was categorised into one of the four directions (θ) using the cross-domain mean 10 m wind direction at each simulation hour. Similarly, $\overline{T_{urban}}$ and $\overline{T_{urban}^{(\theta)}}$ are derived for each of the four urban cases, in which $L_U = 2, 4, 8, 16$ km.

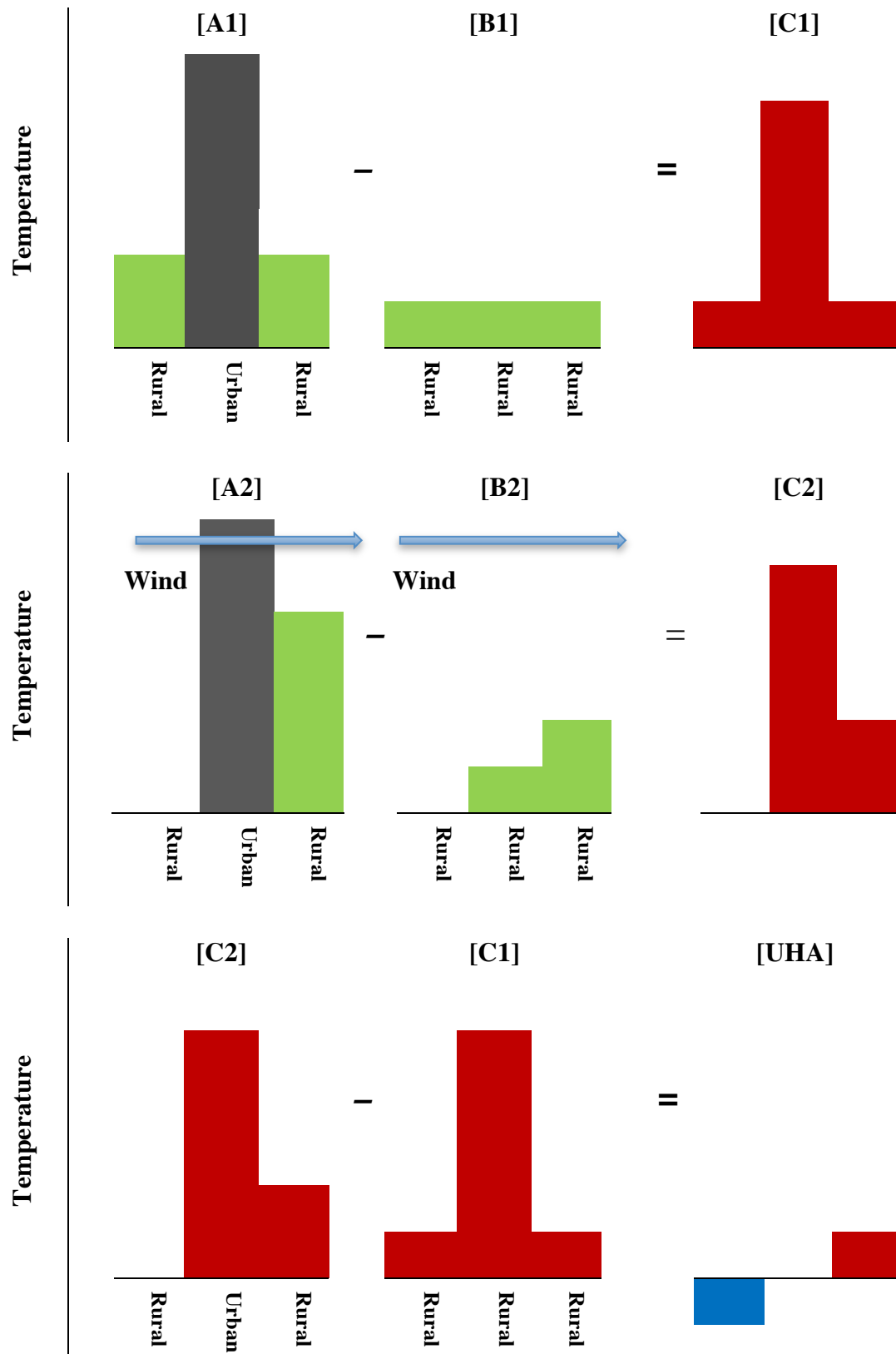


Figure 5.2. Hypothetical UHA calculation that excludes RHA effects. Diagrams named with [A] are for elevated temperatures due to RHA+UHA (i.e. output of the

idealised urban simulations), [B] for elevated temperatures due to RHA only (i.e. output of the rural simulations), and [C] for the difference between [A] and [B] (i.e. elevated temperatures due to UHA only). In the top row, all wind directions (i.e. wind from left to right and right to left) were considered, and the resulting pattern [C1] represents the time-mean UHII field ($\overline{\Delta T}$). In the middle row, only one wind direction (i.e. wind from left to right) is considered, and the resulting [C2] represents the directional time-mean UHII field ($\overline{\Delta T^{(\theta)}}$). In the bottom row, [C2] and [C1] are copied from above, and [C2]-[C1] yields [UHA], which is the UHA field ($\overline{T_{UHA}^{(\theta)}}$) that is free from the local-UHI and RHA effect.

In Stage I, by subtracting the rural time-mean ($\overline{T_{rural}}$) from $\overline{T_{urban}}$ for each of the four urban cases ($L_U = 2, 4, 8, 16$ km), where all wind directions were considered, as indicated in Equation 1 below, the resulting pattern depicts the time-mean UHI intensity (UHII) field ($\overline{\Delta T}$). This is illustrated hypothetically in the top row of Figure 5.2. The same calculation was then applied for the directional time-means, indicated by Equation 2, to show how the resulting UHII field ($\overline{\Delta T^{(\theta)}}$) was modified by wind direction (illustrated in the middle row of Figure 5.2). The resulting 2D UHII field for each wind direction was then rotated to align to a westerly, and then the mean of these four directional rotated UHII fields was taken, represented as $\overline{\Delta T^{(\theta)}}$.

$$\overline{\Delta T} = \overline{T_{urban}} - \overline{T_{rural}} \quad (1)$$

$$\overline{\Delta T^{(\theta)}} = \overline{T_{urban}^{(\theta)}} - \overline{T_{rural}^{(\theta)}} \quad (2)$$

The operations of (1) and (2) have been shown to remove RHA effects (Chapter 4). The result of this step ($\overline{\Delta T}$ or $\overline{\Delta T^{(\theta)}}$) still contains the UHA information. An example why this approach was used is that a strong regional temperature gradient within domain 4 under e.g. a northerly wind flow would be present in both the urban and rural time-mean temperature fields (e.g. $\overline{T_{urban}}$ and $\overline{T_{rural}}$). By subtracting the northerly wind flow rural time-mean from the urban time-mean, the resulting field (e.g. $\overline{\Delta T}$) has effectively removed any regional effect (as these were contained in both time-means).

In Stage II, to isolate the UHAI effect, the time-mean UHII field ($\overline{\Delta T}$) was subtracted from the time-mean directional UHII field ($\overline{\Delta T^{(\theta)}}$), as shown in Equation 3, for each of the four urban sizes, i.e. $L_U = 2, 4, 8, 16$ km. This is shown hypothetically in the bottom row of Figure 5.2, i.e. whether the downwind air temperature for a given wind direction is warmer or cooler than if the mean downwind temperature was calculated using all wind directions.

$$\overline{T_{UHA}^{(\theta)}} = \overline{\Delta T^{(\theta)}} - \overline{\Delta T} \quad (3)$$

The UHA methodology is further adapted to use only two opposing wind directions when creating the time-mean UHII ($\overline{\Delta T}$): (i) mean of north and south, and (ii) mean of east and west. This step was taken because the land-use configurations for the urban cases are symmetrical (i.e. square), therefore removing any noise from adjacent wind directions that were not being analysed. The approach taken to rotate the UHII field ($\overline{\Delta T^{(\theta)}}$) to a single direction was also applied to the UHAI results. This was achieved

by flipping (as the land-use is symmetrical) the northerly UHAI field, then taking the mean with the southerly UHAI field. The same approach was then applied to the east and west UHAI fields. The resulting two UHAI fields were then rotated to the same (westerly) direction and the mean was taken. The result, $\overline{T_{UHA}^{(\theta)}}$, is effectively the mean UHAI field of all wind directions.

Results from previous studies (Heaviside et al., 2015; Chapters 4 and 5) showed UHAI ($\overline{T_{UHA}^{(\theta)}}$) to be negative upwind and positive downwind to be a product of the methodology. A negative UHAI component at an upwind location does not refer to cooling, but reflects to the advected heat which is induced by the wind flow from the opposite direction and is hidden inside $\overline{\Delta T}$; once Equation 3 is applied to this location, because upwind $\overline{\Delta T^{(\theta)}}$ contains zero temperature elevation but upwind $\overline{\Delta T}$ contains a positive temperature, this gives a negative value for $\overline{T_{UHA}^{(\theta)}}$. Therefore, as illustrated by the bottom row of Figure 5.2, the total UHAI component was interpreted as the difference between positive and negative values. However, it is noted that within the urban land use, cooling may be present from the surrounding rural land use (i.e. the opposite effect to UHA) and this is out of the scope of this study.

5.4. Results and Discussion

5.4.1. Semi-idealised urban heat islands

The modelled time-mean UHII fields ($\overline{\Delta T}$, as illustrated by [C1] in the top diagram of Figure 5.2) for four urban size cases are shown in Figure 5.3a. It is clear from Figure 5.3 that an increase in UHI area and intensity are related to an increase in urban size (L_U). The largest UHII of up to 3.6°C are found near the centre of the 16-km urban size. A glow is noted in the rural areas directly surrounding the urban areas and is indicative of the UHA effects. However, it is difficult to visualise UHA in the UHII plots as the signal is obscured by the overall UHI pattern. It is important to note these values of $\overline{\Delta T}$ are derived from mean night-time cases under stable conditions, therefore could change based on prevailing conditions, and that a single urban category does not reflect all urban land-use variability within real urban areas. For example, this semi-idealised case may not be translated directly to real cases, due to complexity caused by different urban geometries, construction materials and vegetation quantities.

In order to explore this relationship, the mean $\overline{\Delta T}$ of all urban grid cells is taken for each case, noted as $\overline{\Delta T'}$ (i.e. for the 4-km case $\overline{\Delta T'}$ is the mean of 16 urban grid cells) and interpreted as the average UHII of the urban square. $\overline{\Delta T'}$ was found to increase with urban size, ranging from 2.0°C to 3.2°C (2 km to 16 km respectively). The relationship between the average UHII and the urban size is found to follow a logarithmic law, as shown in the bottom right panel of Figure 5.3. The relationship can be represented through a simple linear regression ($R^2=0.99$) in Equation 4:

$$\overline{\Delta T}' = 0.58 (\log L_U) + 1.6 \quad (4)$$

where \log denotes the natural logarithm. The logarithmic nature of the relationship between urban size and UHII is similar to Oke (1973) where long-time maximum UHIIs, observed across a range of large U.S. and European cities, were linearly related to \log of city population (i.e. a proxy for urban size). To compare the semi-idealised urban results with real cases from Oke (1973) urban size (L_U) for the European cities was estimated using a population density of 3000 people per km^2 (based on the West Midlands region, Birmingham City Council 2011). The UHII data for the European cities from Oke (1973) is plotted alongside the idealised UHII results ($\overline{\Delta T}'$) in Figure 5.3b. Although each study shows a strong positive linear trend, the slope of the semi-idealised cases is approximately a third of that found by Oke (1973). The semi-idealised results were the time-mean UHII, whereas Oke's (1973) results were the maximum UHII over a long time period, thus explaining the main difference in slope. Furthermore, the WRF-BEP configuration does not consider anthropogenic heat sources and only the middle WRF-BEP urban land-use type was used.

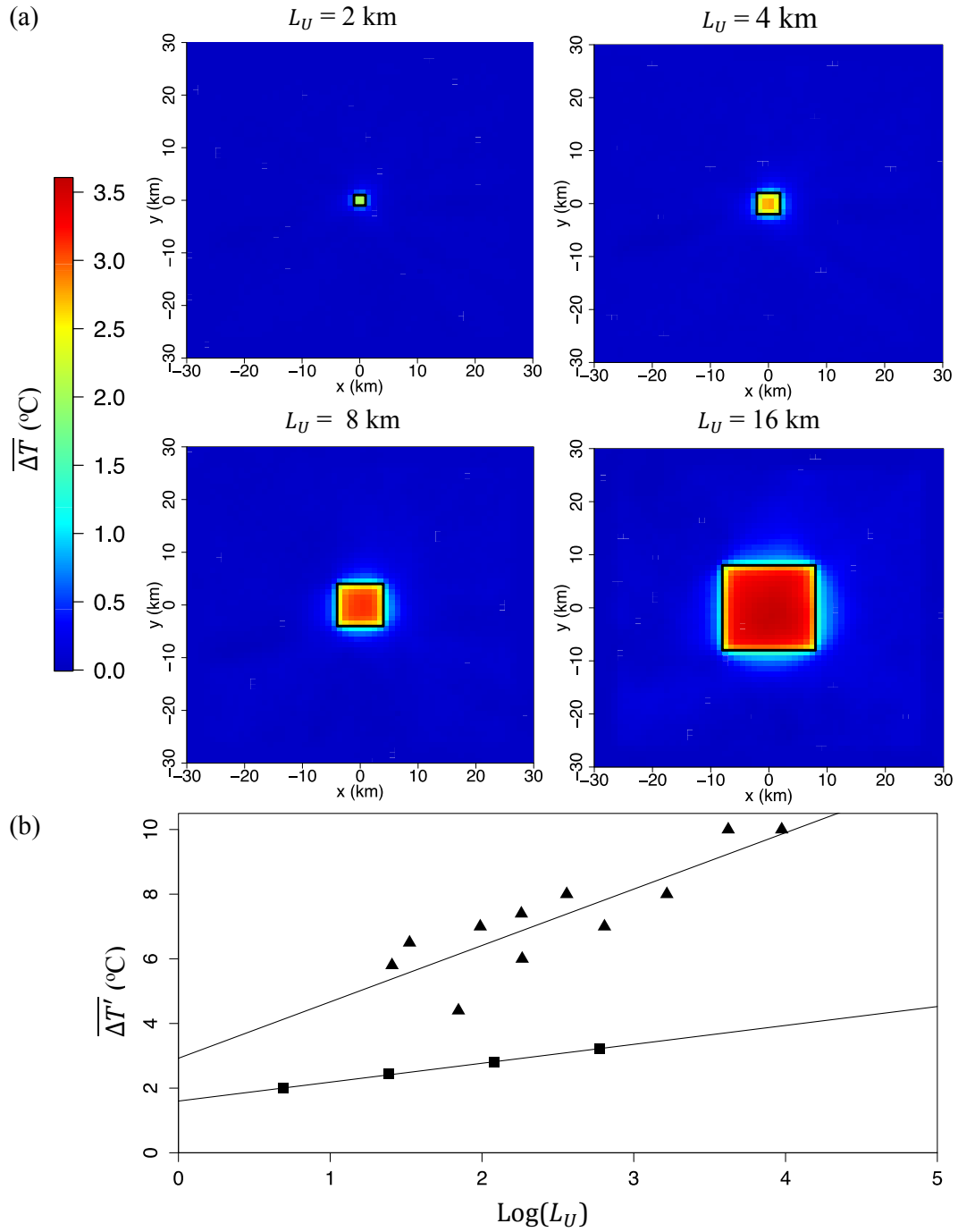


Figure 5.3. (a) Domain 4 time-mean 2 m UHII field ($\overline{\Delta T}$) for each urban size ($L_U = 2, 4, 8, 16$ km) where all wind directions are used. The black box shows the outer boundary of the urban land use. (b) The relationship between the mean UHII of all urban grid cells, $\overline{\Delta T'}$, and the log urban size (L_U) is given in black squares; $\overline{\Delta T'} = 0.58 (\log L_U) + 1.6$. A comparison with Oke's (1973) relationship between urban

size (converted from population) and maximum UHII for European cities is shown in black triangles; $\overline{\Delta T} = 1.75 (\log L_U) + 2.92$.

5.4.2. Semi-idealised urban heat advection

Although it is clear from the time-mean UHII field ($\overline{\Delta T}$) presented in Figure 5.3 that the majority of the UHI was contained within the urban land-use boundary, there was evidence of heat transport outwards from the urban into rural areas. In order to visualise this clearly, and before the UHA methodology is applied, an example of the directional UHII ($\overline{\Delta T^{(\theta)}}$) is presented in Figure 5.4. Three notable features are observed for this directional UHII: (i) the location of the peak UHII is shifted from the centre to near the downwind boundary of the urban land use, (ii) a clear heat spread from the urban into the downwind rural area is evident, and (iii) the UHII downwind of the urban centre is greater: 3.9°C versus 3.6°C for the all direction case (Figure 5.3). The advected UHI effect is approximately 2.5°C at the rural grid cells closest to the urban boundary, and its influence is shown to extend approximately 8-km downwind. It is noted that the heat pattern extending from the urban into the rural land use is curved. This is due to the use of real meteorology, i.e. the four wind directions each contain wind flows in a 90-degree arc.

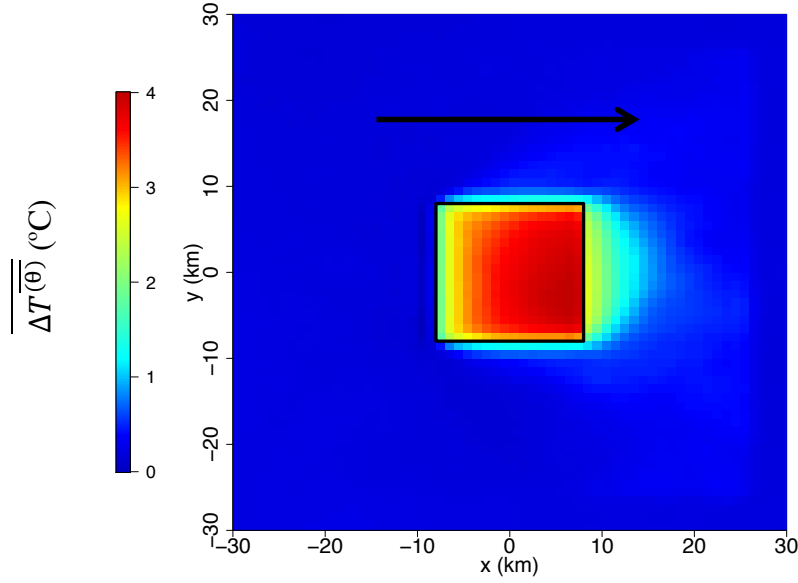


Figure 5.4. Directional time-mean UHII ($\overline{\Delta T^{(\theta)}}$) calculated as the rotated mean of the N, S, E and W wind direction UHII fields for the 16-km urban size. The black arrow represents the mean wind direction (wind flow $< 5 \text{ m s}^{-1}$). The black box shows the outer boundary of the urban land use.

Whilst Figure 5.4 shows heat from the UHI advected into the downwind rural area, it does not clearly differentiate between the UHAI and UHII fields. In order to separate the UHA effects, the UHA methodology described in Section 5.3.2 was applied. The resulting time-mean UHAI field, denoted as $\overline{T_{UHA}^{(\theta)}}$, is presented as a single direction that contains information of all wind directions (similar to Figure 5.4) in Figure 5.5. The results shows that the UHAI is present for each urban size. Visually, the UHAI and area of influence increases with each urban size increment. The downwind positive UHAI, over one degree for the 16-km case, shows the majority of the effect to occur outside the urban boundary. However, a significant portion of the UHA is found within the urban boundary. Notably, the negative and positive UHA effects are symmetrical for each urban size. This has been discussed in Section 5.3.2 and

matches the hypothetical methodology shown in Figure 5.2. This symmetry was unattainable in previous applications of the UHA methodology (Heaviside et al., 2015; Chapters 2 – 4) due to complex land-use patterns.

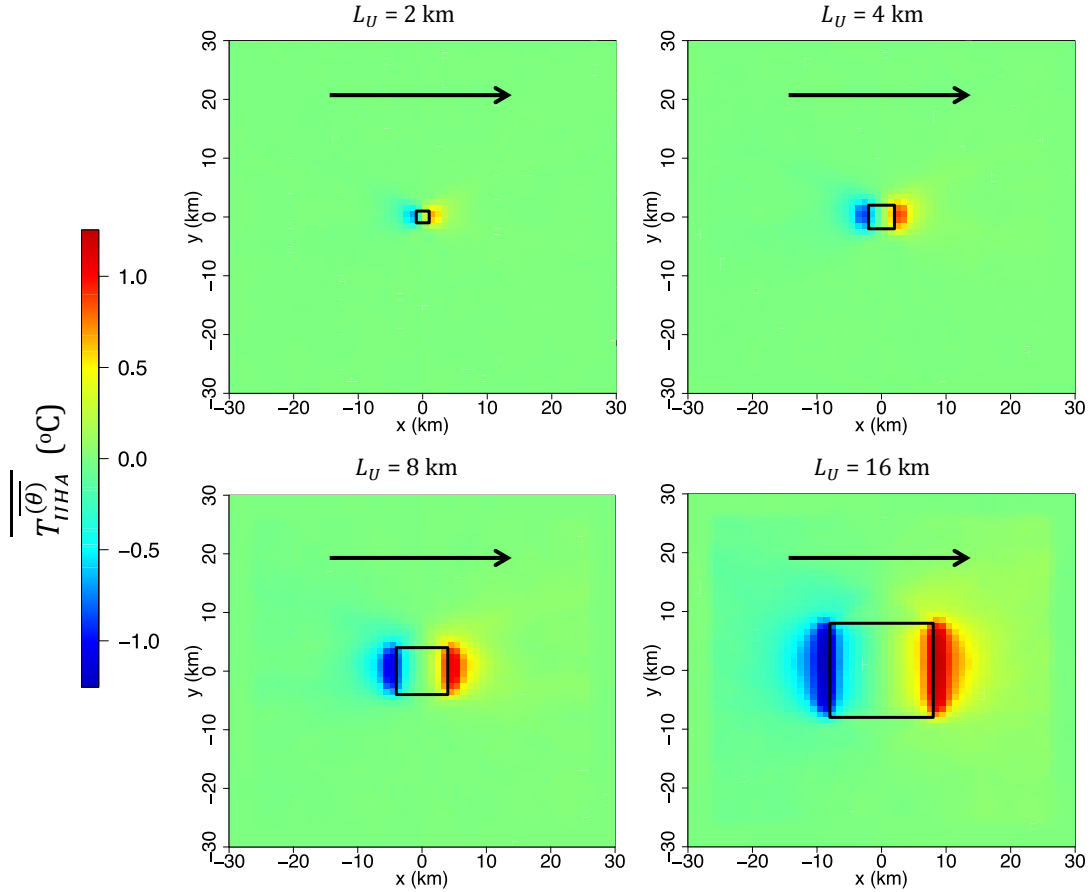


Figure 5.5. Rotated time-mean UHAI field ($\overline{T_{UHA}^{(\theta)}}$) for each idealised urban size (L_U). The black rectangle in each plot represents the urban outline, and black arrow the wind direction wind flow $< 5 \text{ m s}^{-1}$).

To explore the characteristics of the UHAI ($\overline{T_{UHA}^{(\theta)}}$) shown in Figure 5.5, a horizontal transect (left to right) was taken through the centre of each urban area. These transects, presented in Figure 5.6a, show the negative upwind, and positive downwind UHAI contributions, and the clear symmetry between them. An unexpected UHAI dip

at approximately 25 km distance for the 16-km urban size is explained by the numerical treatment at the nested domain boundary. This would prevent urban sizes larger than 16 km being analysed for UHA in a 60-km domain size. The domain size could be increased, albeit with increased computational time, in future studies to accommodate larger urban sizes.

As discussed in the methodology, the total UHAI ($\overline{T_{UHA}^{(\theta)}}$) is the difference between the negative and positive UHAI values. Thus the differences between positive and negative UHAI values were calculated (Figure 5.6b). In order to find a more precise location of the peak UHAI the “splinefun” package in R was used to cubically interpolate the UHAI between the 1-km WRF grid spacing in Figure 5.6b. Using this spline interpolation the results show the amount of UHAI ($\overline{T_{UHA}^{(\theta)}}$) received at a particular location increases with distance from the urban centre, until peaking directly after the urban land-use boundary (indicated by the vertical lines on Figure 5.6b). Beyond this peak, the UHAI for each urban size decreases with distance. A maximum UHAI of 1.1, 1.6, 2.0 and 2.4°C at distances from the urban centre: 2.2, 3.3, 5.4 and 9.4 km are found (for the 2, 4, 8 and 16 km urban size respectively). It was also found that the peak UHAI occurs at a mean distance of 1.3 km from the urban boundary (i.e. the adjacent rural grid cell). However, this distance may be a consequence of the 1 km model resolution rather than a fundamental UHA property.

The UHA is also shown to extend considerably from the urban boundary for different urban sizes. For example, the 16-km urban case has a 0.5°C UHAI extending up to 9 km from the urban boundary. The peak UHAI for the 16-km urban case of approximately 2.4°C corresponds to the same level of advected UHI in the immediate

downwind rural areas shown in the earlier directional UHII result (Figure 5.4). This is the same for each urban size and provides further justification to combine the negative and positive UHAI values.

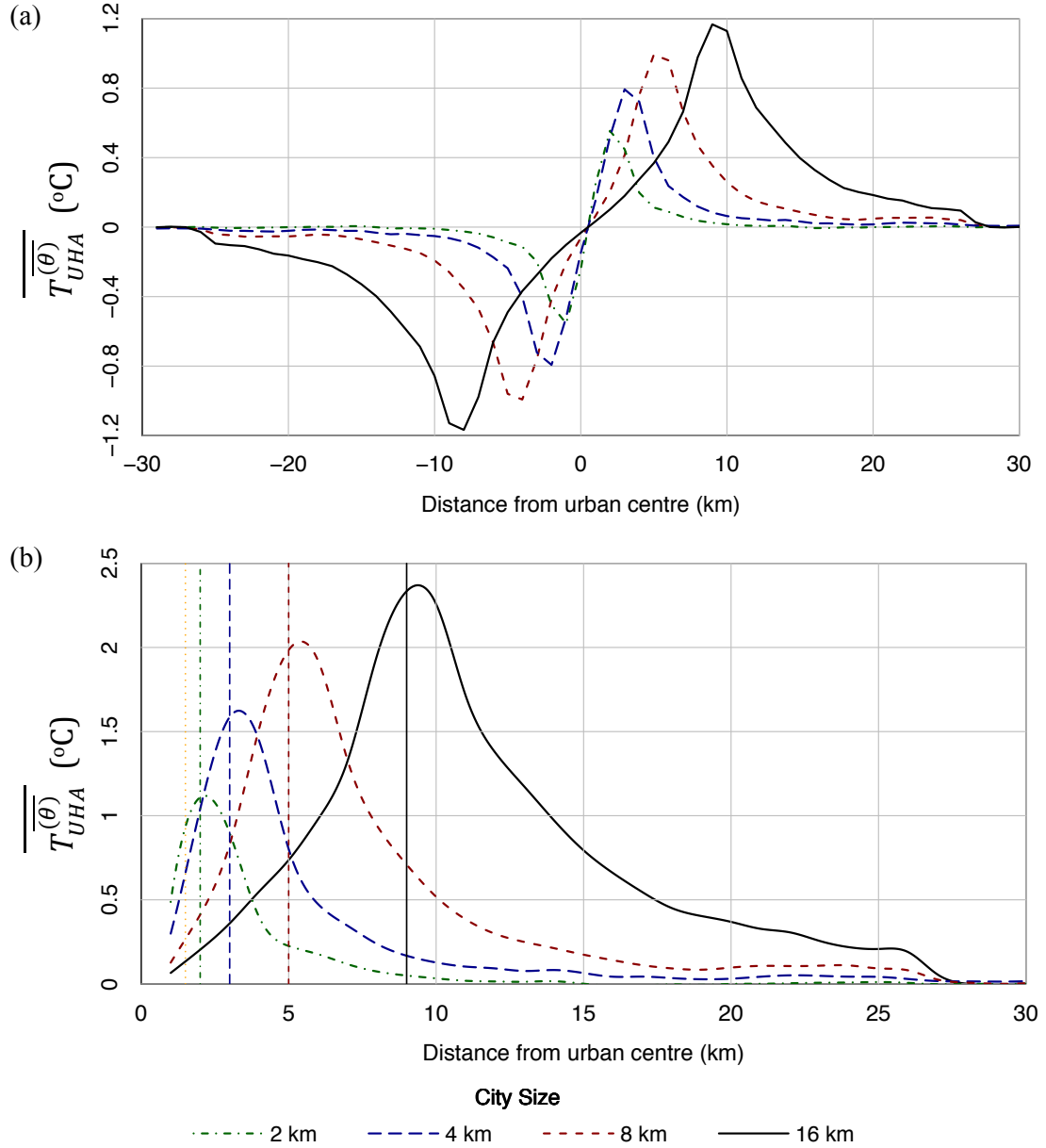


Figure 5.6. (a) Horizontal transects through the rotated time mean directional UHAI fields ($T_{UHA}^{(\theta)}$) for each urban size (shown in Figure 5.5). (b) The negative and positive UHAI transects from Figure 5.6a were combined to show the total UHAI contribution. Spline interpolation is used to smooth each UHAI transect, with the

most noticeable effect for the peak UHAI. The vertical lines in a corresponding line type represent the urban boundary for each size.

5.4.3. Scaled UHA statistical model

The similarity of the profiles of the UHAI transects shown in Figure 5.6 suggests that it may be feasible to create a simple statistical model to fit all the profiles. The intention is to provide a means to calculate UHAI without the need to run intensive computer simulations. In order to accomplish this, the main factors affecting UHAI need to be explored statistically. Linear regression was used to show the relationship between distance (D) that the peak UHAI value is found (D_{MAX}) and urban size (L_U). A significant relationship ($R^2 = 0.99$) was found, shown in Figure 5.7a and Equation 4. The same approach was then applied to the relationship between the UHAI maximum ($\overline{T_{UHA MAX}^{(\theta)}}$) and $\log(L_U)$. This subsequently yielded a significant linear relationship shown in Figure 5.7b and Equation 5 ($R^2 = 0.99$).

$$D_{MAX} = 0.51 L_U + 1.22 \quad (4)$$

$$\overline{T_{UHA MAX}^{(\theta)}} = 0.60 \log(L_U) + 0.75 \quad (5)$$

We can then adopt the following scaling approach: (i) the distance from urban centre, D , is scaled by D_{MAX} , and (ii) the UHAI value ($\overline{T_{UHA}^{(\theta)}}$) at each distance is scaled by the peak UHAI ($\overline{T_{UHA MAX}^{(\theta)}}$). The profiles of UHAI transects, expressed by two new scaled

variables, $D' = D/D_{MAX}$, and $\overline{T_{UHA}^{(\theta)'}} = \overline{T_{UHA}^{(\theta)}} / \overline{T_{UHA MAX}^{(\theta)}}$, are presented in Figure 5.7c.

It is clear that the UHAI transects for each urban size show a close resemblance. The log of the resulting transformed mean transect (i.e. D'' is at 0.1 resolution from the four curves at D') is illustrated in Figure 5.7d. These steps are summarised in (6) and (7).

$$D'' = \log \left(\frac{D}{D_{MAX}} \right) \quad (6)$$

$$\overline{T_{UHA}^{(\theta)''}} = \log \left(\frac{\overline{T_{UHA}^{(\theta)}}}{\overline{T_{UHA MAX}^{(\theta)}}} \right) \quad (7)$$

A Fourier series was then used to approximate the log relationship of the mean transformed transect curve ($\overline{T_{UHA}^{(\theta)''}}$) as expressed in Equation 8. The parameters for this equation were estimated using the nonlinear least squares function in R.

$$\begin{aligned} \overline{T_{UHA}^{(\theta)''}} = & -3.24 + 2.18 \cos(D'') + 0.92 \cos(2D'') - 1.37 \sin(D'') \\ & + 0.32 \sin(2D'') + 0.23 \sin(3D'') \end{aligned} \quad (8)$$

The information generated through fitting the UHAI transects from different urban sizes has therefore formed a simple UHAI statistical model. For any given urban size L_U and distance D , the UHAI value can be estimated using this methodology. The UHAI transects that the model outputs along with the original modelled cases are shown in Figure 5.8. The statistical model is able to satisfactorily replicate the modelled urban cases, however the peak UHAI is slightly underestimated. Whilst this

methodology is derived for a simplified urban case, and does not show all urban complexities (or variation in meteorology), it can be used as a simple means to estimate UHAI. However, this approximation is based on a single land-use type and wind speeds $< 5 \text{ m s}^{-1}$. The statistical model is also based on a standalone square urban area (i.e. does not consider the interactions, perhaps non-linear, between multiple urban areas) and does not contain vegetation (therefore UHA results may be higher than expected in reality). Addressing these issues could form the base of future research.

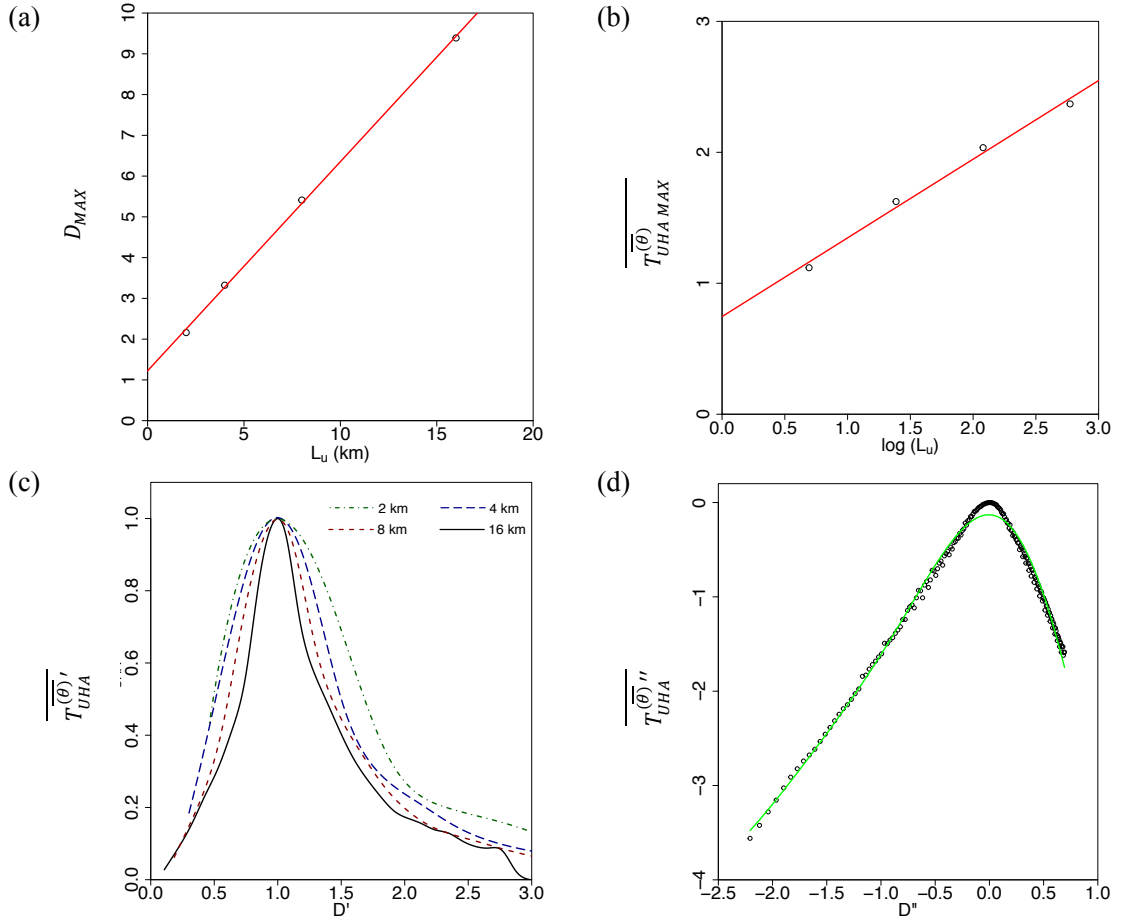


Figure 5.7. (a) The relationship between urban size (L_u) and peak UHAI distance from the urban centre (D_{MAX}). The equation of the line is given at (4). (b)

Relationship between log urban size (L_U) and peak UHAI ($\overline{T_{UHA}^{(\theta)}}$). The equation of the line is given at (5). (c) Decomposed UHAI transects (the original transects are shown in Figure 5.6b). (d) Log mean of the collapsed UHAI transects found in Figure 5.7c shown in dots. The equation of the Fourier line is given at (6).

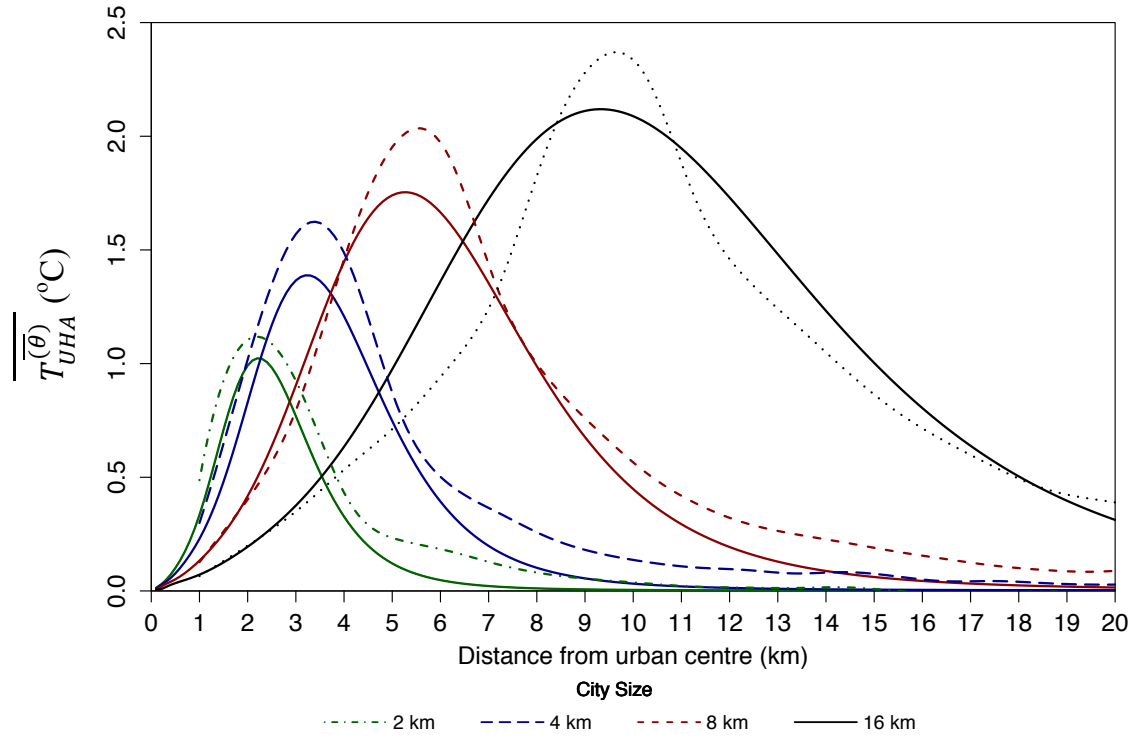


Figure 5.8. UHAI statistical model output for $L_U = 2, 4, 8$ and 16 km are shown solid lines and the original modelled output in dashed lines.

5.5. Conclusions

Previous attempts to quantify UHA were hampered by complex urban land-use patterns. To overcome this, semi-idealised simulations were conducted using the WRF-BEP mesoscale model configuration. Within the inner model domain, the land use was replaced with simplified, square, representations of cities up to 16 km in size. A rural only land-use simulation was also conducted and used to remove any non-

urban, RHA effects from the results. Six periods in 2013 and 2014 were run that contained 450 hours of stable (clear skies and low wind speeds) night-time meteorological conditions. A time-mean 2 m temperature field was calculated as the difference between each urban and rural simulations considering: (i) all wind directions, and (ii) directional cases.

The all wind direction time-mean UHII field had a temperature difference between the urban and rural simulations up to 3.6°C for the hypothetical 16-km urban size. The UHII was found to be related to the logarithm of urban size, agreeing with the observational analysis conducted by Oke (1973). For the directional UHII cases, a clear pattern of heat transport from the urban to rural land use was shown. The spatial location of the peak UHII was found to intensify and move to the (inside) downwind boundary of the urban land use.

UHA was separated from the underlying UHII, resulting in a clear UHA field free from complexities caused by real land-use patterns. A horizontal transect was taken through each UHAI field. This showed symmetrical negative and positive UHAI values (opposing wind directions) that were subsequently combined to derive the downwind-only UHAI field. This addition created the same UHAI as found with the earlier advected UHII results. The results showed a UHAI up to 2.4°C for the hypothetical 16-km urban size. The largest UHAI were found in the downwind rural grid cell directly adjacent to the urban boundary (i.e. 1-km away). A UHAI effect of 0.5°C was found to extend up to 9-km downwind of the urban boundary for the 16-km urban size. A significant UHAI, 1.1°C, was initiated by the smallest urban size, 2 km. Whilst a 2.4°C UHAI (16-km urban size) appears large and double that found in

observations (Chapter 2), the urban land use in these simulations did not contain vegetation (i.e. urban fraction was set to 1) or an anthropogenic heat source. This is in contrast to (the majority of) real cities where vegetation (including urban parks) and moisture would reduce the overall UHAI.

The maximum UHAI was related to the log urban size (similar to the UHII). The distance at which this maximum UHAI occurred was linearly related to the urban size. Using this scaling rule, all UHAI transects for the four tested urban sizes were collapsed on top of one another reasonably well. As each transect (once collapsed) was similar to one another, this information was used to create a predictive statistical UHAI model. The model takes input of urban size, and estimates the downwind UHAI with distance. This statistical UHAI model has practical benefits, for example, it may be used to estimate UHAI in areas not currently considered at risk, i.e. outside the traditional UHI concept. The statistical UHAI model could also be used to correct biases in temperature observations taken near urban areas (assuming changes to the model configuration to represent local, real conditions), and the information may help assess the extent of “contamination” of climate records by nearby urban settlements. The model may also help mitigate heat-health and infrastructure risks, particularly when combined with a changing climate. However, further work may be taken to extend this research by: (i) expanding the domain sizes to encompass larger cities (and to avoid smoothing effects at the domain boundary), (ii) create more complex idealised urban representations, i.e. an urban area upwind of another urban area, (iii) test different urban land-use types, and (iv) fully idealised weather conditions could be used to control wind speed and direction. This would enable interpretation of UHA under different weather scenarios.

Overall, this paper has shown that simplifying urban land use in WRF substantially improves quantification of UHA. This work builds on and provides justification to a UHA methodology that was not previously fully tested due to the complexities of urban land use. It is anticipated that the statistical UHAI model developed from the results can be used as a tool to help mitigate UHI and UHA impacts.

Chapter 6.

Conclusions

6.1. Introduction

The overall aim of this thesis was to quantify the effects of urban heat advection (UHA) using a combination of observational analyses and numerical modelling. Discussed in the earlier Chapters, UHA is the transport of warm air generated by urban areas downwind. As a process, UHA was previously overlooked within the broader UHI field. This was in part due to limitations with previous methodologies, stemming from a lack of high-quality urban observation networks. The knowledge of UHA is important to fully appreciate the true impact of urban areas on their surrounding environments. For example, UHA should be carefully considered when analysing long-term climate records taken near urban areas.

UHA was successfully quantified in this thesis by separating the aim into four objectives, forming the body of this thesis. Chapter 2 focussed on observational analysis using a new high-density urban observation network, finding a mean UHAI up to 1.2°C. Chapter 3 applied this new understanding of UHA, and adapted the methodology to work at any weather station. The results showed that even small urban areas created significant biases on air temperatures recorded at stations largely considered rural. Using the Weather Research and Forecasting (WRF) model, Chapter 4 identified that previous attempts to model UHA were over predicted due to not accounting for regional heat advection. However, the WRF modelling was unable to simplify complex UHA signals due to the heterogeneous underlying land use. Therefore, Chapter 5 reduced this UHA complexity by use of semi-idealised numerical modelling (i.e. creation of hypothetical urban areas). The results showed a clear relationship between UHA and log urban size, and this information was used to

develop a simple statistical model was developed. A full summary and conclusion for each Chapter is provided below, followed by a general synthesis containing limitations and overall conclusions.

6.2. Chapter 2. Observations of urban heat island advection from a high-density monitoring network

A new high-density urban observation network named the “Birmingham Urban Climate Laboratory” was analysed to separate a spatial UHA signal from the background temperature (i.e. the UHI). The network consisted of 29 weather stations that provided data across the city at approximately 3-km resolution, i.e. sub-city scale. Over a 20-month period, under nocturnal clear skies and low wind speeds ($< 2 \text{ m s}^{-1}$) a mean UHII up to 4.3°C was found in the city. A methodology to separate UHA was then applied to the dataset. A simple example is provided in the following paragraph to explain the methodology.

A heater is placed in the centre of two people (A and B) who sit at opposite sides of a table. A fan is installed at the back of each person that are alternatively turned on and off for equal durations many times (blowing towards the heater only). The person sitting at the upwind side of the heater will sense the room temperature, whereas people sitting at the downwind side will sense an elevated temperature, ΔT . Over a long period (the time-means presented in Chapter 2), both people will sense an elevated temperature, i.e. mean $\Delta T = 0.5^{\circ}\text{C}$. If only the periods when the fan behind person A is turned on are considered (B is off), then person A will sense room the room temperature whereas B will sense the elevated ΔT at all times, i.e. mean $\Delta T =$

1°C. UHA is calculated as the difference between the case where the two fans are blowing in equal durations from the case where only a single fan is blowing. Once this is applied, person A will experience $\Delta T = -0.5^\circ\text{C}$ whereas B will experience $\Delta T = +0.5^\circ\text{C}$. These results will changeover when the fans turned off and on are swapped. Therefore, negative UHA values do not represent cooling, but rather a lack of additional warming (above room temperature) from the heater. The total UHAI was interpreted as the difference between negative and positive values.

Under medium wind speeds ($2 - 3 \text{ m s}^{-1}$) a downwind mean UHAI up to 1.2°C was found. This medium wind speed group was found to contain the highest UHA values, explained by the relationship between the UHII (highest at low wind speeds and cloud cover) and the advective capability at different wind speeds (increased at higher wind speeds). Correlating the UHA results with upwind urban fraction (calculated as the inverse of a normalized difference vegetation index) found UHA to extend 4 – 12 km downwind of Birmingham (approximately city scale).

A degree of spread between UHA results at different stations were found. This was due to limitations in the methodology, largely originating from complex land-use patterns. For example: (i) the use of a central urban station that could itself be biased by wind direction; (ii) small-scale advection features (influence from nearby individual buildings that the methodology is unable to account for); and (iii) UHA from multiple upwind sources (i.e. most stations in the network were surrounded by urban areas). Despite these limitations, Chapter 2 demonstrated the significance of UHA for the first time using a high-density urban observational network.

6.3. Chapter 3. The effects of heat advection on UK weather and climate observations in the vicinity of small urbanised areas

It was conceptualised that the UHA methodology demonstrated in Chapter 2 could be adapted for use at any weather station (i.e. without the need for a high-density observation network). To adapt the methodology, a baseline temperature series for the UK was created by taking the mean of seven rural stations that had reliable hourly temperature records over a 30-year time period. This baseline temperature was adapted for use in the UHA calculation instead of the spatial time-mean temperature field used in Chapter 2.

The UHA calculation in Chapter 3 were only applied to select stations (42 total). These were stations located downwind of an urban area contained in a single wind direction (i.e. it was not necessary to analyse fully rural or urban stations). These stations were identified, along with mapping their upwind urban fraction using an automatic classification based on OS building data. The stations were typically located at small airfields with upwind urban areas approximately 1 km^2 in size. The use of stations with only a single upwind urban area was intended to improve on Chapter 2 where UHA originating from multiple sources were difficult to distinguish.

A mean warming across all stations up to 0.6°C was found at night, under low cloud and wind speeds between $2 - 3 \text{ m s}^{-1}$. The urban areas within a 0.5-km distance from the observations were found to have the greatest influence on air temperatures. The results emphasised that UHA was not a process exclusive to cities and was significant even at small scales. Knowledge of how UHA effects weather and climate stations,

that are likely classified rural, could serve as an important asset in the evaluation of anthropogenic influence on climate change records. However, Chapter 3 highlighted that analysing UHA from smaller, simpler urban patterns (i.e. than Chapter 2) did not remove all noise from the data and thus allow full UHA quantification. One limitation of the approach in Chapter 3 is that non-urban wind directions may each have their own unique advection sources (for example, the difference between grass or forest upwind from a station). Therefore, to limit these effects a controlled approach was needed, as put forward in Chapters 4 and 5.

6.4. Chapter 4. Methodology to separate urban from regional heat advection by use of the Weather Research and Forecasting mesoscale model

Chapters 2 and 3 demonstrated that a large UHA signal exists within observations. To make a more detailed assessment, i.e. beyond what observations could provide, WRF modelling of UHA was required. This Chapter examined previous UHA modelling (Heaviside et al., 2015) and found two key weaknesses. Firstly, the earlier modelling was conducted during a heatwave case study and therefore unable to provide directional time-means over many simulation hours. Secondly, the impact of regional heat advection was not considered. Whilst regional effects may be small in continental studies, the coastal nature of the UK means strong regional temperature gradients exist. Previous UHA modelling (Heaviside et al., 2015) showed UHA up to 2.5°C to extend across large, unrealistic, downwind regions of the domain.

The WRF numerical model was chosen for the analysis because it was already coupled to several urban models (in this case Building Effect Parameterization: BEP

was chosen), and has been extensively evaluated in the urban environment. The simulations were further evaluated in this Chapter using observations from the BUCL network, finding a good agreement with observations. The WRF model was run over six time periods (of stable weather) to provide over 1600 hours of simulations (therefore providing data for an adequate number of wind directions hours), noted “urban-case”. A second set of simulations containing identical meteorology, except with all urban land use set to vegetation, was also conducted. The results from these “rural-case” simulations were used to demonstrate that a large portion of heat previously attributed to UHA by Heaviside et al. (2015) was due to regional heat advection.

By including the rural-case simulations in the UHA calculations, any regional heat effects were effectively removed. Following this calculation, the results indicated that UHA was confined to within and several kilometres downwind of urban areas. Within areas by UHA, the intensity was up to 1.9°C. Whilst offering a substantial improvement to previous UHA modelling, this Chapter was still limited by complex land-use patterns, making UHA difficult to interpret.

6.5. Chapter 5. Semi-idealised urban heat advection simulations using the WRF mesoscale model

The UHA analysis presented in Chapters 2 – 4 were limited by complex urban land-use patterns, thus UHA was not fully quantified. To meet the aim of this theses, a new approach was taken in this Chapter. The same modelling framework presented in

Chapter 4 was used, except the land use was replaced with hypothetical urban cities. These were simple, square representations ranging in size from 2 to 16 km.

The semi-idealised approach was initially used to calculate the mean UHII (up to 3.6°C), and this was linearly related to the log of urban size. The relationship was comparable to that found by Oke (1973), however the slope of the relationship had a gentler gradient. The mean UHII calculated in this Chapter as opposed to the maximum UHII over a long observational period used by Oke (1973) may explain this difference. The improved UHA methodology from Chapter 4, that accounted for regional heat advection was then applied to the semi-idealised simulations. A clear UHA pattern, free from any heterogeneous features previously caused by complex urban land use was found. Due to the simplicity of the land use, a clear symmetry was found between UHA in opposing wind directions (i.e. negative UHAI values matched positive). Whilst this symmetry was hypothesised in previous Chapters, it was not accomplished. The results showed the UHAI up to 2.4°C for the largest urban size, 16 km, with 0.5°C UHAI extended up to 9-km downwind.

The UHA pattern, whilst different in intensity and area followed a similar profile for each modelled urban size. Statistical analysis showed that the maximum UHAI was found to be related to the log of urban size (similar to the UHII). Using this information as a scaling rule, the UHAI results from each urban size were used to create a predictive statistical model. The model estimates downwind UHAI based on urban size, and provides a means to estimate UHA without the need for computationally expensive simulations. This has practical uses, for example correcting temperature biases in long-term air temperature observations taken near

urban areas. However, the model only considers a single urban category and is based on night-time data at low wind speeds and cloud cover, and does not consider the anthropogenic heat flux. The hypothetical cities were also configured in WRF as 100 % urban, which would be unrealistic in real world situations.

6.6. UHA synthesis and concluding remarks

Until recently, most UHI studies assumed that air temperature was in equilibrium with local land use. However, due to wind advection, this is not the case, as highlighted by the creation of a methodology to demonstrate this impact (Heaviside et al., 2015). This insight, based on numerical modelling, was furthered in this thesis by adapting the methodology to work with observations, improving the approach and isolating a complex UHA pattern using semi-idealised modelling. However, several limitations, particularly the variability of UHA and applicability of modelling, were found whilst conducting the analysis. The following discussion synthesises the UHA results in this thesis.

Initial analysis of the high-resolution HiTemp urban network in Chapter 2 found for low wind speeds ($< 2 \text{ m s}^{-1}$) a large mean night time UHII of 4.3°C in Birmingham, a large city of approximately a million inhabitants. The UHII was found to decrease with increasing wind speed (1.3°C for wind speeds $> 3 \text{ m s}^{-1}$). By applying the UHA methodology (summarised above in Section 6.2), hence separating the resulting effects of advection on local air temperature, a significant downwind warming was found. For Birmingham, the mean UHAI was 0.2°C , 0.4°C and 0.3°C for WG 1 ($< 2 \text{ m s}^{-1}$), WG2 ($2 - 3 \text{ m s}^{-1}$) and WG3 ($> 3 \text{ m s}^{-1}$) respectively.

The same analysis, with adaptations (creation of a rural baseline), was applied to selected UK weather stations (that were likely at risk of UHA) in Chapter 3. A mean UHAI of 0.4°C, 0.6°C and 0.4°C was found for the same wind speed groups as Chapter 2. At individual stations the difference between wind directions containing rural and urban sources was up to 2°C. Considering these UHAIs were calculated downwind of urban areas significantly smaller in size to the Birmingham case (approximately 300:1 km² ratio), these results appeared opposite to what would be expected. However, the UHAI differences can be explained by the observation station locations. Many of the HiTemp observations were inside the urban canopy, where flows are highly heterogeneous. Therefore, observations would be expected to contain UHA from multiple sources at different scales (i.e. local and city-scale). For the small-scale UHA cases, stations used in the analysis were only located in the downwind region of a single urban source. For the Birmingham case, it was probable that UHA was underestimated due to challenges associated with complex urban land-use patterns. Considerable variability was also found within the upwind rural directions for the small-scale urban cases. This rural heterogeneity questions the widely used two-station approach (urban – rural) to calculate UHI intensity. Although the UHAI values in Chapters 2 and 3 represent given conditions and time frames, they still represent a notable downwind warming that was rarely previously considered. Furthermore, these findings challenge the traditional urban plume concept (illustrated in Chapter 3), due to downwind warming present at the surface (i.e. not limited to an elevated plume within the urban boundary layer).

Due to the challenges with observing UHA in Chapters 2 and 3, numerical modelling was introduced in Chapter 4. Here, it was demonstrated that the initial methodology

(Heaviside et al., 2015) overestimated UHA. Regional heat advection, especially prevalent due to the island nature of the UK, was found to be the cause. A subsequent refinement to the methodology, showed maximum UHA in the modelled domain around Birmingham to be almost 2°C, smaller than previously modelled. Although, this modelling clearly showed UHA to be a significant feature, similar to previous Chapters, UHA still exhibited large spatial variability making quantification difficult. This issue was addressed in Chapter 5 that used the same UHA methodology and WRF configuration as Chapter 4, but with idealised representations of cities varying from 2 to 16 km. Using this approach, it was possible to clearly define the UHA contribution to local temperatures. A mean UHA up to 2.4°C was found for the 16 km case, with UHA of 0.5°C extending 9 km from the urban land-use boundary. The UHAI results for the semi-idealised modelling were considerably higher than found in the observations and modelling the real case in Chapter 4. However, there are two important considerations. Firstly, this is a clean UHAI pattern across two homogeneous land-use types, therefore avoiding any issues of multiple UHA sources from previous Chapters. Secondly, the urban cases represent solid land-use that is not representative of real cases, i.e. no features like urban parks that would reduce the available heat for advection. Notwithstanding, the final analysis Chapter of this thesis was able to demonstrate how a well-defined, idealised UHA pattern could be scaled statistically.

Whilst the UHA effect was clear, and quantified in this thesis, there were several limitations. Firstly, the mean UHAI was presented throughout this thesis. Therefore, UHAI on individual nights could be higher, for instance during a heatwave. This is a constraint of the UHA methodology that revolves around time-means, hence not

suitable to investigate individual UHA events. Secondly, although most UHA uncertainty was attributed to the complexity of urban land use, other factors like choice of land-use data for quantifying upwind sources or station-specific qualities may have contributed. For example, rural homogeneity was largely assumed, and as Chapter 3 demonstrated this was not the case. Thirdly, the use of numerical modelling presented challenges, for example a simple statistical model was produced from the semi-idealised modelling results, however the model was only based on a single urban land-use type, and for given meteorological conditions. To make the statistical model more representative of real cases it would require running different urban land-use configurations and more simulation hours to provide a greater range of meteorological conditions. Additionally, the interaction of UHA from one (or indeed multiple) hypothetical cities on one another would need modelling.

Overall, the main limitation of this thesis was the inability to explore different UHA processes within the boundary layer and instead only quantifying the resulting impacts on air temperature. This would be the separation of UHA between: (i) horizontal movement through the urban canyon; and (ii) downwards transport by turbulent eddies downwind from the elevated urban plume. To separate these processes and explore the three-dimensional nature of UHA, high-resolution spatial observations would be needed vertically in addition to the surface observations used in Chapters 2 and 3. However, vertical observations in urban areas are not easy to capture. Notwithstanding novel projects are being instigated to overcome this. For example, the use of bio-aerial platforms to capture three-dimensional data within the urban boundary layer (<http://gtr.rcuk.ac.uk/projects?ref=NE%2FN003195%2F1>). Furthermore, a shift in data capture methods to citizen science (Chapman et al., 2016)

will lead to data-rich environments where UHI and UHA analysis can be conducted. Numerical modelling may also be used to separate advection processes, although higher resolutions than applied to this thesis would be required. These are not currently feasible using WRF or similar models due to a “terra incognita” at sub-km scales (Wyngaard, 2004). Instead, a different suite of models would be required, i.e. computational fluid dynamics. However, these are computationally expensive and only cover limited domains.

Despite limitations, this thesis has contributed to our understanding of UHA through a combination of observational and numerical modelling techniques, and provided an ideal basis for future UHA research, particularly the three-dimensional separation of advection process within the boundary layer. The UHA findings provide valuable knowledge that can contribute to mitigating heat related risks. For example, UHA has considerable implications for the analysis of long-term temperature records taken near urban areas. Indeed, Chapter 3 demonstrated a UHA bias already present in many of the observations used for weather and climate analysis. Therefore, the “circle of influence” for a given station should be extended beyond the current 0.5 km interpretation especially near, even small, urban areas. The statistical model developed from scaling the semi-idealised results, that requires only urban size as input (albeit with appropriate fine tuning, i.e. location specific model parameters), could provide a useful means of correcting UHA biases in long-term observations. The UHA findings may also contribute to assessments of urban induced excess heat (especially combined with a changing climate) and associated health-risks, particularly in downwind areas not previously thought to be impacted by urbanisation.

This thesis has therefore highlighted an important, dynamic aspect of the urban modification to local climate and improved our understanding of UHA. The approach to quantify UHA used a transferable methodology that can be readily adapted to other cities worldwide.

References

Ackerman B., Changnon S.A., Dzurisin Jr. G., Gatz D.F., Grosh R.C., Hilberg S.D., Huff F.A., Mansell J.W., Ochs III H.T., Peden M.E., Schickedanz P.T., Semonin R.G., and Vogel J.L. (1978) 'Summary of METROMEX, Volume 2: Causes of Precipitation Anomalies'. Illinois State Water Survey, Bulletin 63, Urbana, IL, pp. 395.

Arnfield A.J. (2003) 'Two decades of urban climate research: A review of turbulence, exchanges of energy and water, and the urban heat island', *International Journal of Climatology*, 23, pp. 1-26. doi: 10.1002/joc.859.

Azevedo J.A., Chapman L., Muller C.L. (2016) 'Quantifying the Daytime and Night-Time Urban Heat Island in Birmingham, UK: A Comparison of Satellite Derived Land Surface Temperature and High Resolution Air Temperature Observations', *Remote Sensing*, 8(2), pp. 153. doi: 10.3390/rs8020153.

Balsamo G., Albergel C., Beljaars A., Boussetta S., Brun E., Cloke H., Dee D., Dutra E., Muñoz-Sabater J., Pappenberger F., Rosnay P., Stockdale T., Vitart F. (2015) 'ERA-Interim/Land: a global land surface reanalysis data set', *Hydrological Earth System Science*, 19, pp. 389-407. doi:10.5194/hess-19-389-2015.

Barlow J.F., Rooney G.G., Hünerbein S.v., Bradley S.G. (2008) ‘Relating Urban Surface-layer Structure to Upwind Terrain for the Salford Experiment (Salfex)’, *Boundary-Layer Meteorology*, 127, pp. 173-191. doi: 10.1007/s10546-007-9261-y.

Barlow J.F. (2014) ‘Progress in observing and modelling the urban boundary layer’, *Urban Climate*, 10(2), pp. 216-240. doi: 10.1016/j.uclim.2014.03.011.

Basara J.B., Illston B.G., Fiebrich C.A., Browder P.D., Morgan C.R., McCombs A., Bostic J.P., McPherson R.A., Schroeder A.J., Crawford K.C. (2010) ‘The Oklahoma City Micronet’, *Meteorological Applications*, 18(3), pp. 252–261. doi: 10.1002/met.189.

Belcher S.E., Coceal O., Goulart E.V., Rudd A.C., Robins A.G. (2015) ‘Processes controlling atmospheric dispersion through city centres’, *J Fluid Mech* 763, pp.51-81. doi: 10.1017/jfm.2014.661.

Birmingham City Council (2011) 2011 Census: Key Statistics for Birmingham and its constituent areas. Available at:
https://www.birmingham.gov.uk/downloads/file/4573/census_2011_ks101_usual_resident_populationpdf (Accessed 10 June 2017).

Bornstein R.D., Johnson S.D. (1977) ‘Urban-rural wind velocity differences’, *Atmospheric Environment*, 11(7), pp. 597-602. doi: 10.1016/0004-6981(77)90112-3.

Bornstein R., Lin Q.L. (2000) 'Urban heat islands and summertime convective thunderstorms in Atlanta: three case studies', *Atmospheric Environment*, 34(3), pp. 507-516. doi: 10.1016/S1352-2310(99)00374-X.

Bohnenstengel S.I., Evans S., Clark P.A., Belcher S.E. (2011) 'Simulations of the London urban heat island', *Quarterly Journal of the Royal Meteorological Society*, 137(659), pp.1625-1640. doi: 10.1002/qj.855.

Bornstein R.D., Johnson S.D. (1977) 'Urban-rural wind velocity differences', *Atmospheric Environment*, 11(7), pp.597-602. doi: 10.1016/0004-6981(77)90112-3.

Bougeault, P., Lacarrere P. (1989) 'Parameterization of Orography-Induced Turbulence in a Mesobeta-Scale Model', *Monthly Weather Review*, 117, pp. 1872–1890. doi: 10.1175/1520-0493(1989)117<1872:POOITI>2.0.CO;2

Brandsma T., Konnen G.P., Wessels H.R.A. (2003) 'Empirical estimation of the effect of urban heat advection on the temperature series of De Bilt (The Netherlands)', *International Journal of Climatology*, 23(7), pp.829-845. doi: 10.1002/joc.902.

Brandsma T., Wolters D. (2012) 'Measurement and Statistical Modeling of the Urban Heat Island of the City of Utrecht (the Netherlands)', *Journal of Applied Meteorology and Climatology*, 51, pp. 1046–1060. doi: 10.1175/JAMC-D-11-0206.1.

Chandler, T.J. (1965) *The Climate of London*. Hutchinson & Co, London. doi: 10.1177/0309133309339794.

Chapman L., Azevedo J.A., Prieto-Lopez T. (2013) 'Urban heat and critical infrastructure networks: a viewpoint', *Urban Climate*, 3, pp. 7-12. doi: 10.1016/j.uclim.2013.04.001.

Chapman, L., Bell, C., Bell, S. (2016) 'Can the crowdsourcing data paradigm take atmospheric science to a new level? A case study of the urban heat island of London quantified using Netatmo weather stations', *International Journal of Climatology*. doi: 10.1002/joc.4940.

Chapman L., Muller C.L., Young D.T., Warren E.L., Grimmond C.S.B., Cai X-M., Ferranti J.S. (2014) 'The Birmingham Urban Climate Laboratory: An open meteorological testbed and challenges of the smart city', *Bulletin of the American Meteorological Society*, 96, pp. 1545–1560. doi: 10.1175/BAMS-D-13-00193.1.

Chemel C., Sokhi R.S. (2012) 'Response of London's Urban Heat Island to a Marine Air Intrusion in an Easterly Wind Regime', *Boundary-Layer Meteorology*, 144, pp. 65-81. doi: 10.1007/s10546-012-9705-x.

Chen F., Kusaka H., Bornstein R., Ching J., Grimmond C.S.B., Grossman-Clarke S., Loridan T., Manning K.W., Martilli A., Miao S., Sailor D., Salamanca F.P., Taha H., Tewari M., Wang X., Wyszogrodzki A.A., Zhang C. (2011) 'The integrated WRF/urban modelling system: development, evaluation, and applications to urban

environmental problems’, *International Journal of Climatology* 31, pp. 273–288. doi: 10.1002/joc.2158.

Chen F., Yang X., Zhu W., (2014) ‘WRF simulations of urban heat island under hot-weather synoptic conditions: The case study of Hangzhou City, China’, *Atmospheric Research*, 138, pp. 364-377. doi: 10.1016/j.atmosres.2013.12.005.

Chen X.L., Zhao H.M., Li P.X., Yin Z.Y. (2006) ‘Remote sensing image-based analysis of the relationship between urban heat island and land use/cover changes’, *Remote Sensing of Environment*, 104, pp. 133-146. doi: 10.1016/j.rse.2005.11.016.

Ching J.K.S., Clarke J.F., Godowitch J.M. (1983) ‘Modulation of heat flux by different scales of advection in an urban environment’, *Boundary-Layer Meteorology*, 25(2), pp. 171-191. doi: 10.1007/BF00123973.

Chou M-D., Suarez M.J. (1994) ‘An efficient thermal infrared radiation parameterization for use in general circulation models’, *NASA Tech. Memo*, pp. 84.

Chow W.T.L., Roth M. (2006) ‘Temporal dynamics of the urban heat island of Singapore’, *International Journal of Climatology*, 26(15), pp. 2243-2260. doi: 10.1002/joc.1364.

Clarke J.F. (1969) ‘Nocturnal urban boundary layer over Cincinnati, Ohio’, *Monthly Weather Review*, 97, pp. 582-589. doi: 10.1175/1520-0493(1969)097<0582:NUBLOC>2.3.CO;2.

Comarazamy D.E., González J.E., Luvall J.C., Rickman D.L., Bornstein R.D. (2013) 'Climate Impacts of Land-Cover and Land-Use Changes in Tropical Islands under Conditions of Global Climate Change', *Journal of Climate*, 26, pp. 1535–1550. doi: 10.1175/JCLI-D-12-00087.1.

Cuchiara G.C., Li X., Carvalho J., Rappenglück B. (2014) 'Intercomparison of planetary boundary layer parameterization and its impacts on surface ozone concentration in the WRF/Chem model for a case study in Houston/Texas', *Atmospheric Environment*, 96, pp.175-185. doi: <https://doi.org/10.1016/j.atmosenv.2014.07.013>.

Dirks R.A. (1974) 'Urban Atmosphere: Warm Dry Envelope Over St. Louis', *Journal of Geophysical Research*, 79(24), pp. 2156-2202. doi: 10.1029/JC079i024p03473.

Dixon P.G., Mote T.L. (2003) 'Patterns and causes of Atlanta's urban heat island-initiated precipitation', *Journal of Applied Meteorology*, 42(9), pp. 1273-1284. doi: 10.1175/1520-0450(2003)042<1273:PACOAU>2.0.CO;2.

Dou J., Wang Y., Bornstein R., Miao S. (2015) 'Observed Spatial Characteristics of Beijing Urban Climate Impacts on Summer Thunderstorms', *Journal of Applied Meteorology and Climatology*, 54, pp. 94–105. doi: 10.1175/JAMC-D-13-0355.1.

Du C., Liu S., Yu X., Li X., Chen C., Peng Y., Dong Y., Dong1 Z., Wang F. (2013) 'Urban Boundary Layer Height Characteristics and Relationship with Particulate

Matter Mass Concentrations in Xi'an, Central China', *Aerosol and Air Quality Research*, 13, pp. 1598-1607. doi: 10.4209/aaqr.2012.10.0274.

Dudhia J. (1989) 'Numerical study of convection observed during the winter monsoon experiment using a mesoscale two-dimensional model', *Journal of the Atmospheric Sciences*, 46, pp. 3077–3107. doi: 10.1175/1520-0469(1989)046<3077:NSOCOD>2.0.CO;2.

Fan S. J., Fan Q., Yu W., Luo X. Y., Wang B. M., Song L. L., Leong K. L. (2011) 'Atmospheric boundary layer characteristics over the Pearl River Delta, China, during the summer of 2006: measurement and model results', *Atmospheric Chemistry and Physics*, 11, pp. 6297-6310. doi: <https://doi.org/10.5194/acp-11-6297-2011>.

Fan Y., Li Y., Bejan A., Wang Y., Yang X. (2017) 'Horizontal extent of the urban heat dome flow', *Scientific Reports*, 7:11681. doi: 10.1038/s41598-017-09917-4.

Ferranti E., Chapman L., Lowe C., McCulloch S., Jaroszweski D., Quinn A. (2016) 'Heat-Related Failures on Southeast England's Railway Network: Insights and Implications for Heat Risk Management', *Weather, Climate and Society*, 8, pp. 177–191. doi: 10.1175/WCAS-D-15-0068.1.

Flagg D.D., Taylor P.A. (2011) 'Sensitivity of mesoscale model urban boundary layer meteorology to the scale of urban representation', *Atmospheric Chemistry and Physics*, 11, pp. 2951–2972. doi: 10.1007/s10546-014-9985-4.

Garratt J.R. (1990) 'The Internal Boundary Layer – A Review', *Boundary-Layer Meteorology*, 50(1), pp. 171-203. doi: 10.1007/BF00120524.

Gedzelman S.D., Austin S., Cernak R., Stefano N., Partridge S., Quesenberry S., Robinson D.A. (2003) 'Mesoscale aspects of the Urban Heat Island around New York City', *Theoretical and Applied Climatology*, 75, pp. 29-42. doi: 10.1007/s00704-002-0724-2.

Giometto M.G., Christen A., Meneveau C., Fang J., Krafczyk M., Parlange M.B. (2016) 'Spatial Characteristics of Roughness Sublayer Mean Flow and Turbulence Over a Realistic Urban Surface', *Boundary-Layer Meteorology*, 160, pp. 425-452. doi: 10.1007/s10546-016-0157-6.

Godowitch J.M., Ching, J.K.S., Clarke J.F. (1987) 'Spatial variation of the evolution and structure of the urban boundary layer', *Boundary-Layer Meteorology*, 38(5), pp. 249-272. doi: 10.1007/BF00122447.

Google Maps (2016) *Map of station locations [online]*. Google. Available at: <https://www.google.co.uk/maps> (Accessed 05 October 2016).

Grimmond C.S.B. (2006) 'Progress in measuring and observing the urban atmosphere', *Theoretical Applied Climatology*, 84, pp. 2-22. doi: 10.1007/s00704-005-0140-5.

Grimmond C.S.B., Roth M., Oke T.R., Au Y.C., Best M., Betts R., Carmichael G., Cleugh H., Dabberdt W., Emmanuel R., Freitas E., Fortuniak K., Hanna S., Klein P., Kalkstein L.S., Liu C.H., Nickson A., Pearlmutter D., Sailor D., Voogt J. (2010) 'Climate and More Sustainable Cities: Climate Information for Improved Planning and Management of Cities (Producers/Capabilities Perspective)', *World Climate Conference*, 3, pp. 247-274. doi: 10.1016/j.proenv.2010.09.016.

Gutiérrez E., González J.E., Martilli A., Bornstein R., Arend M. (2015) 'Simulations of a Heat-Wave Event in New York City Using a Multilayer Urban Parameterization', *Journal of Applied Meteorology and Climatology*, 54(2), pp. 283-301. doi: 10.1175/JAMC-D-14-0028.1.

Haeger-Eugensson M., Holmer B. (1999) 'Advection caused by the urban heat island circulation as a regulating factor on the nocturnal urban heat island', *International Journal of Climatology*, 19, pp. 975-988. doi: 10.1002/(SICI)1097-0088(199907)19:9<975::AID-JOC399>3.0.CO;2-J.

Hajat S., Vardoulakis S., Heaviside C., Eggen B. (2014) 'Climate change effects on human health: projections of temperature-related mortality for the UK during the 2020s, 2050s and 2080s', *Journal of Epidemiology and Community Health*, 68(7), pp. 641-648. doi: 10.1136/jech-2013-202449

Heaviside C., Cai X-M., Vardoulakis S. (2015) 'The effects of horizontal advection on the urban heat island in Birmingham and the West Midlands, United Kingdom

during a heatwave’, *Quarterly Journal of the Royal Meteorological Society*, 141, pp. 1429–1441. doi: 10.1007/s10546-012-9705-x.

Heaviside C., Vardoulakis S., Cai X-M. (2016) ‘Attribution of mortality to the Urban Heat Island during heatwaves in the West Midlands, UK.’, *Environmental Health*, 15(1), pp. 27. doi: 10.1186/s12940-016-0100-9

Hidalgo J., Masson V., Gimeno L. (2010) ‘Scaling the Daytime Urban Heat Island and Urban-Breeze Circulation,’ *Journal of Applied Meteorology*, 49, pp. 889-901. doi: 10.1175/2009JAMC2195.1.

Hildebrand P.H., Ackerman B. (1984) ‘Urban effects on the Convective Boundary Layer’, *Journal of the Atmospheric Sciences*, 41, pp. 76-91. doi: 10.1175/1520-0469(1984)041<0076:UEOTCB>2.0.CO;2.

Howard L. (1833) *The Climate of London*. Dalton: London.

IPCC (2014) *Climate Change (2014) Synthesis Report. Contribution of Working Groups I, II and III to the Fifth Assessment Report of the Intergovernmental Panel on Climate Change* [Core Writing Team, R.K. Pachauri and L.A. Meyer (eds.)]. IPCC, Geneva, Switzerland, pp. 151.

Ivajnsiĉ A., Kaligariĉ M., Źibera I. (2014) ‘Geographically weighted regression of the urban heat island of a small city’, *Applied Geography*, 53, pp. 341-353. doi: 10.1016/j.apgeog.2014.07.001.

Jauregui E. (1997) 'Heat island development in Mexico City', *Atmospheric Environment*, 31(22), pp. 3821-3831. doi: 10.1016/S1352-2310(97)00136-2.

Johnson D.B. (1985) 'Urban modification of diurnal temperature cycles in Birmingham, U.K.', *Journal of Climatology*, 5, pp. 221-225. doi: 10.1002/joc.3370050208.

Johnson H., Kovats R.S., McGregor G., Stedman J., Gibbs M., Walton H., Cook L., Black E. (2005) 'The impact of the 2003 heat wave on mortality and hospital admissions in England', *Health Statistics Quarterly*, 25, pp. 6-11.

Jones P.D., Groisman P.Y.A., Coughlan M., Plummer N. Wang W-C., Karl T.R. (1990) 'Assessment of urbanization effects in time series of surface air temperature over land', *Nature*, 347, pp. 169-172. doi: 10.1038/347169a0.

Kalnay E., Cai M. (2003) 'Impact of urbanization and land-use change on climate', *Nature*, 423, pp. 528-531. doi: 10.1016/j.uclim.2013.04.00.1.

Klysik K., Fortuniak K. (1999) 'Temporal and spatial characteristics of the urban heat island of Łódź, Poland', *Atmospheric Environment*, 33, pp. 3885-3895. doi: 10.1016/S1352-2310(99)00131-4.

Knight S., Smith C., Roberts M. (2010) 'Mapping Manchester's urban heat island', *Weather*, 65(7), pp. 188-193. doi: 10.1002/wea.542.

Kolokotroni M., Giridharan R. (2008) 'Urban heat island intensity in London: An investigation of the impact of physical characteristics on changes in outdoor air temperature during summer', *Solar Energy*, 82, pp. 986-998. doi: 10.1016/j.solener.2008.05.004.

Krüger E., Emmanuel R. (2013) 'Accounting for atmospheric stability conditions in urban heat island studies: The case of Glasgow, UK', *Landscape and Urban Planning*, 117, pp. 112 – 121. doi: 10.1016/j.landurbplan.2013.04.019.

Lee DO. (1975) 'Rural atmospheric stability and the intensity of London's urban heat island', *Weather*, 30, pp. 102-109. doi: 10.1002/j.1477-8696.1975.tb03342.x.

Lee S-H., Kim S-W., Angevine W.M., Bianco L., McKeen S.A., Senff C.J., Trainer M., Tucker S.C., Zamora R.J. (2011) 'Evaluation of urban surface parameterizations in the WRF model using measurements during the Texas Air Quality Study 206 field campaign', *Atmospheric Chemistry and Physics*, 11, pp. 2127–2143. doi: 10.5194/acp-11-2127-2011.

Li D.H.W., Yang L., Lam J.C. (2012) 'Impact of climate change on energy use in the built environment in different climate zones: a review', *Energy*, 42, pp. 103–112. doi: 10.1016/j.energy.2012.03.044.

Liao J., Wang T., Wang X., Xie M., Jiang Z., Huang X., Zhu J. (2014) 'Impacts of different urban canopy schemes in WRF/Chem on regional climate and air quality in

Yangtze River Delta, China', *Atmospheric Research*, 145–146, pp. 226-243. doi: 10.1016/j.atmosres.2014.04.005.

Lindén J., Grimmond C. S. B., Esper J. (2015) 'Urban warming in villages', *Advances in Science and Research*, 12, pp. 157-162. doi: <https://doi.org/10.5194/asr-12-157-2015>.

Loridian T., Grimmond C.S.B. (2012) 'Multi-site evaluation of an urban land-surface model: intra-urban heterogeneity, seasonality and parameter complexity requirements', *Quarterly Journal of the Royal Meteorological Society*, 138, pp. 1094-1113. doi: 10.1002/qj.963.

Loridian T., Lindberg F., Jorba O., Kotthaus S., Grossman-Clarke S., Grimmond C.S.B. (2013) 'High Resolution Simulation of the Variability of Surface Energy Balance Fluxes Across Central London with Urban Zones for Energy Partitioning', *Boundary-Layer Meteorology*, 147, pp. 493-523. doi: 10.1007/s10546-013-9797-y.

Lowry W.P. (1977) 'Empirical Estimation of Urban Effects on Climate: A Problem Analysis', *Journal of Applied Meteorology*, 16, pp. 129-135. doi: 10.1175/1520-0450(1977)016<0129:EEOUEO>2.0.CO;2.

Martilli A. (2002) 'Numerical Study of Urban Impact on Boundary Layer Structure: Sensitivity to Wind Speed, Urban Morphology, and Rural Soil Moisture', *Journal of Applied Meteorology*, 41(12), pp. 1247-1266. doi: 10.1175/15200450(2002)041<1247:NSOUIO>2.0.CO;2.

Martilli A., Clappier A., Rotach M.W. (2002) ‘An urban surface exchange parameterization for mesoscale models’, *Boundary-Layer Meteorology*, 104, pp. 261–304. doi: 10.1023/A:1016099921195.

Mavrogianni A., Davies M., Batty M., Belcher S.E., Bohnenstengel S.I., Carruthers D., Chalabi Z., Croxford B., Demanuele C., Evans S., Giridharan R., Hacker J.N., Hamilton I., Hogg C., Hunt J., Kolokotroni M., Martin C., Milner J., Rajapaksha I., Steadman J.P., Stocker J., Wilkinson P., Ye Z. (2011) ‘The comfort, energy and health implications of London’s urban heat island’, *Building Services Research and Technology*, 32(1), pp. 35–52. doi: 10.1177/0143624410394530.

McCarthy M.P., Best M.J., Betts R.A. (2010) ‘Climate change in cities due to global warming and urban effects’, *Geophysical Research Letters*, 37, L09705. doi: 10.1029/2010GL042845.

Met Office (2012): *Met Office Integrated Data Archive System (MIDAS) Land and Marine Surface Stations Data (1853-current)*. NCAS British Atmospheric Data Centre. Available at:

<http://catalogue.ceda.ac.uk/uuid/220a65615218d5c9cc9e4785a3234bd0> (Accessed: 15 May 2015).

Met Office (2016) *National Meteorological Library and Archive Fact sheet 17 — Weather observations over land*. Available at:

http://www.metoffice.gov.uk/binaries/content/assets/mohippo/pdf/p/6/10_0230_fs_17_observations.pdf (Accessed 26 June 2017).

Miao S. (2009) ‘An Observational and Modeling Study of Characteristics of Urban Heat Island and Boundary Layer Structures in Beijing’, *Journal of Applied Meteorology and Climatology*, 48, pp. 484-501. doi: <https://doi.org/10.1175/2008JAMC1909.1>.

Mlawer E.J., Taubman S.J., Brown P.D., Iacono M.J., Clough S.A. (1997) ‘Radiative transfer for inhomogeneous atmospheres: RRTM, a validated correlated-k model for the longwave’, *Journal of Geophysical Research: Atmospheres*, 102, pp. 16663–16682. doi: 10.1029/97JD00237.

Muller C.L., Chapman L., Grimmond C.S.B., Young D.T., Cai, X-M. (2013) ‘Toward a Standardized Metadata Protocol for Urban Meteorological Networks’, *Bulletin of the American Meteorological Society*, 94, pp. 1161-1185. doi: 10.1175/BAMS-D-12-00096.1.

Oberndorfer E., Lundholm J., Bass B., Coffman R.R., Doshi H., Dunnett N., Gaffin S., Kohler M., Liu K.K.Y., Rowe B. (2007) ‘Green roofs as urban ecosystems: Ecological structures, functions, and services’, *American Institute of Biological Sciences*, 57(10), pp. 823-833. doi: 10.1641/B571005.

Oke T.R. (1973) ‘City size and the urban heat island’, *Atmospheric Environment*, 7, pp. 769-779. doi: 10.1016/0004-6981(73)90140-6.

Oke T.R. (1976) ‘The distinction between canopy and boundary-layer urban heat islands’, *Atmosphere*, 14(4), pp. 268-277. doi: 10.1080/00046973.1976.9648422.

Oke T.R. (1982) 'The energetic basis of the urban heat island', *Quarterly Journal of the Royal Meteorological Society*, 108, pp. 1-24. doi: 10.1002/qj.49710845502.

Oke T. R. (1987) *Boundary Layer Climates*. 2nd edition. London, UK: Routledge.

Oke T.R. (2006) 'Initial Guidance to Obtain Representative Meteorological Observations at Urban Sites', IOM Report No.81, WMO/TD. No. 1250. World Meteorological Organization, Geneva.

Oke T.R. (1995) The Heat Island of the Urban Boundary Layer: Characteristics, Causes and Effects. In: Cermak J.E., Davenport A.G., Plate E.J., Viegas D.X. (eds) *Wind Climate in Cities*. NATO ASI Series (Series E: Applied Sciences), vol 277. Springer, Dordrecht. doi: https://doi.org/10.1007/978-94-017-3686-2_5.

ONS (Office for National Statistics) (2013) '2011 Census analysis – comparing rural and urban areas of England and Wales.' Available at: http://www.ons.gov.uk/ons/dcp171776_337939.pdf (Accessed 8 September 2016).

OS MasterMap® Building Heights [FileGeoDatabase geospatial data], Scale 1:2500, Tiles: tq15ne, tq15nw, tq15se, tq15sw, tq16ne, tq16nw, tq16se, tq16sw, tq17ne, tq17nw, tq17se, tq17sw, tq18ne, tq18nw, tq18se, tq18sw, tq19ne, tq19nw, tq19se, tq19sw, Updated: 29 November 2014, Ordnance Survey (GB), Using: EDINA Digimap Ordnance Survey Service, <<http://digimap.edina.ac.uk>>, Downloaded: 2016-06-27 15:11:36.774

Pal S., Xueref-Remy I., Ammoura L., Chazette P., Gibert F., Royer P., Dieudonné E., Dupont J.-C., Haeffelin M., Lac C., Lopez M., Morille Y., Ravetta F., (2012) 'Spatio-temporal variability of the atmospheric boundary layer depth over the Paris agglomeration: An assessment of the impact of the urban heat island intensity', *Atmospheric Environment*, 63, pp. 261-275. doi: <https://doi.org/10.1016/j.atmosenv.2012.09.046>.

Park H-S. (1986) 'Features of the heat island in seoul and its surrounding cities', *Atmospheric Environment*, 20(10), pp. 1859-1866. doi: 10.1016/0004-6981(86)90326-4.

Parker D.E. (2006) 'A demonstration that large-scale warming is not urban', *Journal of Climate*, 19, pp. 2882-2895. doi: 10.1175/JCLI3730.1.

Parker D., Horton B. (2005) 'Uncertainties in central England temperature 1878–2003 and some improvements to the maximum and minimum series', *International Journal of Climatology*, 25, pp. 1173–1188. doi: 10.1002/joc.1190.

Pasquill F., Smith F.B. (1983) *Atmospheric Diffusion*, 3rd Edition. Ellis Horwood Limited: Chichester. doi: 10.1002/qj.49711046416.

Patz J.A., Campbell-Lendrum D., Hollowat T., Foley J.A. (2005) 'Impact of regional climate change on human health', *Nature*, 438, pp. 310-317. doi: 10.1038/nature04188.

Pineda N., Jorba O., Jorge J., Baldasano J.M. (2004) 'Using NOAA AVHRR and SPOT VGT data to estimate surface parameters: application to a mesoscale meteorological model', *International Journal of Remote Sensing*, 25(1), pp. 129-143. doi: 10.1080/0143116031000115201.

Reuter H.I., Nelson A., Jarvis A. (2007) 'An evaluation of void filling interpolation methods for SRTM data', *International Journal of Geographical Information Science*, 21(9), pp. 983-1008. doi: 10.1080/13658810601169899.

Robine J-M., Cheung S.L., Le Roy S., Van Oyen H., Griffiths C., Michel J.P., Herrmann F.R. (2008) 'Death toll exceeded 70,000 in Europe during the summer of 2003', *Comptes Rendus Biologies*, 331, pp. 171-175. doi: 10.1016/j.crv.2007.12.001.

Rooney G.G. (2001) 'Comparison of upwind land use and roughness length measured in the urban boundary layer', *Boundary-Layer Meteorology*, 100(3), pp. 469-485. doi: 10.1023/A:1019265913011.

Rooney G.G., Longley I.D., Barlow J.F. (2005) 'Variation of urban momentum roughness length with land use in the upwind source area, as observed in two U.K. cities', *Boundary-Layer Meteorology*, 115(1), pp. 69-84. doi: 10.1007/s10546-004-2987-x.

Rotach M. W. (1995) 'Profiles of Turbulence in and above an Urban Street Canyon', *Atmospheric Environment*, 29, pp. 1473-1486. doi: [https://doi.org/10.1016/1352-2310\(95\)00084-C](https://doi.org/10.1016/1352-2310(95)00084-C).

Runnalls K.E., Oke T.R. (2000) 'Dynamics and controls of the surface urban heat island of Vancouver, British Columbia', *Physical Geography*, 21(4), pp. 283-304. doi: 10.1080/02723646.2000.10642711.

Ryu Y-H., Baik J-J., Han J-Y. (2013) 'Daytime urban breeze circulation and its interaction with convective cells', *Quarterly Journal of the Royal Meteorological Society*, 139, pp. 401-413. doi: 10.1002/qj.1973.

Salamanca F., Martilli A. (2010) 'A new building energy model coupled with an urban canopy parameterization for urban climate simulations—Part I. Formulation, verification and a sensitive analysis of the model', *Theoretical Applied Climatology*, 99, pp. 331–344. doi: 10.1007/s00704-009-0142-9.

Salamanca F., Martilli A., Tewari M., Chen F. (2011) 'A Study of the Urban Boundary Layer Using Different Urban Parameterizations and High-Resolution Urban Canopy Parameters with WRF', *American Meteorological Society*, 50, pp. 1107-1128. doi: 10.1175/2010JAMC2538.1.

Santamouris M. (2014) 'Cooling the cities – A review of reflective and green roof mitigation technologies to fight heat island and improve comfort in urban environments', *Solar Energy*, 103, pp. 682 – 703. doi: 10.1016/j.solener.2012.07.003.

Santamouris M. (2015) 'Analyzing the heat island magnitude and characteristics in one hundred Asian and Australian cities and regions', *Science of The Total Environment*, 512, pp. 582-598. doi:10.1016/j.scitotenv.2015.01.060.

Santamouris M., Papanikolaou N., Livada I., Koronakis I., Georgakis C., Argiriou A., Assimakopoulos D.N. (2001) 'On the impact of urban climate on the energy consumption of buildings', *Solar Energy*, 70(3), pp. 201-216. doi: 10.1016/S0038-092X(00)00095-5.

Shepard J.M., Pierce H., Negri A.J. (2002) 'Rainfall modification by major urban areas: Observations from spaceborne rain radar on the TRMM satellite', *Journal of Applied Meteorology*, 41(7), pp. 689-701. doi: 10.1175/1520-0450(2002)041<0689:RMBMUA>2.0.CO;2

Skamarock W.C., Klemp J.B., Dudhia J., Gill D.O., Barker D.M., Duda M.G., Huang X-Y., Wang W., Powers J.G. (2008) 'A Description of the Advanced Research WRF Version 3', NCAR Technical Note NCAR/TN-475+STR. doi: 10.5065/D68S4MVH.

Smith C.L., Webb A., Levermore G.J., Lindley S.J., Beswick K. (2011) Fine-scale spatial temperature patterns across a UK conurbation. *Climate Change*, 109, pp. 269-286. doi: 10.1007/s10584-011-0021-0.

Spronken-Smith R.A., Oke T.R., Lowry W.P. (2000) Advection and the surface energy balance across an irrigated urban park. *International Journal of Climatology*, 20(9), pp. 1033-1047. doi: 10.1002/1097-0088(200007)20:9<1033::AID-JOC508>3.0.CO;2-U.

Stathopoulou M., Cartalis C. (2006) 'Daytime urban heat islands from Landsat ETM+ and Corine land cover data: An application to major cities in Greece', *Solar Energy*, 81, pp. 358-368. doi: 10.1016/j.solener.2006.06.014.

Stensrud D.J. (2007) *Parameterization Schemes: Keys to Understanding Numerical Weather Prediction Models*. Cambridge University Press: Cambridge, UK, 459 pp.

Stewart I.D. (2011) 'A systematic review and scientific critique of methodology in modern urban heat island literature', *International Journal of Climatology*, 31, pp. 200-217. doi: 10.1002/joc.2141.

Stewart I.D., Oke T.R. (2012) 'Local climate zones for urban temperature studies', *Bulletin of the American Meteorological Society*, 93, pp. 1879-1900. doi: 10.1175/BAMS-D-11-00019.1.

Stone B., Hess J.J., Frumkin H. (2010) 'Urban Form and Extreme Heat Events: Are Sprawling Cities More Vulnerable to Climate Change Than Compact Cities?', *Environmental Health Perspectives*, 118(10), pp. 1425-1428. doi: 10.1289/ehp.0901879.

Stull, R.B. (1988). *An Introduction to Boundary Layer Meteorology*, Kluwer Academic, The Netherlands.

Szymanowski M., Kryza M. (2009) 'GIS-based techniques for urban heat island spatialization', *Climate Research*, 38(2), pp. 171-187. doi: 10.3354/cr00780.

Takane Y., Ohashi Y., Kusaka H., Shigeta Y., Kikegawa Y. (2013) 'Effects of Synoptic-Scale Wind under the Typical Summer Pressure Pattern on the Mesoscale High-Temperature Events in the Osaka and Kyoto Urban Areas by the WRF Model', *Journal of Applied Meteorology and Climatology*, 52, pp. 1764-1778. doi: 10.1175/JAMC-D-12-0116.1.

Tewari, M., Chen F., Wang W., Dudhia J., LeMone M.A., Mitchell K., Ek M., Gayno G., Wegiel J., Cuenca R.H. (2004) 'Implementation and verification of the unified NOAA land surface model in the WRF model'. *20th conference on weather analysis and forecasting/16th conference on numerical weather prediction*, pp. 11–15.

Thornes T. (2015) 'Variations of temperature, wind speed and humidity within Birmingham New Street Station during hot weather', *Weather*, 70, pp. 129-134. doi: 10.1002/wea.2358.

Tomlinson C.J., Chapman L., Thornes J.E., Baker C.J. (2012) 'Derivation of Birmingham's summer surface urban heat island from MODIS satellite images', *International Journal of Climatology*, 32, pp. 214-224. doi: 10.1002/joc.2261.

Tomlinson C.J., Prieto-Lopez T., Bassett R., Chapman L., Cai X-M., Thornes J.E., Baker C.J. (2013) 'Showcasing urban heat island work in Birmingham - measuring, monitoring, modelling and more', *Weather*, 68, pp. 44-49. doi: 10.1002/wea.1998.

Unger J., Sumeghy Z., Szegedi S., Kiss A., Geczi R. (2010) ‘Comparison and generalisation of spatial patterns of the urban heat island based on normalized values’, *Physics and Chemistry of the Earth*, 35, pp. 107-114. doi: 10.1016/j.pce.2010.03.001.

United Nations (UN), Department of Economic and Social Affairs, Population Division (2014). ‘World Urbanization Prospects: The 2014 Revision, Highlights (ST/ESA/SER.A/352)’. Available at:
<https://esa.un.org/unpd/wup/publications/files/wup2014-highlights.Pdf> (Accessed 26 June 2017).

Unwin D.J. (1980) ‘The synoptic climatology of Birmingham’s urban heat island’, 1965-74. *Weather*, 35, pp. 43–50. doi: 10.1002/j.1477-8696.1980.tb03484.x.

Vaisala (2012) Weather Transmitter WXT520 User’s Guide. Available at:
<http://www.vaisala.com/Vaisala%20Documents/User%20Guides%20and%20Quick%20Ref%20Guides/M210906EN-C.pdf>. (Accessed 21 February 2016).

Voogt J.A., Oke T.R. (2003) ‘Thermal remote sensing of urban climates’, *Remote Sensing of Environment*, 86, pp. 370-384. doi: 10.1016/S0034-4257(03)00079-8.

Warren, E.L., Chapman L., Young D.T., Muller C.L., Grimmond C.S.B., Cai X-M. (2016) ‘The Birmingham Urban Climate Laboratory—A high density, urban meteorological dataset, from 2012–2014’, *Scientific Data*, 3, pp. 160038. doi: 10.1038/sdata.2016.38.

Wickham C., Rohde R., Muller R.A., Wurtele J., Curry J., Groom D., Jacobsen R., Rosenfeld A., Mosher S. (2013) 'Influence of Urban Heating on the Global Temperature Land Average using Rural Sites Identified from MODIS Classifications', *Geoinformatics & Geostatistics: An Overview*, 1:2. doi: 10.4172/2327-4581.1000104.

World Meteorological Organization (WMO) (2008) Guide to Meteorological Instruments and Methods of Observation. Seventh Edition.

Wong K.K., Dirks R.A. 1978. 'Mesoscale Perturbations on Airflow in the Urban Mixing Layer', *American Meteorological Society*, 17, pp. 677-688. doi: 10.1175/1520-0450(1978)017<0677:MPOAIT>2.0.CO;2.

Wyngaard J.C. (2004) 'Toward Numerical Modeling in the "Terra Incognita"', *Journal of Atmospheric Sciences*, 66, 1816-1826. doi: 10.1175/1520-0469(2004)061<1816:TNMITT>2.0.CO;2.

Yang X., Li Y., Luo Z., Chan, P.W. (2017) 'The urban cool island phenomenon in a high-rise high-density city and its mechanisms', *International Journal of Climatology*, 37, pp. 890–904. doi: 10.1002/joc.4747.

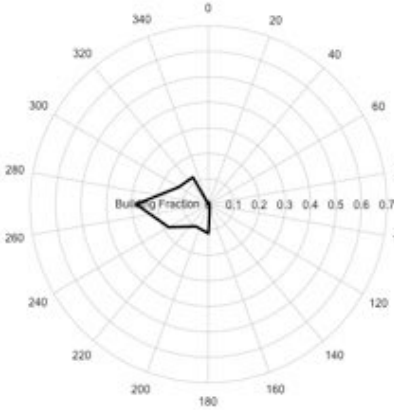

Zhang D-L., Shou Y-X., Dickerson R.R. (2009) 'Upstream urbanization exacerbates urban heat island effects', *Geophysical Research Letters*, 36. doi: 10.1029/2009GL041082.

Zhang D-L., Shou Y-X., Dickerson R.R., Chen F. (2012) ‘Impact of Upstream Urbanization on the Urban Heat Island Effects along the Washington–Baltimore Corridor’, *Journal of Applied Meteorology and Climatology*, 50, pp. 2012-2029. doi: 10.1175/JAMC-D-10-05008.1.

Zhou L.M., Dickinson R.E., Tian Y., Fang J., Li Q., Kaufmann R.K., Tucker C.J., Myneni R.B. (2004) ‘Evidence for a significant urbanization effect on climate in China’, *Proceedings of the National Academy of Sciences of the United States of America*, 101, pp. 9540-9544. doi: 10.1073/pnas.0400357101.

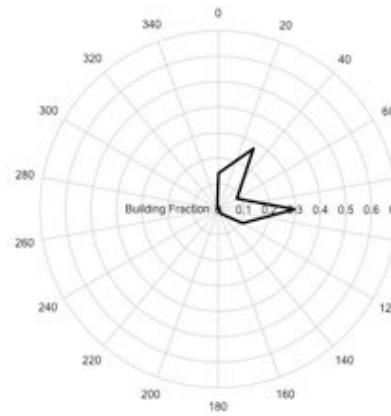
Appendix

Station metadata (accessed through the Met Office Integrated Data Archive System that provides UK land-surface observations from 1853 to present). In total, 42 stations from the UK Met Office network were identified as having an adjacent urban area (approximately 1 km² size) in a single wind sector. The stations are typically located at airfields due to historical associations between aviation and meteorology, although these selected stations should not be considered an exclusive list of those likely to be influenced by UHA. Station data with surrounding urban land use in all directions, near coasts or in areas of high terrain, were not analyzed. In these cases station data could also be affected by UHA but the effect would be difficult to determine. In addition 1-hr data were required, and with a large percentage of UK stations capturing only daily data, this limits the numbers available for analysis. The satellite imagery was used to visually check the automatic building fraction classification.

Station name (ID)	Latitude, Longitude	Building fraction at 30-degree arcs extending 0.5 km from each station	Satellite imagery of stations (Google Maps 2016)
Dyce (161)	57.2051, -2.2037		

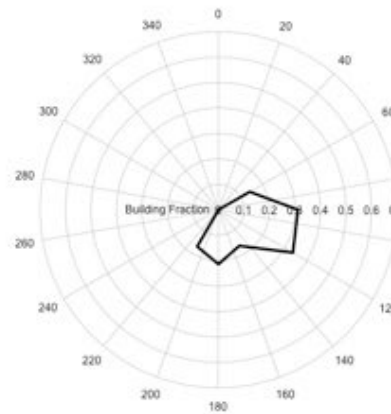
Dishforth
Airfield
(342)

54.1346,
-1.41293



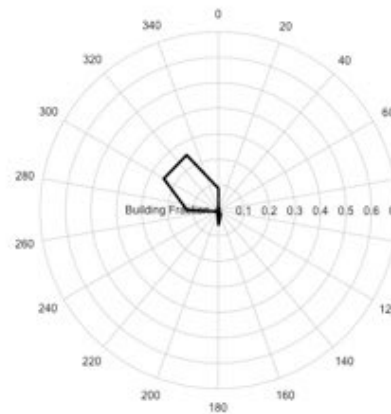
Linton-on-
Ouse
(346)

54.045,
-1.24956



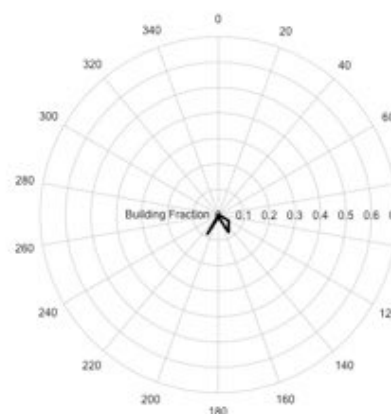
Leconfield
(370)

53.8744,
-0.44009



Scampton
(381)

53.3066,
-0.54649



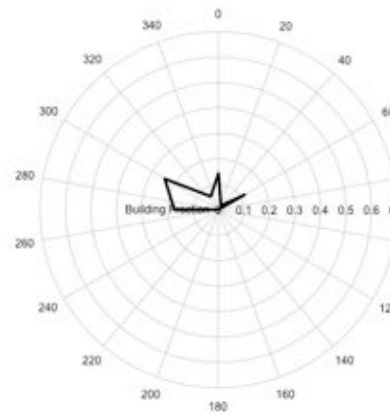
Waddington
(384)

53.1751,
-0.52173



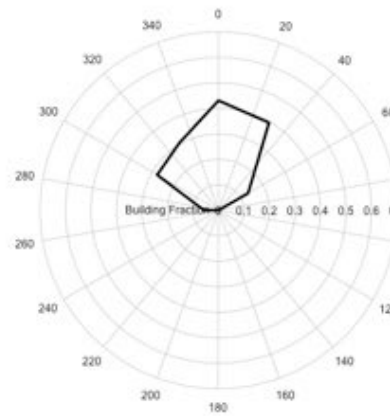
Cranwell
(386)

53.0309,
-0.50194



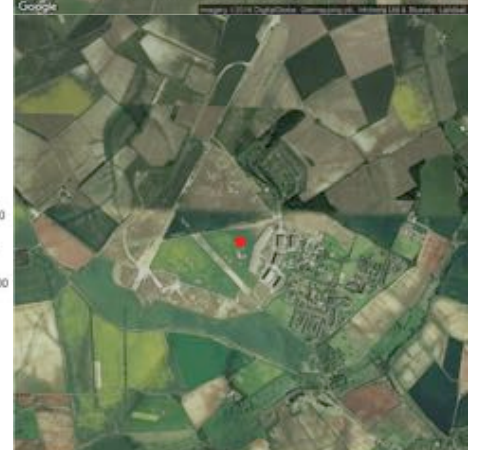
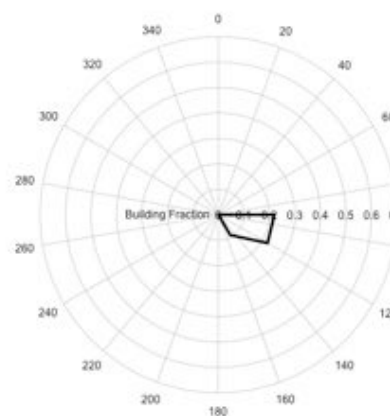
Coningsby
(393)

53.0935,
-0.17119



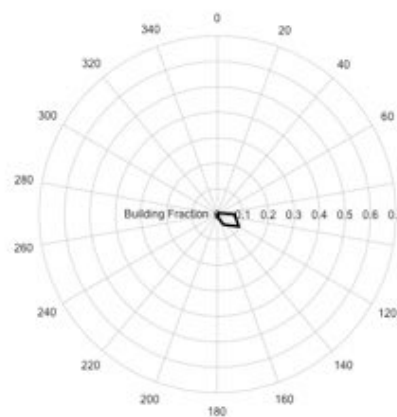
Binbrook
(394)

53.4451,
-0.20053



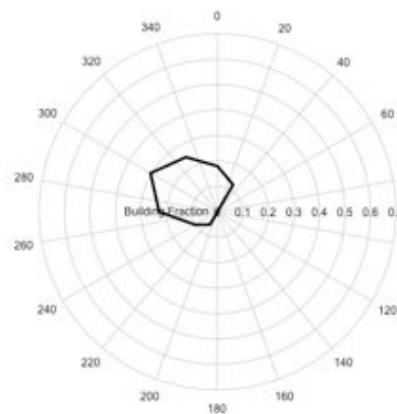
Marham
(409)

52.651,
0.56772



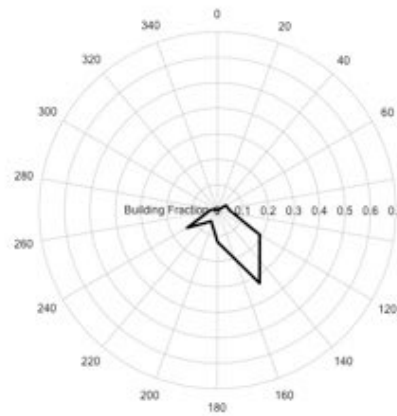
Coltishall
(429)

52.7563,
1.35321



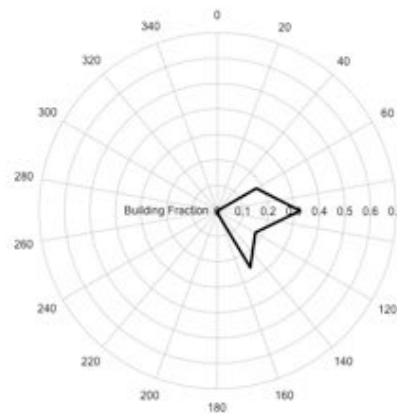
Honington
(438)

52.3400,
0.77203



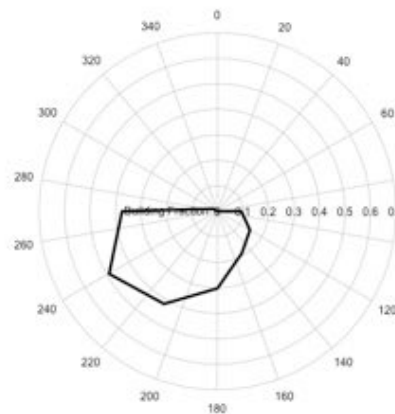
Wattisham
(440)

52.1234,
0.9591



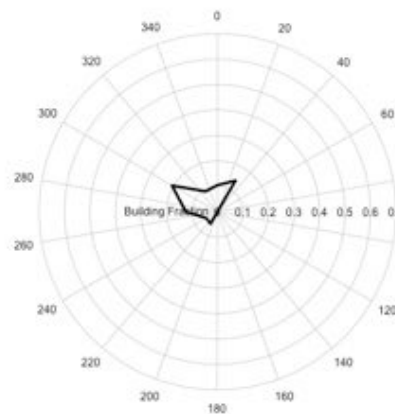
Wyton
(457)

52.3531,
-0.11452



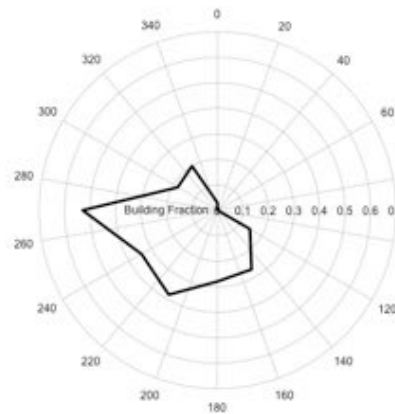
Stansted
(484)

51.8805,
0.22456



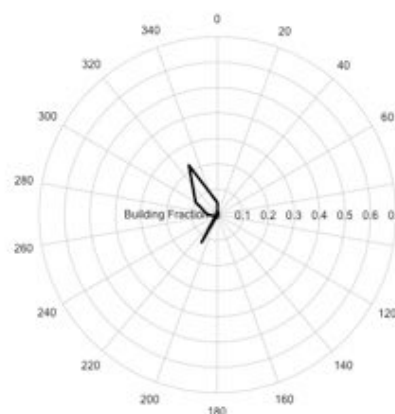
Nottingham
Watnall
(556)

53.0053,
-1.24969



Finningley
(562)

53.4824,
-1.00682



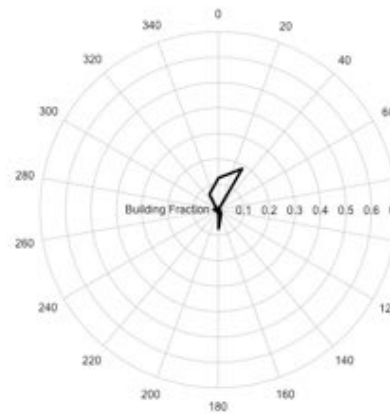
Cottesmore
(576)

52.7270,
-0.65439



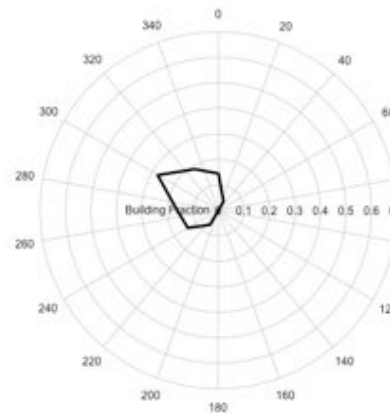
Coventry
Airport
(600)

52.3653,
-1.48886



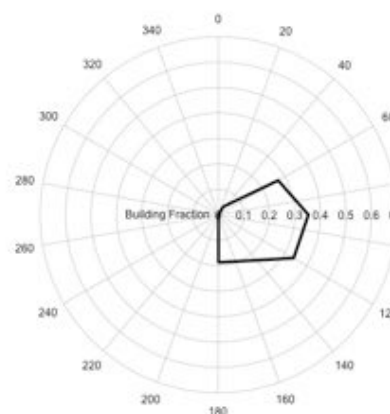
Benson
(613)

51.6199,
-1.09712

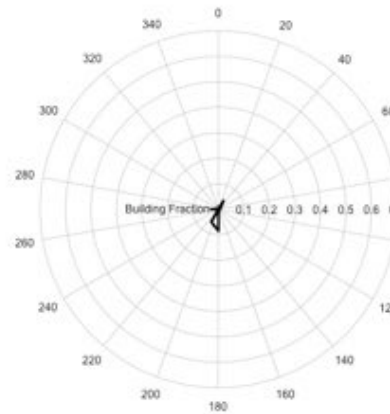


Shawbury
(643)

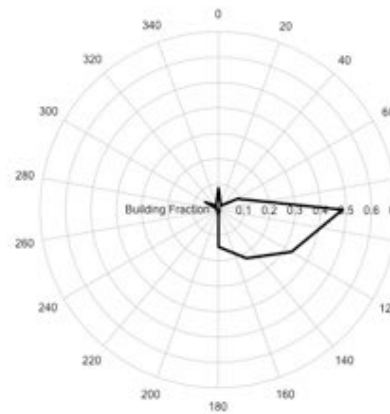
52.7943,
-2.66329



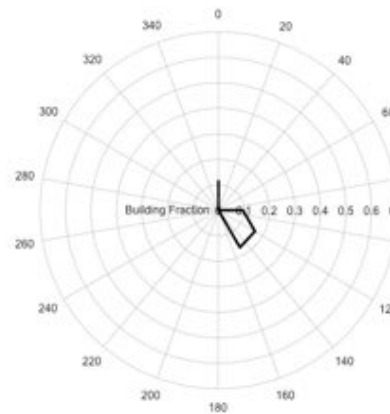
Pershore
(657) 52.148,
-2.03979



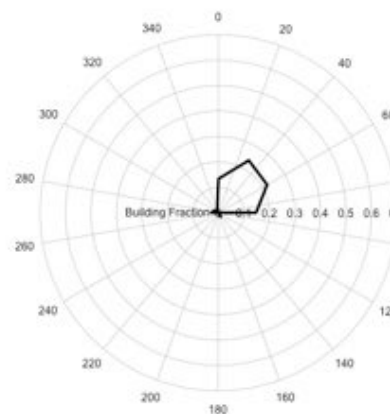
Herstmonceux
West End
(811) 50.8904,
0.31818



Hurn
(842) 50.7789,
-1.83483

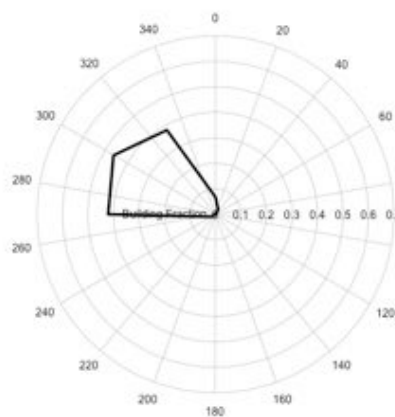


Middle
Wallop
(847) 51.1493,
-1.56851



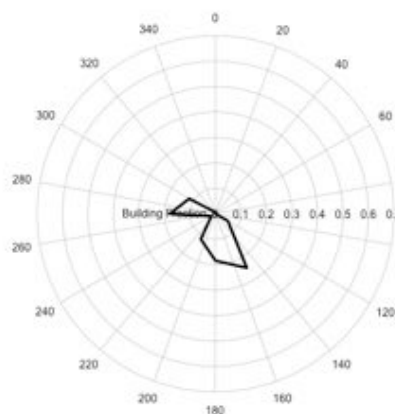
Odiham
(862)

51.2385,
-0.94346



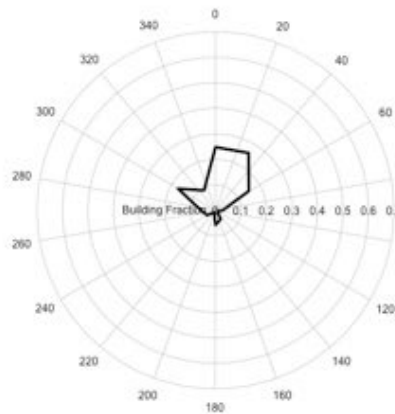
Larkhill
(888)

51.2012,
-1.80443



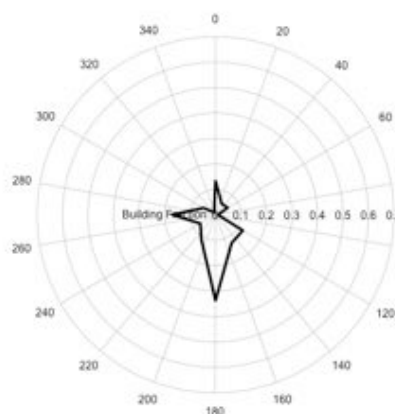
Boscombe
Down
(889)

51.1613,
-1.75317

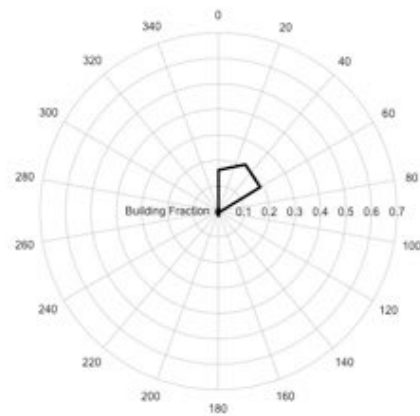


Carlisle
(1070)

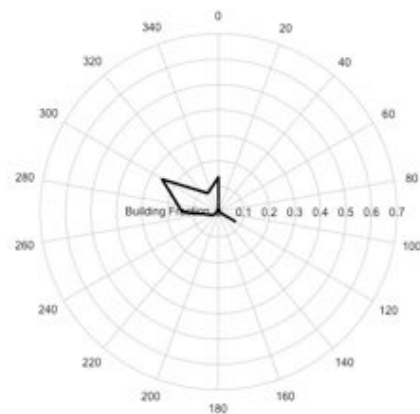
54.9342,
-2.96223



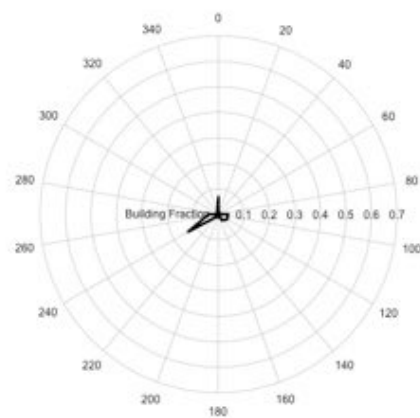
Rhyl No. 2
(1137) 53.259,
-3.50754



Hawarden
Airport
(1144) 53.1752,
-2.98499



Yeovilton
(1302) 51.0059,
-2.64148

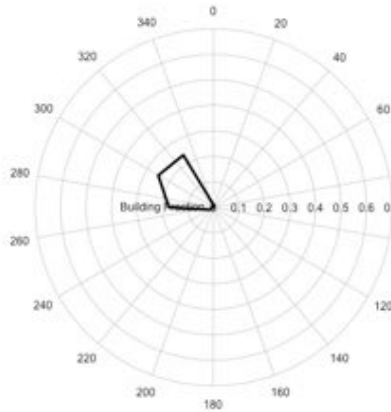


Chivenor
(1346) 51.0886,
-4.14743



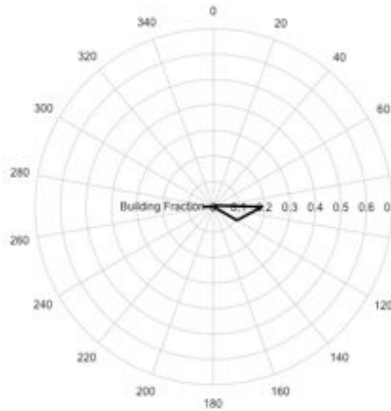
Topcliffe
(16596)

54.2045,
-1.38856



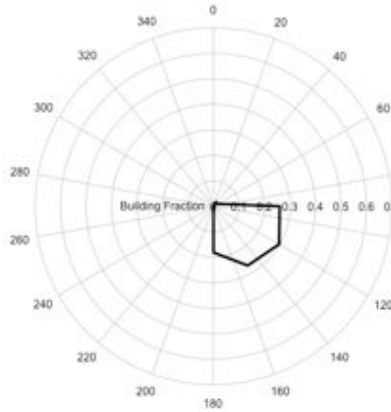
High
Wycombe
HQAIR
(17176)

51.6813,
-0.80528



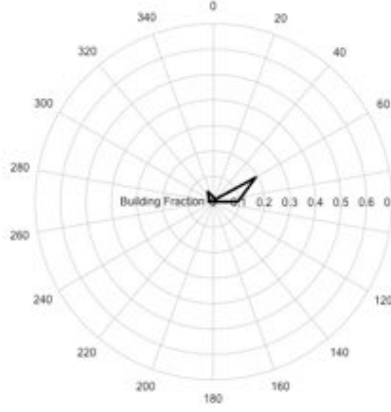
Leeming
(17314)

54.2968,
-1.53145



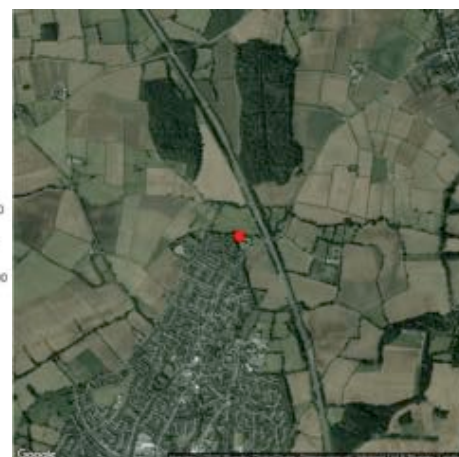
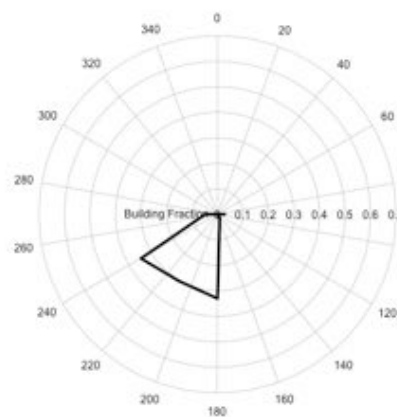
Bristol
Lulsgate
(18912)

51.3850,
-2.71285



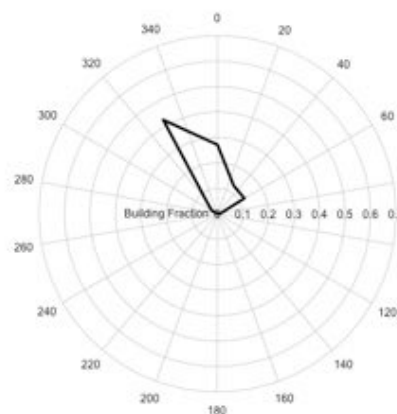
Shepshed
(18995)

52.7814,
-1.28383



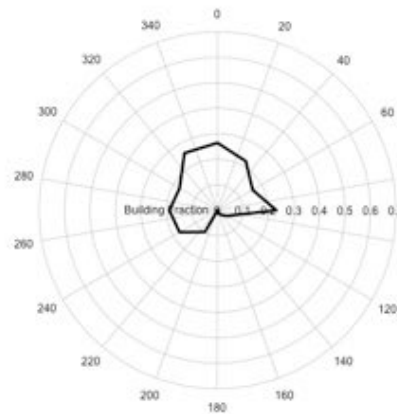
Hereford
Credenhill
(24996)

52.0796,
-2.80102



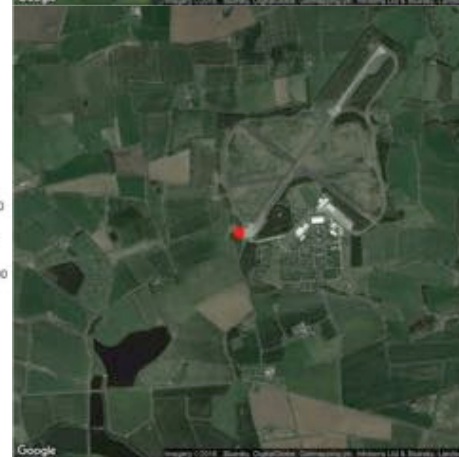
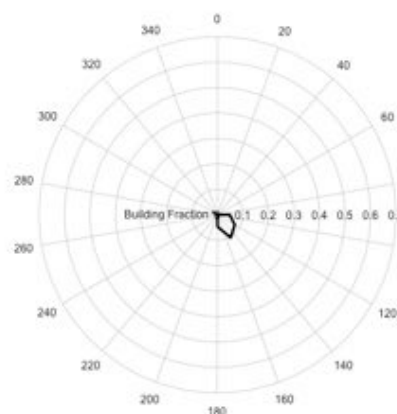
Keele
Unviersity
Roof
(25054)

53.0008,
-2.27272



Albemarle
(30523)

55.0197,
-1.88012



Woodford
(55511)

53.3388,
-2.15313

